

BOND STRENGTH OF ASTM A 1035 GRADE 100 REINFORCING STEEL

BY

Michael Gregory Briggs

April
2008

Submitted to the graduate program in Civil Engineering
and to the Graduate Faculty of the University of Kansas
in partial fulfillment of the requirements for the degree
of Master of Science.

Dr. David Darwin, Chairman

Committee members:

Dr. JoAnn Browning

Dr. Caroline Bennett

Date Defended: _____

Copyright 2008
Michael Gregory Briggs

The Thesis Committee for Michael Briggs certifies
that this is the approved Version of the following thesis:

BOND STRENGTH OF ASTM A 1035 GRADE 100 REINFORCING STEEL

Dr. David Darwin, Chairman

Committee members:

Dr. JoAnn Browning

Dr. Caroline Bennett

Date Approved: _____

ABSTRACT

The bond strength of ASTM A 1035 Grade 100 deformed reinforcing steel is evaluated relative to the values predicted using the development expressions in ACI 318-05 and ACI 408R-03. A total of 69 large-scale beam-splice specimens were tested at the University of Kansas, North Carolina State University, and the University of Texas at Austin, of which 64 failed in bond. Specimens contained bottom-cast lap-splices of No. 5, No. 8, and No. 11 Grade 100 reinforcement and were tested in four-point bending to provide a constant moment over the length of the splices. Parameters known to effect bond strength that were varied between specimens include the splice length, bar size, concrete covers and spacing, concrete compressive strength, and the amount of confining transverse reinforcement.

Lap splices developed bar stresses varying from 68 ksi to 155 ksi prior to splitting bond failure. Analysis of the results indicates that the ACI 318-05 development expression is unconservative. The inclusion of a high strength reinforcement factor $\psi_h = 1.48$ is recommended for use with Grade 100 steel above 80 ksi bar stress. The ACI 408R-03 development expression with $\phi = 0.82$ is conservative for use with Grade 100 steel. Both development expressions underestimate the contribution to bond strength of confining transverse reinforcement.

Keywords: ASTM A 1035; bond; confinement; deformed reinforcement; development; Grade 100; lap connections; reinforced concrete; splice; structural engineering.

ACKNOWLEDGEMENTS

The project was made possible due to the funding of MMFX Technologies, Inc. Additional support was provided by the Dayton Superior Corporation; W.R. Grace and Co.; the University of Kansas Department of Civil, Environmental, and Architectural Engineering; LRM Industries; Builder's Steel; and the Kansas Department of Transportation.

I am eternally grateful for Drs. David Darwin and JoAnn Browning taking me on as a research assistant and allowing me the pleasure of working with them both. The guidance and insight provided were priceless and will undoubtedly continue to be so in ways I cannot yet imagine.

I would like to thank Shelby Miller for her teamwork, dedication, and ingenuity. We both definitely had (and still have) a lot to learn, but working with you was a pleasure and vital to the success of our little endeavor.

The assistance and expertise of those who helped us get the job done was invaluable. I would like to offer a very special thanks to Jim Weaver, Matt Maksimowicz, Jay Bernard, our hourly employees, and any of our fellow grad students that we could sweet-talk into helping with pours and tests. This project literally could not have been done without their help.

The accomplishments of our counterparts at North Carolina State University and the University of Texas at Austin are greatly appreciated. Their hard work not only taught Shelby and I valuable lessons but also provided a great amount of additional data and observations for our work.

Finally, I would like to thank my family for their support, both financial and emotional, and allowing me to pursue whatever course my heart chose in life. Also, thanks for reading to me as a child and encouraging me to do likewise. I think I will be reaping the benefits of that for the many years yet to come.

TABLE OF CONTENTS

ABSTRACT.....	iii
ACKNOWLEDGEMENTS.....	iv
TABLE OF CONTENTS.....	v
LIST OF TABLES.....	vii
LIST OF FIGURES.....	viii
CHAPTER 1: INTRODUCTION.....	1
1.1 General.....	1
1.2 Previous Work.....	2
1.3 Discussion.....	3
1.4 Objective and Scope.....	11
CHAPTER 2: BEAM-SPLICE TESTS.....	13
2.1 General.....	13
2.2 Test Specimens.....	15
2.3 Materials.....	21
2.4 Specimen Fabrication.....	25
2.5 Test Setup and Procedure.....	29
2.6 Calculation of Bar Stress.....	32
CHAPTER 3: RESULTS AND OBSERVATIONS.....	34
3.1 General.....	34
3.2 Behavior and Observations.....	37
3.3 Load-Deflection.....	37
3.4 Cracking.....	38
3.5 Evaluation of Development Expressions.....	42
CHAPTER 4: CONCLUSIONS AND RECOMMENDATIONS.....	57
4.1 Summary.....	57
4.2 Conclusions and Recommendations.....	57
4.3 Suggestions for Future Study.....	59
REFERENCES.....	60

APPENDIX A: MATERIAL PROPERTIES	63
APPENDIX B: DETAILS OF TEST RESULTS	64
B.1 Series 1 Specimens	66
B.2 Series 2 Specimens	69
B.3 Series 3 Specimens	72
B.4 Series 4 Specimens	80
B.5 Series 5 Specimens	88

LIST OF TABLES

Table 2.1 – Matrix of test specimens from all schools	15
Table 2.2 – Matrix of KU test specimens	16
Table 2.3 – Flexural design details and beam dimensions for KU specimens	17
Table 2.4 – Splice, cover, and shear design details for KU specimens	20
Table 3.1 – Splice parameters and bar stress at failure for KU specimens.....	34
Table 3.2 – Bar stress and total load in KU specimens at splitting	42
Table 3.3 – Test and predicted failure stresses for unconfined KU specimens	44
Table 3.4 – Test and predicted bar stresses at failure for unconfined specimens	45
Table 3.5 – Test and predicted failure stresses for confined KU specimens	47
Table 3.6 – Test and predicted bar stresses at failure for confined specimens	48
Table A.1 – Nominal concrete mix designs.....	63
Table A.2 – Aggregate properties.....	63
Table A.3 – High range water-reducing admixture properties	63
Table A.4 – MMFX Grade 100 reinforcement deformation properties.....	63
Table B.1 – Applied loads and moments and bar stresses at splice failure for KU specimens.....	64
Table B.2 – KU beam-splice specimen details in the ACI 408 Database format.....	65
Table B.3 – Splice-end flexural crack widths at bar stresses bounding 40 and 67 ksi	66

LIST OF FIGURES

Figure 1.1 – Modes of bond failure: (a) local concrete crushing or shear cracking in a pullout failure and (b) splitting crack planes [adapted from ACI 408R-03]	4
Figure 2.1 – Sample notation for a beam-splice specimen	14
Figure 2.2 – Elevation view of typical specimen in test setup.....	18
Figure 2.3 – Cross-sections of the splice region for all specimen types, as tested	19
Figure 2.4 – Photograph of No. 5, 8, and 11 MFX Grade 100 reinforcing steel.....	22
Figure 2.5 – Stress-strain curves for Grade 60 and 100 steels.....	23
Figure 2.6 – Stress-strain curves for 5 and 8 ksi concrete	25
Figure 2.7 – Schematic of the test setup	30
Figure 2.8 – Moment-curvature and strength analysis [after Nawy (2003)]	32
Figure 3.1 – Average strain gage bar stress for Group 5A specimens.....	35
Figure 3.2 – Average strain gage bar stress for Group 5B specimens	36
Figure 3.3 – Load-deflection behavior for specimens in Group 3B	38
Figure 3.4 – Mean and 90% upper-bound regression lines for maximum flexural crack widths in KU beam-splice specimens at bar stresses bounding 40 and 67 ksi	40
Figure 3.5 – Splitting cracks on specimen 8-8-XC1-2.5 at 56 kips total load.....	41
Figure 3.6 – Test-to-prediction ratios for unconfined specimens from all schools	46
Figure 3.7 – Test-to-prediction ratios for confined specimens from all schools	49
Figure 3.8 – Eq. (1.1) T/P scatterplot with the limit of Eq. (1.2) applied.....	50
Figure 3.9 – Eq. (1.1) T/P scatterplot without the limit of Eq. (1.2) applied.....	51
Figure 3.10 – Performance of Eq. (3.1) with $\psi_h = 1.48$	54
Figure 3.11 – Performance of Eq. (1.3) with $\phi = 0.82$	56
Figure B.1 – Specimen 5-5-XC0-3/4 showing the "dog-bone" reduced section	67
Figure B.2 – Load-deflection behavior of Series 1 beam-splice specimens.....	68
Figure B.3 – Specimen 5-5-OC0-3/4 at the conclusion of the test.....	69
Figure B.4 – Specimen 5-5-XC0-3/4 at the conclusion of the test.....	70
Figure B.5 – Load-deflection behavior of Series 2 beam-splice specimens.....	71

Figure B.6 – Specimen 5-5-XC0-2d _b after testing, as viewed from above.....	72
Figure B.7 – Specimen 5-5-XC0-2d _b at the conclusion of the test.....	73
Figure B.8 – Load-deflection behavior of Group 3A beam-splice specimens	74
Figure B.9 – Specimen 8-5-OC0-1.5 at the conclusion of the test	74
Figure B.10 – Specimen 8-5-OC1-1.5 at the conclusion of the test	75
Figure B.11 – Specimen 8-5-OC2-1.5 at the conclusion of the test	76
Figure B.12 – Load-deflection behavior of Group 3B beam-splice specimens.....	77
Figure B.13 – Specimen 8-5-XC0-1.5 at the conclusion of the test	77
Figure B.14 – Specimen 8-5-XC1-1.5 at the conclusion of the test	78
Figure B.15 – Specimen 8-5-XC2-1.5 at the conclusion of the test	79
Figure B.16 – Measured bar stress for specimen 8-5-XC2-1.5	80
Figure B.17 – Load-deflection behavior of Group 4A beam-splice specimens	81
Figure B.18 – Specimen 8-8-OC0-2.5 at the conclusion of the test	82
Figure B.19 – Specimen 8-8-OC1-2.5 at the conclusion of the test	82
Figure B.20 – Measured bar stress for specimen 8-8-OC1-2.5	83
Figure B.21 – Specimen 8-8-OC2-2.5 at the conclusion of the test	84
Figure B.22 – Load-deflection behavior of Group 4B beam-splice specimens.....	84
Figure B.23 – Specimen 8-8-XC0-2.5 at the conclusion of the test	85
Figure B.24 – Specimen 8-8-XC1-2.5 at the conclusion of the test	86
Figure B.25 – Specimen 8-8-XC2-2.5 at the conclusion of the test	86
Figure B.26 – External stirrups used to confine specimen 8-8-XC2-2.5.....	87
Figure B.27 – Load-deflection behavior of Group 5A beam-splice specimens	88
Figure B.28 – Specimen 11-8-OC0-2 at the conclusion of the test	89
Figure B.29 – Measured bar stress for specimen 11-8-OC0-2	90
Figure B.30 – Specimen 11-8-OC1-2 after testing, as viewed from above.....	90
Figure B.31 – Measured bar stress for specimen 11-8-OC1-2	91
Figure B.32 – Specimen 11-8-OC2-2 at the conclusion of the test	92
Figure B.33 – Measured bar stress for specimen 11-8-OC2-2	92
Figure B.34 – Load-deflection behavior of Group 5B beam-splice specimens.....	93

Figure B.35 – Specimen 11-8-XC0-2 at the conclusion of the test	94
Figure B.36 – Measured bar stress for specimen 11-8-XC0-2	94
Figure B.37 – Specimen 11-8-XC1-2 at the conclusion of the test	95
Figure B.38 – Measured bar stress for specimen 11-8-XC1-2	96
Figure B.39 – Specimen 11-8-XC2-2 at the conclusion of the test	96
Figure B.40 – Measured bar stress for specimen 11-8-XC2-2	97

CHAPTER 1: INTRODUCTION

1.1 GENERAL

Reinforced concrete structural members depend on the transmission of force from the concrete to the steel reinforcing bars embedded within the member. Force transfer at the interface between the two materials enables the two materials to work in unison to resist loads. This bond force is provided between the steel reinforcement and surrounding concrete by chemical adhesion, friction, and mechanical interlock. Mechanical interlock is provided by bearing of the ribs on a bar on the surrounding concrete in the plane transverse to its longitudinal axis. Smooth bars achieve bond through only adhesion and friction, while deformed bars benefit from mechanical interlock and typically exhibit greater bond strength than a smooth bar of the same size.

The bond strength of a particular reinforcing configuration refers to the amount of force carried in the reinforcing bar that would cause a bond failure. While bond failure is typically not a concern for bars that run continuously through a member, reinforcing bars must be developed where the bars are terminated. Additionally, splices are needed in most structures due to the limited number of available bar lengths. The force carried at any point along a bar must be developed over the bar length to the free end for both splices and bar terminations. For this reason, design provisions for bond strength, such as those contained in the ACI 318-05 building code, are typically presented in terms of a minimum development length that must be present on either side of points of maximum bar stress. Providing an insufficient development or splice length or applying loads that result in bar forces that exceed the bond strength may cause a reinforced concrete member to fail, potentially leading to a total structural failure.

The work reported here is a portion of a joint research program completed at the University of Kansas (KU), North Carolina State University (NCSU), and the University of Texas at Austin (UT) to study the bond performance of ASTM A 1035 Grade 100 steel reinforcing bars. Twenty-two large scale beam-splice tests were

performed at each school. Grade 100 reinforcement differs from most conventional reinforcing steel in that it can develop higher stresses and it has a roundhouse stress-strain curve, while most lower strength bars exhibit a distinct yield plateau followed by strain hardening. Limited studies of bond behavior of Grade 100 steel using beam-splice specimens have shown disparity in some conclusions. Peterfreund (2003) concluded that the development length can be safely calculated using the provisions in ACI 318-02 at a design stress of 120 ksi, while El-Hacha, El-Agroudy, and Rizkalla (2006) recommended the use of a development length modification factor for bar stresses above 80 ksi. Disagreement between the results and the limited number and scope of the earlier tests indicate that further study, with a broader range of parameters, is required prior to the widespread use of Grade 100 steel with the current design provisions.

The current study focuses on the parameters of splice length, bar size, concrete strength, concrete cover, and quantity of confining reinforcement. Results from the specimens tested at KU, combined with those from NCSU and UT, are used to evaluate the accuracy and margin of safety of the development length criteria used in ACI 318-05 and proposed by ACI Committee 408 in ACI 408R-03 for use with Grade 100 reinforcing steel. An upper-bound limit on the contribution of development length to bond strength is also investigated.

1.2 PREVIOUS WORK

The first beam-splice bond testing of Grade 100 reinforcing steel was performed by Ansley (2002). Four pairs of beams were tested to compare the structural performance of members constructed using Grade 100 tension reinforcement to that of members using Grade 60: one pair with continuous tension steel, two pairs of lap-spliced specimens with differing splice lengths, and one pair of beams for use in a shear test with Grade 100 stirrups. Ansley found the load-deflection behavior of splice specimens to be nearly identical to those with continuous reinforcement up to the failure of the splice. Beyond bar stresses at which

the Grade 60 steel had yielded, the corresponding beam using Grade 100 steel failed at a greater load, but a smaller overall beam deflection.

Peterfreund (2003) examined the use of Grade 100 reinforcing steel in bridge deck applications. Two sets of three beam-splice specimens were tested, one set with No. 4 bars and the other with No. 5, all with different splice lengths. Non-contact lap-splices were used at midspan in all specimens on the two tension bars in each specimen. Strain gages were spaced evenly along the length of both bars in one of the two splices. Peterfreund reported that the development length provisions in ACI 318-02 could be safely used for Grade 100 steel at a design yield stress of 120 ksi, as defined using the 0.2% offset method.

El-Hacha et al. (2006) examined the applicability of the development length provisions in ACI 318-02 and an expression proposed by Zuo and Darwin (2000) to the splice strength of Grade 100 bars. Four pairs of beam-splice specimens were tested, each containing one beam with two spliced No. 6 bars unconfined by transverse reinforcement, and one beam with a single spliced No. 8 bar confined by transverse reinforcement. El-Hacha et al. reported that both the ACI 318-02 and Zuo and Darwin development length expressions became unconservative above 80 ksi. Modified versions of both expressions were proposed for use above bar stresses of 80 ksi, although further testing was recommended due to the limited amount of data.

1.3 DISCUSSION

1.3.1 Bond Behavior

Bond is the force transferred between the concrete and the reinforcing steel embedded within a member, and occurs due to chemical adhesion, friction, and mechanical anchorage. Chemical adhesion occurs along all surfaces of the bar, but is lost after initial movement of the bar relative to the surrounding concrete, termed bar slip. Coincident with initial bar slip, friction forces engage along both the barrel of the bar and on the bearing faces of the bar deformations. Mechanical anchorage is established by bearing of the bar deformations against the concrete surface along the embedded bar and is characterized by the forces required to split the surrounding

concrete plus those mobilized in any confining transverse reinforcement. Mechanical anchorage generally provides the greatest contribution to bond force for deformed reinforcing bars.

The bond strength of an embedded reinforcing bar refers to the maximum bar force able to be sustained by the concrete surrounding the bar in question. Failure can occur by (1) either shearing or crushing the concrete at the interface between the two materials, resulting in a pullout-type failure, or (2) the bar deformations wedging through the concrete causing hoop tensile stresses around the bar, sufficient to crack the surrounding concrete, thus releasing the confinement and causing a splitting failure. Concrete crushing and cracking that occur during bond failure are shown in Figure 1.1.

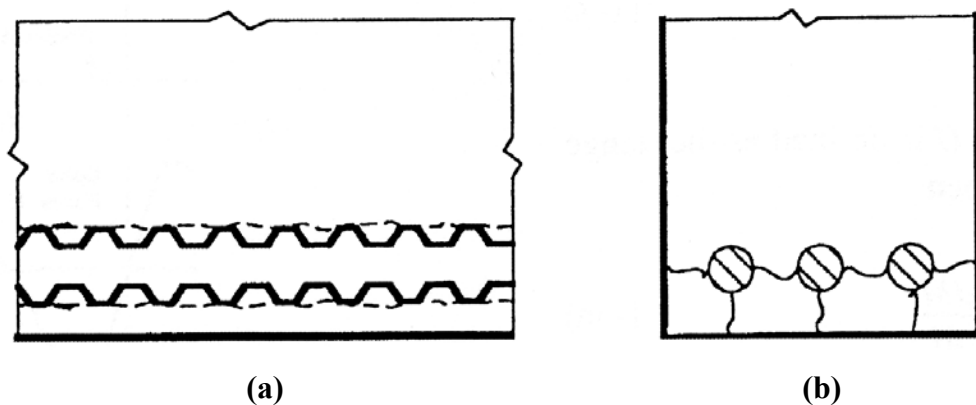


Figure 1.1 – Modes of bond failure: (a) local concrete crushing or shear cracking in a pullout failure and (b) splitting crack planes [adapted from ACI 408R-03]

Bond strength is commonly represented as the total force carried in the reinforcement at bond failure. In design, this is handled by calculating the minimum bonded length required to adequately develop the design bar force or stress. ACI 408R-03 represents the total bond strength as the sum of two resistance forces: T_c , the contribution from the surrounding plain concrete, and T_s , the additional contribution from confining transverse steel placed around the developed or spliced

bar. Both of these factors are a function of numerous parameters related to the member geometry, concrete properties, and the reinforcement itself.

Parameters known to affect bond strength examined in this study include the bonded length, bar size, concrete compressive strength, concrete clear cover and spacing, and the amount of confining transverse reinforcement. Other factors have been identified that affect bond strength, but are generally constant for the specimens tested in this study, and are not discussed here. A detailed discussion of bond behavior is provided in ACI 408R-03.

Increasing the bonded length of the reinforcing bar from the point of interest to the nearest free end will result in increased bond capacity. Although the relationship between bond force and bonded length is nearly linear, it is not proportional given the non-uniform distribution of bond forces along the bonded length.

For a given bonded length and cover to the center of the bar, greater force is required to cause bond failure for a larger bar than a smaller. As the bar size increases, however, bar area increases more quickly than the bond force at failure. Thus, in terms of bar stress, bond strength decreases with increasing bar size. Design equations typically express bond strength in terms of bar stress and diameter.

Increases in concrete compressive strength result in increased bond strengths. The contribution of concrete properties has customarily been represented in most expressions as the square root of the concrete compressive strength $\sqrt{f'_c}$. Darwin, Tholen, Idun, and Zuo (1996a), however, reported that the quarter power of concrete compressive strength $f'_c{}^{1/4}$ provides a more accurate measure of the contribution of concrete strength, especially for $\sqrt{f'_c}$ above 8000 psi, where the square root becomes increasingly unconservative by overestimating the concrete contribution. ACI 318-05 recognizes this limitation by capping the concrete strength that can be used to calculate development length at 10,000 psi when still using $\sqrt{f'_c}$. Zuo and Darwin (1998, 2000) reaffirmed the use of $f'_c{}^{1/4}$ with significant increases in the number of

tests using high-strength concrete, but also noted that use of the quarter power underestimates the contribution of concrete to the additional bond strength provided by confining transverse reinforcement, and found that the use of $f_c^{3/4}$ adequately represents this effect.

The amount of concrete surrounding developed bars, as represented by cover and bar spacing, affects the mode of bond failure, with pullout failures possible for large values of cover and bar spacing. Splitting failures will generally control for smaller values of cover and bar spacing, which results in lower bond strengths. Splitting failures occur along planes through the exterior layer of reinforcement or normal to that layer at each bar location, as shown in Figure 1.1b. For typical member geometry and vertical load application, these planes are horizontal and vertical.

Cover and bar spacing parameters also exert a secondary influence on bond strength. While the minimum cover or spacing determines the weakest splitting plane and thus the location of failure, the relative ratio of the maximum to the minimum cover or spacing value based on whether clear cover or clear spacing controls (c_{max}/c_{min}) also influences the bond strength. Greater bond strengths are observed in specimens where the lesser of side cover and half the clear spacing is not equal to the cover to the tension face than in those where both of these dimensions are equivalent.

Transverse reinforcement impedes the growth of splitting cracks by resisting the hoop tensile stresses that cause them, thereby confining the concrete around the developed bar and increasing bond strength. ACI 408R-03 describes the contribution of transverse reinforcement T_s as a function of the deformation properties of the developed bar, total area of transverse reinforcement crossing the splitting plane in question, and the concrete compressive strength.

Transverse confining reinforcement and concrete cover collectively control the failure mode of the developed or spliced bar. If the resistance to splitting in the weakest splitting plane is sufficient to cause a pullout failure, increases in concrete cover and transverse reinforcement will not further increase bond strength. The

effective contribution of the cover and confinement parameters is thus limited in most descriptive and design expressions. The combination of these parameters is typically grouped in a collective confinement term, above a certain value of which pullout failure is expected to govern.

1.3.2 ACI 318-05 Development Expression

The design provisions in ACI 318-05 are based upon expressions developed by Orangun, Jirsa, and Breen (1975, 1977). The equation for bond strength of deformed straight reinforcing bars in tension contained is expressed in terms of the bonded length required to develop the full yield strength of the reinforcing bar. Rearranging Eq. (12-1) from ACI 318-05 in terms of bar stress and eliminating the terms for bar location, epoxy-coated bars, and lightweight concrete, as they were not applicable to the current study, results in Eq. (1.1), while the corresponding confinement term limit is presented in Eq. (1.2).

$$f_s = \frac{40}{3} \times \frac{\ell_s}{d_b} \times \frac{\sqrt{f'_c}}{\psi_s} \times \left(\frac{c + K_{tr}}{d_b} \right) \quad (1.1)$$

$$K_{tr} = \frac{A_{tr} f_{yt}}{1500sn} \quad (1.1a)$$

$$c = c_{min} + 0.5d_b \quad (1.1b)$$

$$c_{min} = \text{minimum}(c_b, c_s) \quad (1.1c)$$

$$c_s = \text{minimum}(c_{so}, c_{si}) \quad (1.1d)$$

$$\left(\frac{c + K_{tr}}{d_b} \right) \leq 2.5 \quad (1.2)$$

where

A_{tr} = total area of all transverse reinforcement within spacing s crossing the plane of splitting adjacent to the reinforcement being developed (in.²)

c = minimum cover or spacing dimension measured to the center of the bar (in.)

- c_{min} = minimum clear cover or clear spacing dimension (in.)
 c_s = minimum side cover or clear spacing dimension (in.)
 c_{si} = half the clear bar spacing (in.)
 c_{so} = side concrete cover for the reinforcing bar being developed (in.)
 d_b = notional bar diameter calculated on the nominal bar area (in.)
 f'_c = concrete compressive strength based on 6 x 12 in. cylinders (psi)
 = specified concrete compressive strength for member design (psi)
 f_s = stress in reinforcing bar being developed (psi)
 f_{yt} = yield stress of stirrups or ties used as confining transverse reinforcement
 adjacent to the reinforcement being developed (psi)
 K_{tr} = transverse reinforcement index
 ℓ_s = splice/development length (in.)
 n = number of bars being developed in the splitting plane (ea.)
 N_s = number of stirrups or ties providing transverse confinement in the plane of
 splitting adjacent to the reinforcement being developed (ea.)
 s = center-to-center spacing of transverse reinforcement (in.) = $\frac{\ell_s}{N_s}$
 ψ_s = reinforcement size factor, 0.8 for bars No. 6 and smaller, otherwise 1.0

The work of Orangun et al. was first incorporated into the ACI Building Code in ACI 318-89, but simplified into the version presented as Eq. (1.1) in the 1995 edition of the code. Equation (1.1) is based upon the assumption of two separate contributions to total bond strength, T_c and T_s , discussed in Section 1.3.1.

1.3.3 ACI 408R-03 Development Expression

Ongoing research has greatly expanded the number and variety of test data available for study in the field of bond and development since the work performed by Orangun et al. (1975, 1977). ACI Committee 408 on the Bond and Development of Reinforcement reviewed and analyzed the available data and expressions characterizing bond strength and recommended an expression for the development of

straight reinforcing bars in tension in ACI 408R-03, rearranged in terms of bar stress as Eq. (1.3). As in Eq. (1.1), the terms representing the effects of bar position, epoxy coating, and lightweight concrete have been removed as they are not applicable to the current study. Equation (1.4) displays the upper limit on the confinement term.

$$f_s = \phi \left[76.3 \frac{\ell_s}{d_b} \left(\frac{c\omega + K_{tr}}{d_b} \right) + 2400\omega \right] f_c'^{1/4} \quad (1.3)$$

$$K_{tr} = \left(\frac{0.52t_r t_d A_{tr}}{sn} \right) f_c'^{1/2} \quad (1.3a)$$

$$t_r = 9.6R_r + 0.28 \leq 1.72 \quad (1.3b)$$

$$t_d = 0.78d_b + 0.22 \quad (1.3c)$$

$$\omega = \left(0.1 \frac{c_{max}}{c_{min}} + 0.9 \right) \leq 1.25 \quad (1.3d)$$

$$c_{max} = \text{maximum}(c_b, c_s) \quad (1.3e)$$

$$c_s = \text{minimum}(c_{so}, c_{si} + 0.25) \quad (1.3f)$$

$$\left(\frac{c\omega + K_{tr}}{d_b} \right) \leq 4.0 \quad (1.4)$$

where

c_{max} = greater of the bottom cover and the lesser of the side cover or clear spacing dimensions (in.)

R_r = relative rib area of the bar being developed

t_d = term representing the effect of bar size on the transverse confinement contribution to bond strength (in.)

t_r = term representing the effect of relative rib area on the transverse confinement contribution to bond strength

- ϕ = strength reduction factor, evaluated at both 1.00 for best-fit analysis and 0.82 for the load and ϕ factors used in ACI 318-05
- ω = term representing the effect of the side cover or clear spacing to bottom cover ratio

Equation (1.1b) and (1.1c) are used to calculate terms in Eq. (1.3). The conflicting definitions of c_s and K_r should be noted between Eq. (1.1) and (1.3), and the appropriate equations used accordingly.

When adopted by ACI Committee 408, Eq. (1.3) was modified slightly from its original form as formulated by Zuo and Darwin (1998, 2000). An equation of this form has been continually updated through additional research and analyses by Darwin et al. (1992, 1996a, 1998), and is a modified version of the original equation presented by Orangun et al. (1975, 1977). The expression maintains the basic assumption that total bond force equals the summation of concrete and confining steel contributions, T_c and T_s , respectively. The key differences from Eq. (1.1) recognized by Eq. (1.3) are the use of $f_c'^{1/4}$ for T_c , $f_c'^{3/4}$ for T_s , and the incorporation of the cover ratio ω , relative rib area R_r , and reliability-based strength reduction factor ϕ . Additionally, Eq. (1.1) was based upon an original analysis of 62 specimens with minimal variation in concrete compressive strength. Equation (1.3) was developed using a database of 416 specimens (Zuo and Darwin 1998) and recalibrated using ACI Committee 408 Database 10-2001 of 478 (ACI 408R-03) bottom-cast beam-splice test results. ACI 408R-03 reports that Eq. (1.3) offers effectively unbiased predictions of bond strength for the parameters included in the equation, while Eq. (1.1) becomes increasingly inaccurate and unconservative when evaluated at high concrete compressive strengths, bar stresses, and bonded lengths.

1.3.4 ASTM A 1035 Grade 100 Reinforcing Steel

ASTM first approved a standard specification for Grade 100 reinforcing steel in 2004. The deformed low-carbon chromium steel reinforcing bars have a specified minimum yield strength of 100 ksi according to ASTM A 1035-06. El-Hacha et al.

(2006), however, reported that the bars may reach a yield strength of 115 to 120 ksi using the 0.2% offset method. ASTM A 1035 also requires a minimum tensile strength of 150 ksi and 7% elongation at failure for bar sizes of No. 3 through No. 11. The stress-strain behavior of Grade 100 steel is characterized by a roundhouse curve that lacks a definitive yield plateau.

ASTM A 1035 steel contains between 8.0 and 10.9% chromium by weight; a maximum of 1.5% manganese, 0.50% silicon, 0.15% carbon; and trace quantities of nitrogen, sulfur, and phosphorous. Aside from the high yield strength, the alloying causes the steel to have enhanced corrosion resistance properties, including an increased corrosion chloride threshold and a lower rate of corrosion than conventional ASTM A 615 reinforcing steel. This combination of attributes creates an attractive structural material due to potential material and life-cycle cost savings.

1.4 OBJECTIVE AND SCOPE

The objective of this study is to evaluate the accuracy and applicability of expressions recommended by ACI 318-05 and ACI 408R-03 for use in predicting the bond strength of deformed straight ASTM A 1035 Grade 100 reinforcing bars in tension. The study is part of a joint research program conducted at KU, NCSU, and UT.

The experimental work performed at KU involves 22 large-scale beam-splice tests with No. 5, No. 8 and No. 11 Grade 100 tension reinforcement. A total of 69 beam-splice specimens were tested at the three schools. Parameters investigated include splice length, bar size, concrete strength, concrete cover, and quantity of confining transverse reinforcement. Target concrete compressive strengths were 5,000 and 8,000 psi. Test specimens containing splices not confined by transverse reinforcement were designed to fail at bar stresses of 80 and 100 ksi, while confined splice specimens were designed to fail at stresses 20 and 40 ksi higher than the matching unconfined specimens.

Based upon the beam-splice test results from the joint study, recommendations are made regarding the use and applicability of the development length expressions found in ACI 318-05 and ACI 408R-03 with Grade 100 steel.

CHAPTER 2: BEAM-SPLICE TESTS

2.1 GENERAL

The contents of this chapter are adapted from Miller (2007) and Briggs et al. (2007).

2.1.1 Experimental Program

As recommended by ACI Committee 408 (2003), beam-splice specimens were used to study the bond behavior of the reinforcing steel. Splice lengths, confining transverse reinforcement, concrete properties, and cover dimensions were selected to achieve a bond failure within the splice at stress levels in the tension steel of 80, 100, 120, or 140 ksi as predicted using Eq. (1.3).

Of the 69 beams tested in the study, 22 specimens were tested at the University of Kansas (KU) with the following parameters:

No. 5 bars:

¾-in. and $2d_b$ cover

18, 25, 32, and 43 in. splice lengths, ℓ_s

5000 psi target concrete compressive strength, f'_c

All splices unconfined

No. 8 bars:

1½-in. and 2½-in. cover

27, 36, 47, and 63 in. splice lengths, ℓ_s

5000 and 8000 psi target concrete compressive strength, f'_c

0, 2, 4, 5, and 8 No. 4 bar stirrups confining the splice

No. 11 bars:

2-in. cover

58 and 79 in. splice lengths, ℓ_s

8000 psi target concrete compressive strength, f'_c

0, 4, and 9 No. 4 bar stirrups confining the splice

2.1.2 Notation

Test specimens are identified using a notation system common to the three universities. The notation designates the size of the spliced bars, the concrete compressive strength in ksi, the bar stress level for splices without confining steel, the level of confinement, and the concrete clear cover. Beams were designed in groupings of six with identical cover, dimensions, and span lengths. The beams in a series differ in terms of splice length (two lengths were used) and level of confinement (three levels were used). Beams are identified as shown in Figure 2.1.

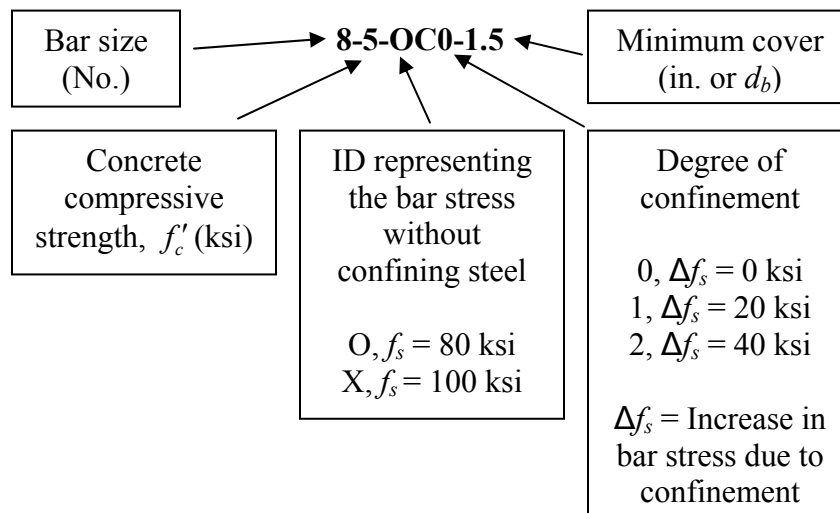


Figure 2.1 – Sample notation for a beam-splice specimen

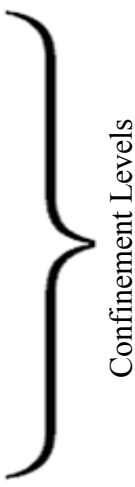
2.1.3 Collective Test Program

Each school was responsible for three series of specimens plus two sets of two beams from a series for which another university had primary responsibility. Table 2.1 summarizes the test program. Duplicate beams are shown in bold. The test specimens include those from the original program of 66 beams plus three extra specimens tested at UT for the purpose of evaluating the effect of concrete compressive strength. These specimens are duplicates of specimen 8-8-OC_-1.5 at the 0, 1, and 2 levels of confinement, but were cast with 5 ksi concrete instead of 8 ksi concrete. To avoid confusion with specimens already titled 8-5-OC_-1.5, which

have a different splice length, these three additional specimens are designated as 8-5-SC_-1.5, in which ‘S’ denotes a “special” design bar stress without confining steel.

Table 2.1 – Matrix of test specimens from all schools

f'_c (ksi)	d_b (No.)	Cover (in.)	KU		NCSU		UT*	
			O**	X**	O	X	O	X
5	5	3/4	0	0			0	0
		2d _b	0	0			0	0
		3d _b					0	0
	8	1.5	0,1,2	0,1,2			0,2	0,2
		2.5			0,1,2	0,1,2		
	11	2			0,1,2	0,1,2		
		3					0,1,2	0,1,2
8	8	1.5			0,2	0,2	0,1,2	0,1,2
		2.5	0,1,2	0,1,2				
	11	2	0,1,2	0,1,2				
		3			0,1,2	0,1,2		
Total Specimens			22		22		22	



Confinement Levels

*Does not show UT specimens 8-5-SC0-1.5, 8-5-SC1-1.5, and 8-5-SC2-1.5

**ID representing the bar stress without confining transverse steel

2.2 TEST SPECIMENS

2.2.1 General

Five series of specimens were constructed and tested at KU, as shown in Table 2.2. Series 1 and 2 are duplicates of beams tested at UT, while Series 3, 4, and 5 are complete sets of six. The series are split into groups according to splice length; ‘A’ denotes the shorter of the two splice lengths (and lower bar stress at splice failure), while ‘B’ is the longer (with the higher bar stress at splice failure).

The test specimens were designed as typical reinforced concrete beams subjected to four-point loading to provide a constant moment region in the middle portion of the member, the location of the splice. The absence of shear in the central portion of the beam eliminates the need for shear reinforcement around the splices, allowing transverse reinforcement to be used solely as confinement for the splices.

Figure 2.2 displays an elevation of a typical specimen, and cross-sections of the splice region are shown in Figure 2.3.

Table 2.2 – Matrix of KU test specimens

Series	Group	Specimen	Bar Size	Nominal f'_c	Minimum Design Cover, c	Nominal Section, $b \times h$	Splice Length, ℓ_s	Design Stress
			(No.)	(ksi)	(in.)	(in. x in.)	(in.)	(ksi)
1	A	5-5-OC0-3/4	5	5	0.75	14 x 20	32	80
	B	5-5-XC0-3/4					43	100
2	A	5-5-OC0-2d _b	5	5	1.25	35 x 10	18	80
	B	5-5-XC0-2d _b					25	100
3	A	8-5-OC0-1.5	8	5	1.5	14 x 30	47	80
		8-5-OC1-1.5						100
		8-5-OC2-1.5						120
	B	8-5-XC0-1.5					63	100
		8-5-XC1-1.5						120
		8-5-XC2-1.5*						140
4	A	8-8-OC0-2.5	8	8	2.5	14 x 21	27	80
		8-8-OC1-2.5						100
		8-8-OC2-2.5						120
	B	8-8-XC0-2.5					36	100
		8-8-XC1-2.5						120
		8-8-XC2-2.5						140
5	A	11-8-OC0-2	11	8	2	24 x 26	58	80
		11-8-OC1-2						100
		11-8-OC2-2						120
	B	11-8-XC0-2					79	100
		11-8-XC1-2						120
		11-8-XC2-2**						140

*T-beam with $b_f = 28$ in. and $h_f = 7$ in.

**T-beam with $b_f = 38$ in. and $h_f = 7$ in.

The design methods described in the following sections were used for the specimens tested at KU, although the procedures were similar at all three universities.

2.2.2 Flexural Design

The specimens tested at the University of Kansas were designed to achieve a stress in the tension steel of 150 ksi at flexural failure. A strength design approach was used to calculate flexural capacity, using the Whitney stress block to represent

concrete in compression. Values of β_1 from ACI 318-05 were used based upon the nominal concrete compressive strength. Flexural design details are shown in Table 2.3.

Table 2.3 – Flexural design details and beam dimensions for KU specimens

Specimen		Design Beam Dimensions						Longitudinal Reinforcement				
Group	Designation	Support Spacing	Span, L	Width, b	Height, h	Effective Depth, d	Depth to A_s' , d'	Bar Size	Number of Bars, n	Area of Tension Steel, A_s	Area of Compr. Steel, A_s'	Target Bar Stress, f_s
		(ft)	(ft)	(in.)	(in.)	(in.)	(in.)	(No.)	(ea.)	(in. ²)	(in. ²)	(ksi)
1A	5-5-OC0-3/4	7	15	14	21*	18.94	1.81	5	4	1.76	1.76	80
1B	5-5-XC0-3/4	7	15	14	21*	18.94	1.81	5	4	1.76	1.76	100
2A	5-5-OC0-2d _b	7	15	35	10	8.44	1.75	5	4	1.76	0.80	80
2B	5-5-XC0-2d _b	7	15	35	10	8.44	1.75	5	4	1.76	0.80	100
3A	8-5-OC0-1.5	10	21	14	30	28.00	1.75	8	2	1.58	0.40	80
	8-5-OC1-1.5	10	21	14	30	28.00	1.75	8	2	1.58	0.40	100
	8-5-OC2-1.5	10	21	14	30	28.00	1.75	8	2	1.58	0.40	120
3B	8-5-XC0-1.5	10	21	14	30	28.00	1.75	8	2	1.58	0.40	100
	8-5-XC1-1.5	10	21	14	30	28.00	1.75	8	2	1.58	0.40	120
	8-5-XC2-1.5	10	21	28**	30	28.00	2.00	8	2	1.58	3.16	140
4A	8-8-OC0-2.5	10	21	14	21	18.00	2.00	8	2	1.58	1.58	80
	8-8-OC1-2.5	10	21	14	21	18.00	2.00	8	2	1.58	1.58	100
	8-8-OC2-2.5	10	21	14	21	18.00	2.00	8	2	1.58	1.58	120
4B	8-8-XC0-2.5	10	21	14	21	18.00	2.00	8	2	1.58	1.58	100
	8-8-XC1-2.5	10	21	14	21	18.00	2.00	8	2	1.58	1.58	120
	8-8-XC2-2.5	10	21	14	21	18.00	2.00	8	2	1.58	1.58	140
5A	11-8-OC0-2	11	24	24	26	23.50	1.75	11	2	3.12	0.40	80
	11-8-OC1-2	11	24	24	26	23.50	1.75	11	2	3.12	0.40	100
	11-8-OC2-2	11	24	24	26	23.50	1.75	11	2	3.12	0.40	120
5B	11-8-XC0-2	11	24	24	26	23.50	1.75	11	2	3.12	0.40	100
	11-8-XC1-2	11	24	24	26	23.50	1.75	11	2	3.12	0.40	120
	11-8-XC2-2	11	24	38**	26	23.50	1.97	11	2	3.12	3.56	140

*Height of Series 1 specimens was 20 in. for the middle 6 ft. of the beam.

**T-beam flange width, b_f . General beam width b identical to other beams in group.

The specimens in Series 1 and 2 contained four No. 5 bars as tension reinforcement. Specimens in Series 3 and 4 contained two No. 8 bars, while those in Series 5 used two No. 11 bars as tension reinforcement.

All specimens contained longitudinal bars in the compression region to anchor the stirrups used as shear reinforcement and the confining transverse reinforcement. The specimens in Series 1 and 4 were designed using compression steel to provide adequate flexural capacity for the beam, while all other designs, except specimens 8-

5-XC2-1.5 and 11-8-XC2-2, ignored the presence of top steel because the bars were small and not required to provide flexural strength. Specimens in Series 1 and Series 2 contained four No. 5 bars and four No. 4 bars, respectively. Specimens in Series 4 used two No. 8 bars, while specimens in both Series 3 and 5 used two No. 4 bars.

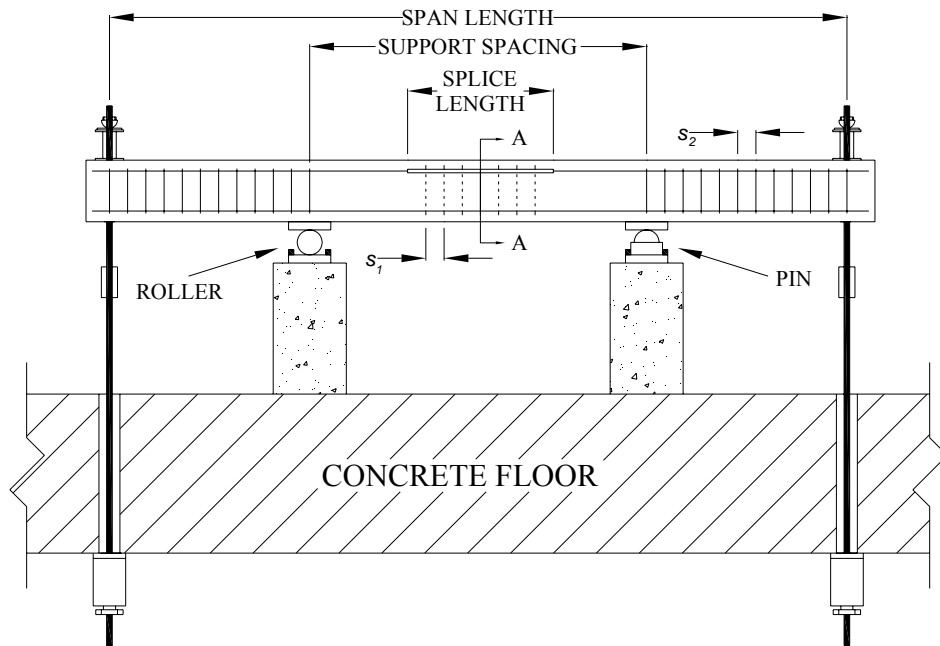
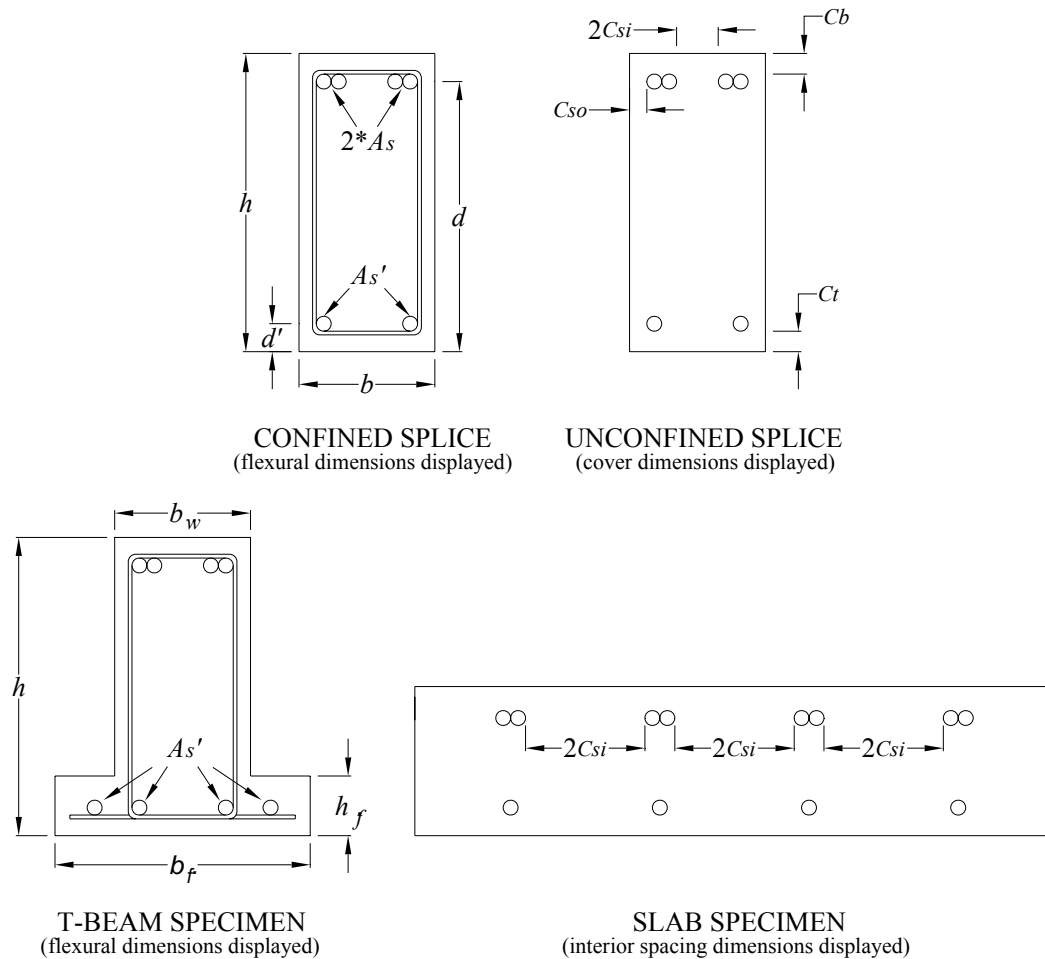


Figure 2.2 – Elevation view of typical specimen in test setup

Early in the testing program, specimen 8-5-XC2-1.5 failed in flexure in the compression region near the support. As a result, both that specimen and 11-8-XC2-2, which were designed to reach stresses of 140 ksi at splice failure, were redesigned as T-beams with additional compression reinforcement to increase their flexural capacity and avoid flexural failures. Specimen 8-8-XC2-2.5, the other beam tested at KU with a predicted bar stress of 140 ksi, had already been cast and failed in bond in the splice region and therefore was not redesigned. The flanges on both T-beam specimens were 14 in. wider than the original web width and 7 in. deep. Specimen 8-5-XC2-1.5 contained four No. 8 bars as compression reinforcement, while specimen 11-8-XC2-2 contained two No. 4 bars and four No. 8 bars. All other properties of the beams remained identical to the matching specimens in the respective series.



SECTION A-A

Figure 2.3 – Cross-sections of the splice region for all specimen types, as tested

2.2.3 Shear Design

Shear reinforcement for the portions of the beams outside of the central constant moment region was designed in accordance with procedures outlined in ACI 318-05. The spacing of closed stirrups s_2 varied between 4 and 5 in, as displayed in Table 2.4. Series 1 through 4 used No. 4 closed stirrups as shear reinforcement, while Series 5 used No. 5 stirrups. The closed stirrups were made from Grade 60 steel fabricated with 135° hooks at one corner. All stirrups used in specimens in Series 1 and 5 were bent at a fabricating shop; some of the stirrups used in Series 2, 3, and 4 were fabricated at KU.

Table 2.4 – Splice, cover, and shear design details for KU specimens

Specimen		Splice Design									Shear Reinforcement	
Group	Designation	Splice Length, ℓ_s (in.)	Bottom Cover, c_b (in.)	Outside Cover, c_{so} (in.)	Half Clear Spacing c_{si} (in.)	No. 4 Stirrups, N_s (ea.)	c/c Tie Spacing, s_l (in.)	Bar Size (No.)	Number of Bars, n (ea.)	Target Bar Stress, f_s (ksi)	Bar Size (No.)	c/c Spacing, s_2 (in.)
1A	5-5-OC0-3/4	32	0.75	1.13	1.13	--	--	5	4	80	4	4
1B	5-5-XC0-3/4	43	0.75	1.13	1.13	--	--	5	4	100	4	4
2A	5-5-OC0-2d _b	18	1.25	3.75	3.75	--	--	5	4	80	4	4
2B	5-5-XC0-2d _b	25	1.25	3.75	3.75	--	--	5	4	100	4	4
3A	8-5-OC0-1.5	47	1.5	1.5	3.5	--	---	8	2	80	4	4.5
	8-5-OC1-1.5	47	1.5	1.5	3.5	4	11 3/4	8	2	100	4	4.5
	8-5-OC2-1.5	47	1.5	1.5	3.5	8	5 7/8	8	2	120	4	4.5
3B	8-5-XC0-1.5	63	1.5	1.5	3.5	--	--	8	2	100	4	4.5
	8-5-XC1-1.5	63	1.5	1.5	3.5	4	15 3/4	8	2	120	4	4.5
	8-5-XC2-1.5	63	1.5	1.5	3.5	8	7 7/8	8	2	140	4	4.5
4A	8-8-OC0-2.5	27	2.5	2.5	2.5	--	--	8	2	80	4	5
	8-8-OC1-2.5	27	2.5	2.5	2.5	2	13 4/8	8	2	100	4	5
	8-8-OC2-2.5	27	2.5	2.5	2.5	5	5 3/8	8	2	120	4	5
4B	8-8-XC0-2.5	36	2.5	2.5	2.5	--	--	8	2	100	4	5
	8-8-XC1-2.5	36	2.5	2.5	2.5	2	18	8	2	120	4	5
	8-8-XC2-2.5	36	2.5	2.5	2.5	5	7 1/4	8	2	140	4	5
5A	11-8-OC0-2	58	2	2	7.18	--	--	11	2	80	5	4.5
	11-8-OC1-2	58	2	2	7.18	4	14 1/2	11	2	100	5	4.5
	11-8-OC2-2	58	2	2	7.18	9	6 1/2	11	2	120	5	4.5
5B	11-8-XC0-2	79	2	2	7.18	--	--	11	2	100	5	4.5
	11-8-XC1-2	79	2	2	7.18	4	19 3/4	11	2	120	5	4.5
	11-8-XC2-2	79	2	2	7.18	9	8 3/4	11	2	140	5	4.5

2.2.4 Splice Design

Specimens were designed with lap splices centered at midspan of the beams. Two splice lengths ℓ_s were selected for each series that, as calculated by Eq. (1.3), would result in bond failure at bar stresses of 80 and 100 ksi if the splices were not confined by transverse reinforcement. These specimens were designated as “OC_” or “XC_” in which “O” denotes the shorter splice length and “X” the longer. Stirrups provided two levels of confinement, “_C1” and “_C2”, designed to increase the bar stress at failure for each splice length by 20 or 40 ksi, respectively. The center-to-center spacing between transverse reinforcement s_l is listed in Table 2.4. The resulting nominal splice strengths are 80, 100, and 120 ksi for specimens OC0, OC1, and OC2, respectively, and 100, 120, and 140 ksi for specimens XC0, XC1, and XC2.

Test specimens containing No. 8 and No. 11 bars were designed to have equal amounts of concrete clear cover on the bottom c_b and sides c_{so} of the spliced bars to help ensure an equal likelihood of failure by bottom or side splitting. The specimens in Series 4 had a clear spacing $2c_{si}$ equal to twice the concrete clear cover, while the specimens in Series 3 and 5 had a clear spacing greater than two times the clear cover. Specimens containing No. 5 bars were designed as slabs and, thus, had clear bar spacings that were greater than twice the bottom cover to simulate typical slab construction. Clear spacing remained twice the side cover. Cover and clear spacing variables are shown in the typical cross-sectional layouts displayed in Figure 2.3, while the values are presented in Table 2.4.

2.2.5 Span Length

All specimens were designed so that the support spacing ensured a distance from either end of the splice to the central supports equal to or greater than the effective depth of the beam d to ensure strain linearity and eliminate shear effects in the splice region in accordance with St. Venant's Principle. The loading span lengths were selected to induce moments causing bar stresses of 150 ksi at appropriately moderate loads. The span lengths were selected in increments of three feet based on the available 3-ft spacing of load points in KU's structural testing laboratory.

2.3 MATERIALS

2.3.1 Reinforcing Steel

ASTM A 1035 Grade 100 reinforcing steel was used as the longitudinal tension reinforcement in the specimens. The stress-strain relationship used for the Grade 100 steel for flexural design was that proposed by Dawood et al. (2004), shown in Eq. (2.1). Glass (2007) performed uniaxial tensile tests on samples of the No. 5, 8 and 11 reinforcement at UT and proposed Eq. (2.2) for No. 5 and 8 bars and (2.3) for No. 11 bars to estimate the stress-strain behavior of the Grade 100 reinforcement, which were used to calculate bar stress when analyzing the test results.

$$f_s = 165(1 - e^{-185\epsilon_s}) \quad (2.1)$$

$$f_s = 156(1 - e^{-220\varepsilon_s}) \quad (2.2)$$

$$f_s = 162(1 - e^{-235\varepsilon_s}) \quad (2.3)$$

where:

f_s = stress in the steel (ksi)

ε_s = strain in the steel

The bar deformation characteristics were measured and the relative rib areas calculated for the Grade 100 bars used in this study. Relative rib area is a measure of the bearing area of deformations on a reinforcing bar normalized to the surface area of that bar between deformations. Relative rib area was measured in accordance with ACI 408.3-01/408.3R-01.

Six-inch digital calipers were used to determine the average width and spacing of the deformations. A knife-edge dial gage spanning two deformations was used to determine the deformation height in five places between the ribs. All measurements were taken on a minimum of five deformations per bar and were accurate to 0.001 in. The relative rib areas were determined to be 0.0767 for No. 5 bars, 0.0838 for No. 8 bars, and 0.0797 for No. 11 bars. The three bars are shown in Figure 2.4.



Figure 2.4 – Photograph of No. 5, 8, and 11 MMFX Grade 100 reinforcing steel

ASTM A 615 Grade 60 steel was used for the remainder of the reinforcement in the specimens including the compression steel, shear stirrups, and confining transverse reinforcement. The Grade 60 steel was not tested, but assumed to follow the bi-linear stress-strain curve recommended by ACI 408R-03 and described by Eq. (2.4). Figure 2.5 plots the stress-strain curves given in Eq. (2.2), (2.3), and (2.4).

$$f_s (\text{ksi}) = \begin{cases} 29000 \times \varepsilon_s & \varepsilon_s \leq 0.00207 \\ 60 & 0.00207 < \varepsilon_s \leq 0.0086 \\ 60 + 614(\varepsilon_s - 0.0086) & \varepsilon_s > 0.0086 \end{cases} \quad (2.4)$$

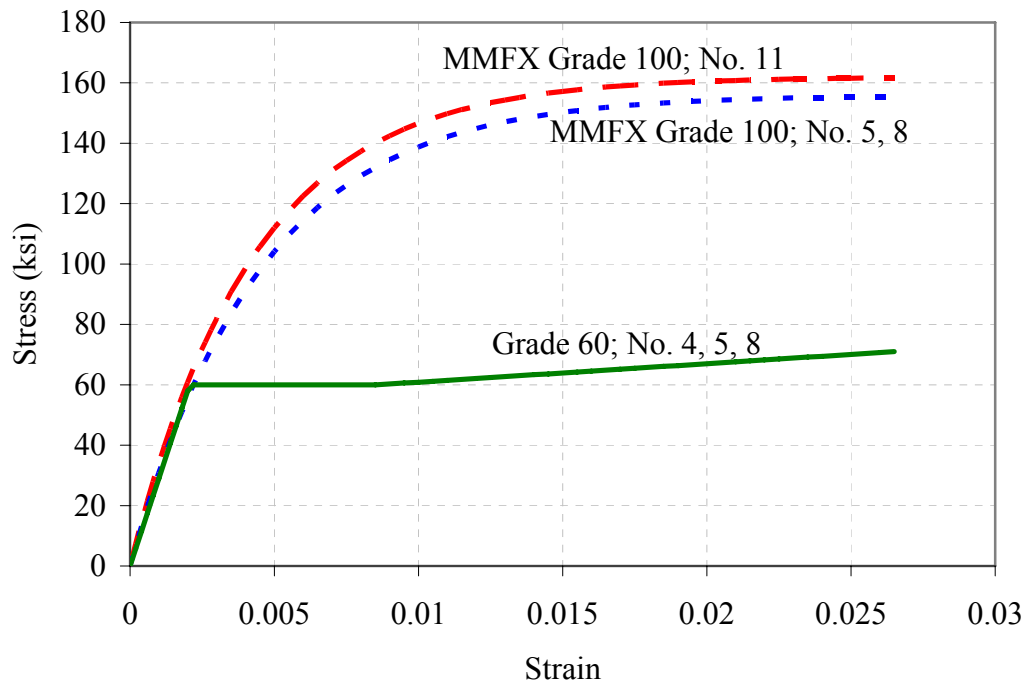


Figure 2.5 – Stress-strain curves for Grade 60 and 100 steels

2.3.2 Concrete

Target concrete compressive strengths of 5 and 8 ksi were selected to represent concrete found in actual construction because mixes with specified strengths of 4 and 6.5 ksi often reach 5 and 8 ksi, respectively. All specimens were cast with normalweight, non-air-entrained concrete consisting of Ash Grove Type I/II

portland cement, water, Kansas River sand, and crushed limestone coarse aggregate with a maximum aggregate size of ¾-in. High-range water-reducing admixtures (HRWRAs) were used in all 8 ksi mixes and as needed in 5 ksi mixes to meet workability targets.

Concrete stress f_c and strain ε_c were estimated using a modified concrete stress-strain relationship developed by Hognestad (1951). The modified Hognestad relationship is listed as Eq. (2.5). Figure 2.6 shows stress-strain curves for 5 and 8 ksi concrete.

$$f_c = \begin{cases} f_c'' \left[2 \left(\frac{\varepsilon_c}{\varepsilon_0} \right) - \left(\frac{\varepsilon_c}{\varepsilon_0} \right)^2 \right] & \text{for } \varepsilon_c \leq \varepsilon_0 \\ f_c'' \left[0.15 \left(\frac{\varepsilon_0 - \varepsilon_c}{\varepsilon_{cu} - \varepsilon_0} \right) + 1 \right] & \text{for } \varepsilon_c \geq \varepsilon_0 \end{cases} \quad (2.5)$$

$$f_c'' = 0.85 f_c' \quad (2.5a)$$

$$\varepsilon_0 = \frac{1.7 f_c'}{E_c} \quad (2.5b)$$

$$E_c = 1.8 \times 10^6 + 460 f_c' \quad (2.5b)$$

where:

f_c = concrete stress

f_c' = concrete compressive strength

f_c'' = peak concrete stress

ε_c = concrete strain

ε_0 = concrete strain at peak stress

ε_{cu} = ultimate concrete strain at crushing = 0.0038

E_c = approximate concrete modulus of elasticity

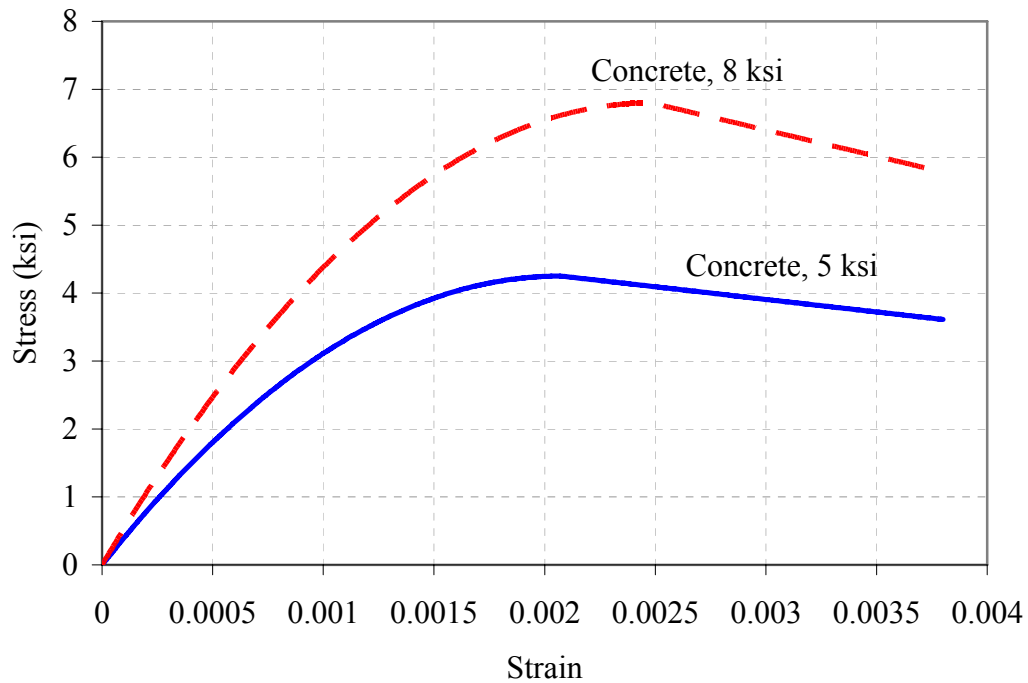


Figure 2.6 – Stress-strain curves for 5 and 8 ksi concrete

2.4 SPECIMEN FABRICATION

2.4.1 Formwork

Specimens were cast in individual forms constructed of $\frac{3}{4}$ -in. plywood and 2x4s. The forms were protected using a multiple-layer polyurethane coating, and mineral oil was used as a release agent for all surfaces exposed to concrete. $\frac{3}{8}$ -in. all-thread low carbon steel rods were used in all specimens, with the exception of the two slab-beams in Series 2, to maintain correct width and transfer lateral force from the fluid concrete pressure to the form stringers. The rods passed through the specimen approximately 6 in. from the compression face of the beam at a spacing of 2 ft center-to-center throughout the entire length of the beam and remained in the concrete during the splice tests.

Because the test apparatus required the load rods to be spaced at 36 in. transversely at the ends of the span, specimens in Series 2 and specimen 11-8-XC2-2, a T-beam, required blockouts to reduce the section width at the loading points to

accommodate the load rods. No longitudinal bars were terminated due to these changes, and adequate cover was maintained for all longitudinal steel.

2.4.2 Reinforcement Cage Details

The beam specimens were constructed 1 ft longer than the design loading span to accommodate the loading apparatus. Longitudinal reinforcement was terminated 1 in. from the end of the specimen to allow for construction tolerances. Shear reinforcement was continued at the typical spacing to the end of the longitudinal reinforcement.

Grade markings were allowed within the splice region. The grade markings did not interrupt the typical deformation pattern for either the No. 8 or No. 11 bars, and while deformations were removed on the No. 5 bars to accommodate the grade stamp, the markings were staggered with such frequency that some portion of a grade marking would remain within the splice length on every specimen.

The cages were assembled using standard 8-in. and 10-in. wire ties. The reinforcement was cut with a band saw, and band saw cut ends of tension reinforcement were used within the splices to avoid inconsistencies in material properties and bar geometry common to the shear-cut ends of the as-delivered bars.

Transverse anchor bars were welded within 2 in. of the end of the longitudinal reinforcement on all specimens, except those in two of the earliest test specimens, 8-5-OC0-1.5 and 8-5-XC0-1.5. An early specimen not included in this report exhibited bond failure near the loading apparatus at one end of the beam, precipitating a shear failure in that specimen. The anchor bars used in subsequent specimens provided additional bearing area to ensure proper bar development at the termination of longitudinal steel. Additionally, the welded anchor bars kept the cages square and rigid during transport.

Cover tolerances were achieved using standard steel reinforcement chairs attached directly to the longitudinal bars, a stirrup, or to a short piece of reinforcing bar of the size needed to maintain the appropriate cover of the supported longitudinal bar. Support bars and chairs were placed within the splice region as necessary.

2.4.3 Concrete Placement and Curing

The beams were cast using ready mix concrete. In most cases, they were cast in pairs. Workability was adjusted as needed by adding water that had been withheld during batching or by adding a high-range water reducer. Due to variability between concrete loads, all specimens using a specific mix design were not cast with identical batch quantities, although all 5 ksi and 8 ksi beams were each cast using the same two nominal mix designs reported in Appendix A.

The beams were cast in two layers, beginning and ending at the ends of the beams, while placing the bottom and top layers of concrete in the splice regions of both beams from the middle portion of the batch to help ensure placement of the best quality concrete in the splice region. Concrete samples for strength specimens and standard concrete tests were taken in accordance with ASTM C 172 immediately before and after placing the first lift in both of the splice regions and were combined prior to testing the plastic concrete and casting the strength specimens. The concrete in the beams was consolidated using internal vibration after a complete layer had been placed.

After casting, beams were typically cured in the forms and covered with wet burlap and plastic sheeting on the exposed face until approximately three-quarters of the desired compressive strength had been reached, at which point the forms were stripped and the beams set on blocks to air-dry on all faces. Some specimens were stripped prior to attaining three-quarters of the final strength and were instead completely covered in wet burlap and wrapped in plastic sheeting. During moist curing, beams were rewet a minimum of once per day.

2.4.4 Strength Specimens

Standard 6 x 12 in. concrete cylinders were cast in accordance with ASTM C 192 along with the splice specimens. The cylinders were stored next to the beams as they cured and were stripped simultaneously with the beams.

Cylinders cast in disposable plastic molds were used to track the strength of the concrete as the beams cured. Three cylinders per beam were cast in steel molds;

these cylinders were used to establish the concrete compressive strength when the beams were tested. The cylinders were capped in accordance with ASTM C 617 before testing and tested immediately after the completion of the splice test. Strengths were recorded to the nearest 10 psi, in accordance with ASTM C 39. Generally, if multiple beams were tested within a 24-hour period, the compressive strengths of two beams cast simultaneously were treated as equivalent, and all cylinder strengths were averaged.

2.4.5 Specimen Measurements

The specimens were marked to indicate the locations of the load apparatus, pin and roller supports, ends of the splice region, and the beam centerline. All longitudinal measurements were taken from the centerline to eliminate any inconsistencies for specimens slightly longer or shorter than the nominal length. The markings were 'PS' for the pedestal support, 'SR' to indicate the end of the splice region, and 'CL' for the centerline of the beam. Specimens were also marked with cardinal directions for reference in photographs.

Width, height, and length were measured along the external faces of each specimen before testing. Height and width measurements were taken at 11 locations along all sides of each beam, including the pin and roller support locations, both ends of the splice region, and the centerline of the beam. Length was typically measured on each side of the beam on both the compression and tension faces. To ensure accurate measurements, any excess concrete or surface variations were removed from corners of the beams with an abrasive block or angle grinder. Measurements were taken to 1/32-in. accuracy.

Because of the inaccuracies inherent to measuring cover prior to casting, clear cover values are based on post-break measurements obtained from concrete debris broken at splice failure or with an air chisel after the completion of testing. Measurements were taken at each end of the splice because the moment is assumed to be highest there due to the self-weight of the beam. Concrete was also removed to expose the compression reinforcement in these locations.

Clear cover measurements taken at each splice end (based on original orientation at casting) include bottom cover to the tension reinforcement c_b , external side cover c_{so} , and top cover to the compression reinforcement. Additionally, the internal clear spacing between splices $2c_{si}$ was measured. Measurements to the tension reinforcement were made to the bar deformations, whereas the top cover was measured to the solid bar stock. All concrete cover measurements were made with calipers accurate to 0.001 in.

2.5 TEST SETUP AND PROCEDURE

2.5.1 General

All specimens were designed to be tested in four-point bending. Prior to testing, each beam was inverted from its casting position for safety and ease of marking cracks. This was done by rotating the beams while they were supported on longitudinal No. 8 bars cast into and projecting out of the ends of the beams. The beams were initially cast tension-face down to avoid any top-bar effect on the primary reinforcement, which is known to reduce bond strength of reinforcing bars.

As shown in Figure 2.7, the two central reactions were provided by pin and roller supports made of cold-worked, solid round-stock steel bars in contact with the compression face through 1-in. thick cold-rolled bearing plates. The pin and roller were mounted on concrete pedestals that were, in turn, supported by a 2-ft thick reinforced concrete structural floor. All surfaces involved in load transfer were covered with a layer of Hydrostone, a 10,000 psi high strength gypsum plaster, which is used to prevent movement between the surfaces and ensure even load distribution.

Beams in Series 3 and 4 were supported by a 6-in. diameter roller and pin, both 12 in. long, with appropriately sized bearing plates above and below, with the exception of specimen 8-5-XC2-1.5, a T-beam. All other beams, including 8-5-XC2-1.5, were supported on 30-in. long, 2⁵/₈-in. diameter round-stock, on 30×6-in. bearing plates. Pin supports were fabricated by welding the round-stock to the lower bearing plate, allowing no translation between the two.

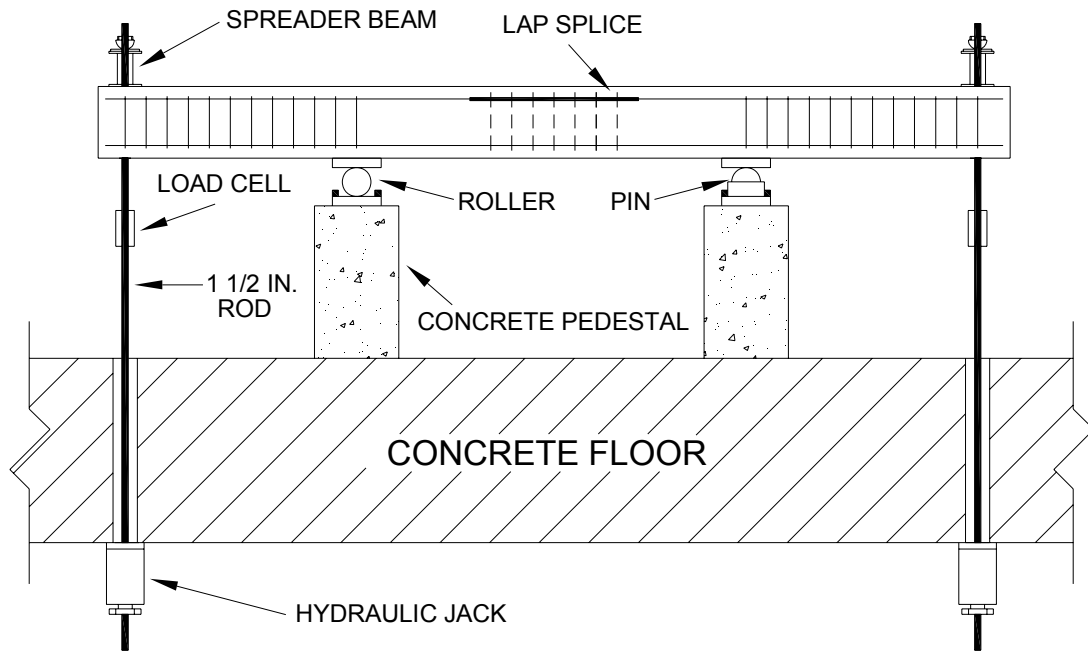


Figure 2.7 – Schematic of the test setup

At each end of the beam, loads were applied through a W8×48 steel spreader beam spanning the tension face. Each spreader beam was connected to two 1½-in. diameter high-yield threaded rods which were passed through stiffened openings in the wide flange section. These rods were pulled downward through the structural concrete floor by load-equalized hydraulic jacks connected to a central pump. Load cells on each of the four load rods were independently calibrated from 0 to 100 kips, approximately twice the highest load required for any test on a single rod.

2.5.2 Instrumentation

Three linear variable differential transformers (LVDTs) were used to record the vertical beam deflections; one at midspan and one at each load application point at the end of the span. A dial gage was attached to each LVDT stand so that beam deflections could also be recorded by hand. Applied load was measured using load cells located on each rod consisting of a group of four strain gages arranged on the rod in a full Wheatstone bridge. Readings from the LVDTs and load cells were

monitored and recorded using a data acquisition (DA) system. The DA system recorded readings from the LVDTs and the load cells at a rate of 4 Hz.

Within each specimen, four 120- Ω ¼-in. strain gages were bonded to the primary tension reinforcement. One strain gage was placed on each spliced bar approximately two inches outside the end of the splice. One deformation on each No. 8 and No. 11 bar was removed using low-heat grinding and polishing to provide a level surface for attaching the strain gage. No. 5 bars typically required the removal of two deformations. Strain gages were applied and sealed following the manufacturer's recommended procedures for submersion in concrete (Vishay 2007). The coating used to seal the strain gages typically covered a number of deformations, all outside of the splice region. Strain gages were read using strain indicator boxes.

2.5.3 Procedure

Prior to each test, the double acting jack system was pumped fully in reverse, after which all slack was taken out of the load rods by tightening the nuts until each load rod was almost engaged with the fully retracted hydraulic jacks. This was done to ensure even loading across all four rods. After zeroing all LVDT, load cell, and strain gage readings on the DA system and strain indicator boxes, zero readings were recorded for each of the three dial gages. Load was applied using a manually-controlled hydraulic pump. Pauses were incorporated in the loading sequence at predetermined load levels to visually inspect the beam, mark visible cracks, measure crack widths using crack comparators, and to record strain and dial gage readings.

The initial load increment was always half of the estimated cracking load to ensure that all instruments and the hydraulic system were operating properly, while the second load step reached the estimated cracking load. The total number and size of load increments varied depending on the estimated capacity of the specimen being tested. Pauses typically were limited to 4 minutes or less. Following specimen failure, the jacks were pumped in reverse until all load was removed from the rods and the jacks were fully retracted.

Due to the brittle nature and large amount of stored energy released in splice failures, the final load step at which cracks were marked and measured was typically set as $\frac{2}{3}$ of the estimated failure load. After this point, the load was increased steadily until failure.

2.6 CALCULATION OF BAR STRESS

2.6.1 General

Moments along the beam specimens were calculated using a two-dimensional analysis in which loads and reactions were assumed to act along the longitudinal centerline of the beam. Reactions and moments were based on load cell readings and the weight of the loading assemblies. The self-weight of the beam was included in the calculations based on average beam dimensions and an assumed density of 150 pcf. Given that specimens generally experienced nearly identical moments at both ends of the splices, splitting failures were assumed to initiate from the splice end with the smallest measured cover dimension.

Test specimens were evaluated using a cracked section analysis with a linear strain distribution throughout the cross-section. Bar stress in the specimens was calculated by both strength and moment-curvature methods. Additionally, bar stress was calculated from the measured strain in the bars obtained with the strain gages placed immediately outside the splices. Figure 2.8, modified from Nawy (2003), is a representation of the moment-curvature and strength methods of analysis.

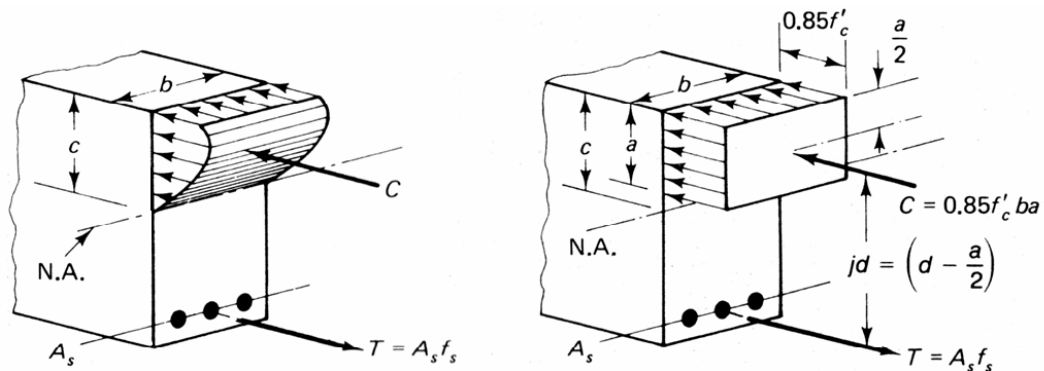


Figure 2.8 – Moment-curvature and strength analysis [after Nawy (2003)]

All longitudinal steel was included in the section analysis calculations for both the strength and moment-curvature methods, regardless of whether the steel was included in the original flexural design. Equations (2.2) and (2.3) were used to calculate the stress in the Grade 100 tension steel, while Eq. (2.4) was used for all other (Grade 60) longitudinal steel. The concrete compressive strength measured from the strength specimens at the time of the test was used for the calculations. For both the strength and moment-curvature methods, concrete in tension was assumed to have cracked and make no contribution to the member forces.

2.6.2 Strength Method

The strength method uses an equivalent stress block to represent the concrete in compression. As in the flexural design of the members, evaluations made with the strength method used the Whitney stress block and the values of β_1 provided in ACI 318-05. The inherent weaknesses in this application of the strength method are recognized, given that the stress block was developed to represent the stress distribution at or near concrete crushing and many of the splice failures occurred well below the crushing strain of the concrete in the extreme compression fiber.

2.6.3 Moment-Curvature Method

The moment-curvature method differs from the strength method of analysis only in that a nonlinear relationship is used throughout the compression region. The concrete's stress-strain curve, as approximated by Eq. (2.5), was used to represent this distribution. In a comparison of analysis methods, Zuo and Darwin (1998) concluded that the moment-curvature method is a more realistic representation of the material behavior and, thus, would provide better and more consistent results than the strength method.

2.6.4 Measured Bar Strain

Measured strain in the spliced bars was recorded during the tests. From the average of the final bar strain values recorded prior to splice failure, the bar stress was calculated using either Eq. (2.2) or Eq. (2.3), as appropriate given the bar size.

CHAPTER 3: RESULTS AND OBSERVATIONS

3.1 GENERAL

Twenty-two beam-splice specimens were tested at KU and a total of 69 at the three schools. Table 3.1 presents the primary splice strength parameters and the maximum bar stress within the splice at failure for each KU test specimen. The bar stresses reported include those calculated by the moment-curvature method, strength method, and using bar strain as measured by strain gages. Specimen dimensions and details of the KU tests are located in Appendix B.

Table 3.1 – Splice parameters and bar stress at failure for KU specimens

Group	Specimen	Bar Size (No.)	Concrete Strength, f'_c (psi)	Cover Dimensions			Splice Length, ℓ_s (in.)	Stirrups Confining Splice, N (ea.)	Bar Stress at Failure, f_s		
				c_b (in.)	c_{so} (in.)	c_{si} (in.)			Strength (ksi)	Moment Curvature (ksi)	Measured Bar Strain*
1A	5-5-OC0-3/4	5	5,490	0.73	1.08	1.02	32	0	73.9	77.0	--
1B	5-5-XC0-3/4		4,670	0.66	0.92	1.09	43	0	79.5	82.2	--
2A	5-5-OC0-2db		5,490	1.05	3.72	3.67	18	0	83.1	86.9	--
2B	5-5-XC0-2db		4,670	0.98	3.80	3.64	25	0	87.8	91.2	--
3A	8-5-OC0-1.5	8	5,260	1.34	1.41	3.63	47	0	75.1	78.1	--
	8-5-OC1-1.5		4,720	1.54	1.51	3.32		4	122.1	123.5	--
	8-5-OC2-1.5		6,050	1.34	1.44	3.37		8	125.4	127.3	--
3B	8-5-XC0-1.5		5,940	1.35	1.41	3.62	63	0	87.0	90.0	--
	8-5-XC1-1.5		4,720	1.46	1.52	3.36		4	127.5	128.7	--
	8-5-XC2-1.5		5,010	1.30	1.53	3.23		8	141.4	143.0	<i>148.9</i>
4A	8-8-OC0-2.5		8,660	2.25	2.25	2.64	27	0	75.9	79.5	--
	8-8-OC1-2.5		7,790	2.37	2.19	2.54		2	85.3	88.7	<i>81.1</i>
	8-8-OC2-2.5		7,990	2.16	2.28	2.63		5	112.3	115.0	--
4B	8-8-XC0-2.5	7,990	2.32	2.38	2.61	36	0	87.7	91.1	--	
	8-8-XC1-2.5	7,790	2.46	2.35	2.48		2	108.1	111.0	--	
	8-8-XC2-2.5	8,660	2.25	2.44	2.57		5	114.5	117.4	--	
5A	11-8-OC0-2	11	9,370	1.82	1.83	6.89	58	0	64.5	67.9	70.6
	11-8-OC1-2		9,370	1.55	1.68	7.25		4	91.7	95.5	98.8
	11-8-OC2-2		8,680	1.82	1.94	6.95		9	120.3	123.5	123.4
5B	11-8-XC0-2		9,910	1.76	1.87	7.30	79	0	75.2	78.9	83.3
	11-8-XC1-2		9,910	1.94	2.02	6.98		4	103.2	106.9	103.9
	11-8-XC2-2		8,680	1.71	2.12	6.88		9	134.4	137.3	136.7

**Italicized* bar stresses are estimated because bar strain data was not available at the failure load.

The moment-curvature method consistently yielded higher bar stresses than the strength method. The average difference between the bar stresses at failure calculated by the two methods was 2.9 ksi, and ranged between 1.2 ksi and 3.8 ksi,

with moment-curvature always producing the greater value. Bar stresses determined from measured strain values are listed for the Series 5 specimens, in all of which at least two, but typically three or all four gages were reporting accurate strain values at the conclusion of the test. Values are also reported for specimens 8-5-XC2-1.5 and 8-8-OC1-2.5, although no strain gages in either specimen were still reporting accurately at failure. The reported values for those tests are estimated based upon the nearly linear behavior of the gages prior to gage failure. Plots of the stress determined from strain gages during specimen loading for all eight specimens with reported values are available in Appendix B. The strain gages in all other specimens were damaged during concrete placement, reported erroneous strain values, or failed during testing. A direct cause for the large number of inaccurate and non-responsive gages is unknown. Figures 3.1 and 3.2 show the bar stress during loading by averaging all accurately reporting strain gages for each specimen in Groups 5A and 5B, respectively. The asterisks represent the bar stress at failure calculated by the moment-curvature method.

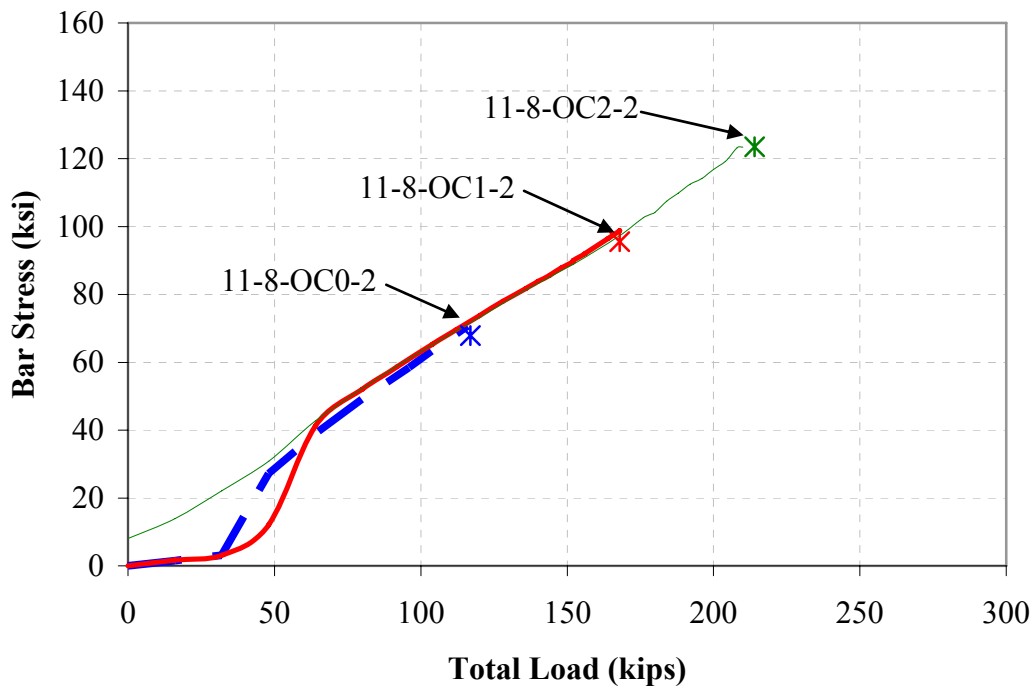


Figure 3.1 – Average strain gage bar stress for Group 5A specimens

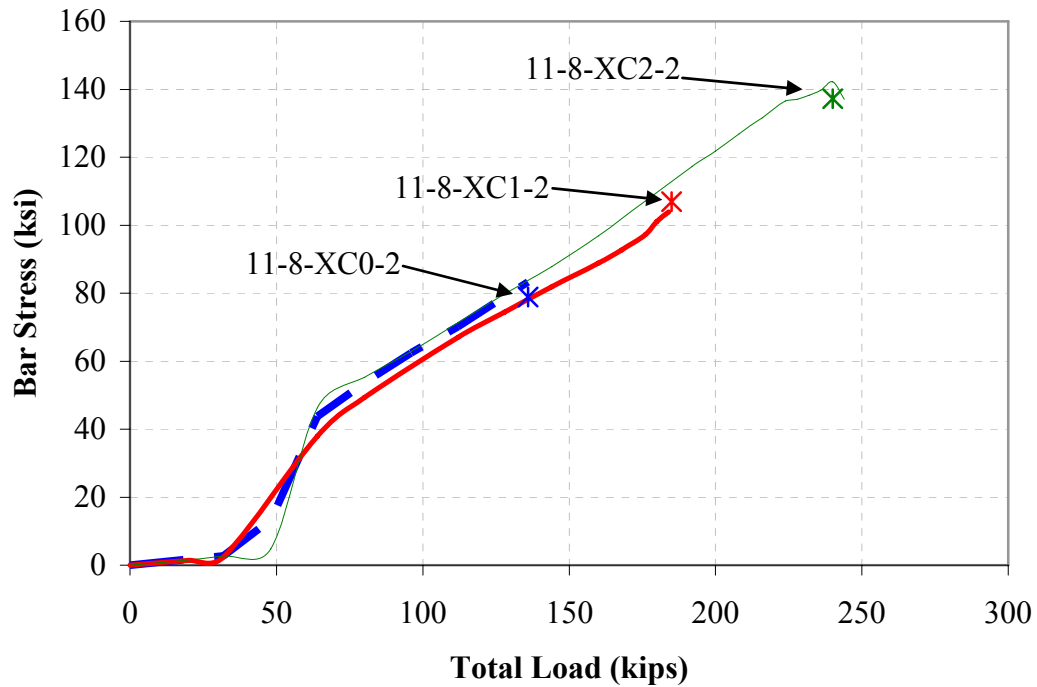


Figure 3.2 – Average strain gage bar stress for Group 5B specimens

Because the strain gage data was recorded by hand, data was not available precisely at the failure load. The load corresponding to the peak bar stress, however, was within 0.6 kips for all Series 5 specimens, except 11-8-OC2-2, for which the final data point was 4.0 kips below the failure load. The strain gage-determined bar stresses at failure for Series 5 specimens ranged from 4.4 ksi higher to 3.0 ksi lower than those stresses calculated by moment curvature, and averaged 1.1 ksi higher.

All bar stress values discussed subsequently are those calculated by the moment-curvature method. As discussed in Section 2.6.3, the moment-curvature method is believed to be more accurate than the strength method. The lack of strain gage data for every test and the similarity between the moment-curvature method and strain gage bar stresses warrants the use of moment-curvature data. Additionally, the use of a single calculation method allows for uniformity between the test results from KU, NSCU, and UT. All bar stresses reported from the tests performed at NSCU and UT were calculated using the moment-curvature method.

3.2 BEHAVIOR AND OBSERVATIONS

The 22 specimens tested at KU failed in bond due to splitting of the concrete cover surrounding the tension lap splices, with 64 of the 69 specimens tested at the three schools exhibiting a splitting bond failure. Five NCSU specimens failed due to crushing of the concrete at the extreme compressive fiber. These specimens were mistakenly constructed with excessive confining transverse reinforcement and are omitted from results reported in this document.

All splitting bond failures exhibited an abrupt loss of load-carrying capacity upon failure with spalling of the concrete cover off the splices. Greater applied loads, and thus stored energy released, typically corresponded with explosive failures that threw chunks of concrete and dust many feet into the air and away from the specimen. “Unconfined” specimens, those without transverse reinforcement confining the splices, exhibited the explosive behavior at lower loads than “confined” specimens, due to the restraint provided to the concrete cover and spliced bars by the confining transverse reinforcement.

During testing of the specimens in Series 1 and 2, the two exterior splices, of the four in each specimen, were observed to fail prior to ultimate failure of the entire specimen. Glass (2007) reported similar behavior in the duplicate specimens tested at UT. Following that initial failure, the total load on the beam dropped slightly, after which loading resumed until the two inner splices failed, typically at a higher load than the partial failure. The highest load applied to the specimen was used in analysis, but always under the assumption that all four spliced bars were contributing to the beam’s resistance.

3.3 LOAD-DEFLECTION

Load-deflection plots are used to examine the flexural behavior of each specimen, including the effect of splice strength and confining transverse reinforcement on the load-carrying and deformation capacities of the specimens. Figure 3.3 displays the load-deflection behavior of the specimens in Group 3B, which is typical to all specimen groups tested in the research program. In the figure, the

total load applied to the specimen is plotted versus the total deflection, which is calculated as the difference between the midspan deflection and average of the endspan deflections at the two load application points. Load-deflection plots for all specimen groups are located in Appendix B. Figure 3.3 shows that the addition of confining transverse reinforcement increases both the deformation capacity and the ultimate load for otherwise identical beam specimens. Increases in both load capacity and ultimate deflection are desirable in terms of structural performance because they provide warning prior to failure. The specimens in Group 3B appeared to develop the first flexural cracks at roughly 30 kips, after which the beam stiffness, represented by the slope of the load-deflection plot, decreases drastically.

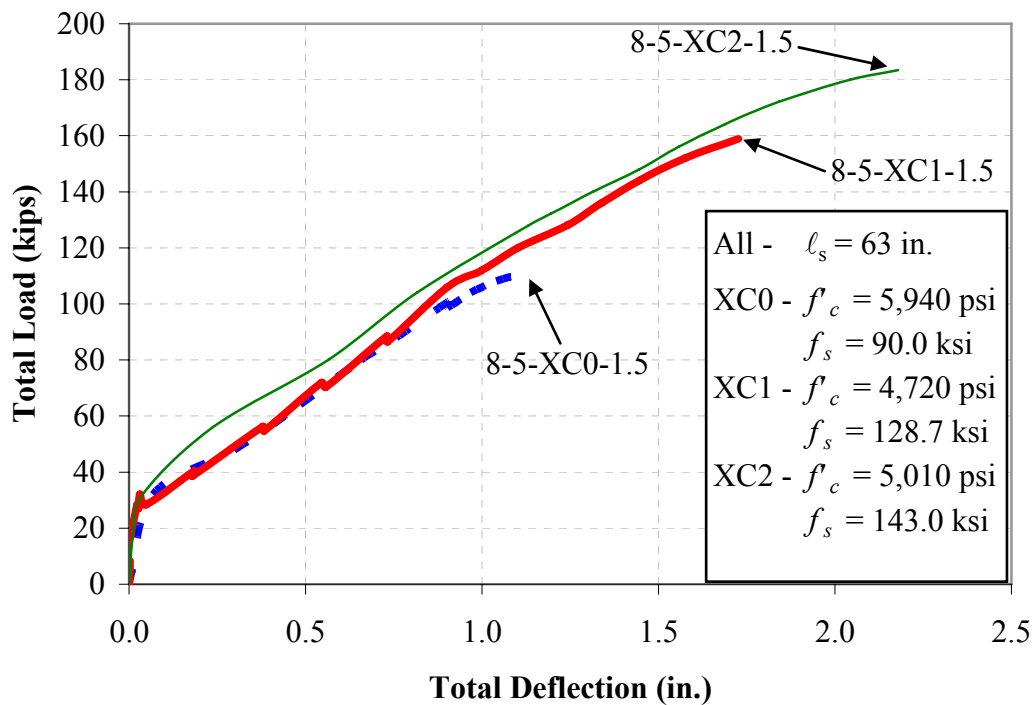


Figure 3.3 – Load-deflection behavior for specimens in Group 3B

3.4 CRACKING

The first cracks to appear during testing were flexural cracks, generally located where the applied moment peaked over the central support points. As loading

continued, splitting, shear, and additional flexural cracks developed. As expected, shear cracks were only observed in the exterior spans between the loading points and central supports. At high loads, crack patterns typically became complicated around internal discontinuities, such as strain gage sites and reinforcing chair locations. Clear card-type crack comparators were used to visually measure crack widths.

3.4.1 Flexural Cracks

Flexural cracks were initially observed at the central support points or at one or both ends of the splice region. Most flexural cracks formed in the early stages of loading. As loading continued, some additional cracks formed while the initial cracks extended further down the specimen. Flexural cracks outside of the two central supports propagated down through the specimen with varying degrees of inclination as expected in shear regions. Flexural cracks typically developed on the tension face at the location of the stirrups used as confining transverse and shear reinforcement, if present, due to the local discontinuity in the concrete.

The widest observable cracks on the specimens were measured after each load increment. At moderate and high loads, these were always the flexural cracks at the ends of the splice region. Figure 3.4 displays the maximum flexural crack widths as a function of bar stress for the loads that produced stresses bounding values of both 40 and 67 ksi for all specimens tested at KU. The crack widths are presented in Table B.3. The values of 40 and 67 ksi represent $\frac{2}{3}f_y$ for 60 and 100 ksi reinforcing steels, respectively, the service load stresses upon which the crack control provisions in Section 10.6.4 of ACI 318-05 are established. The data are separated into two groups, the first of which contains the two data points immediately above and below 40 ksi from each test, while the second contains the data similarly bounding 67 ksi, if available. Three visually-identified outliers are excluded from the 40 ksi data. A linear regression analysis was performed on each group and is shown in Figure 3.4 along with lines representing the 90% upper-bound on crack width. The upper-bound lines were generated using a student t-distribution-based prediction interval with $i-2$

degrees of freedom (10%, $i = 41$ at 40 ksi) (10%, $i = 30$ at 67 ksi), and give crack widths at 40 and 67 ksi corresponding with a 10% probability of exceedance.

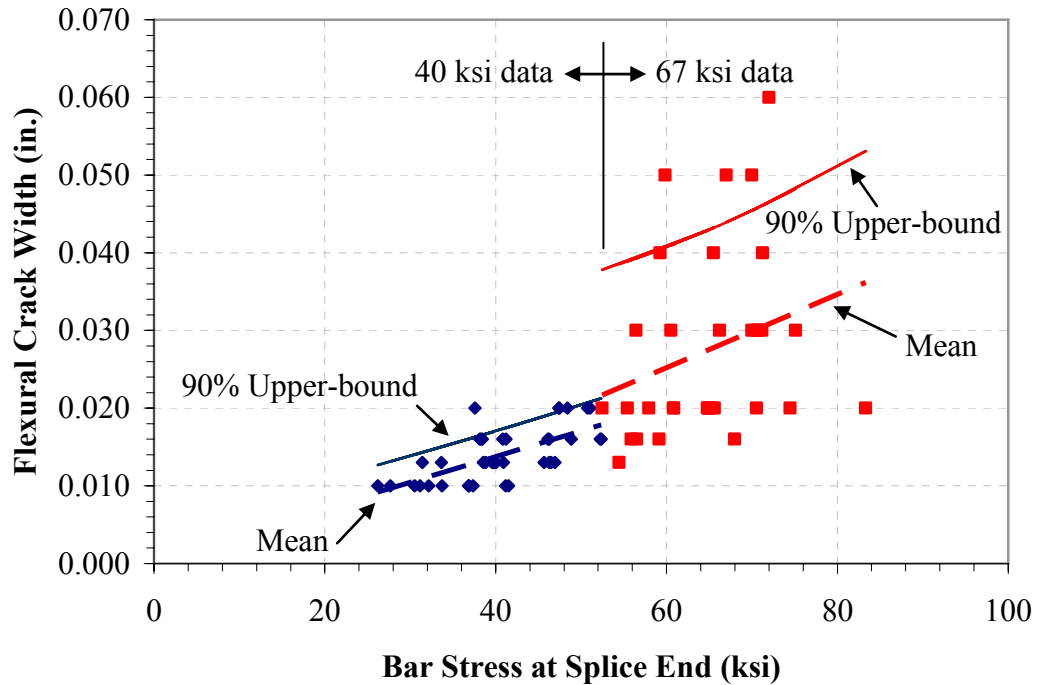


Figure 3.4 – Mean and 90% upper-bound regression lines for maximum flexural crack widths in KU beam-splice specimens at bar stresses bounding 40 and 67 ksi

The average and upper-bound crack widths are 0.014 in. and 0.017 in., respectively, at a bar stress of 40 ksi and 0.028 in. and 0.044 in. at a bar stress of 67 ksi. The crack widths at a service load stress of 40 ksi match expectations and are reasonable at that level of stress, nearly equivalent to the crack size limit of 0.016 in. recommended in ACI 318R-05 Section 10.6.4. The crack widths at 67 ksi, however, significantly exceed the values that a linear relationship between bar stress and crack width would suggest, as evidenced in Figure 3.4 by the discontinuity between both the best-fit and upper-bound lines.

splitting cracks within 12 in. of the end of span at locations of relatively low moment and, thus, bar stress, indicating that bar slip had occurred.

Table 3.2 – Bar stress and total load in KU specimens at splitting crack initiation

Beam ID	Concrete Strength f'_c (psi)	Nominal Section, $b \times h$ (in. x in.)	Minimum Design Cover (in.)	Splice Length, ℓ_s (in.)	Stirrups Confining Splice, N (ea.)	At Splitting Crack Initiation		
						Total Load (kips)	Splice Stress (ksi)	Flexural Crack Width (in.)
5-5-OC0-3/4	5,490	14 x 20	0.75	32	0	---	---	---
5-5-XC0-3/4	4,670			43	0	52	59	0.016
5-5-OC0-2d _b	5,490	35 x 10	1.25	18	0	---	---	---
5-5-XC0-2d _b	4,670			25	0	---	---	---
8-5-OC0-1.5	5,260	14 x 30	1.5	47	0	48	40	0.013
8-5-OC1-1.5	4,720				4	48	40	0.010
8-5-OC2-1.5	6,050				8	80	65	0.020
8-5-XC0-1.5	5,940			63	0	48	40	0.013
8-5-XC1-1.5	4,720				4	72	59	0.030
8-5-XC2-1.5	5,010				8	80	65	0.020
8-8-OC0-2.5	8,660	14 x 21	2.5	27	0	---	---	---
8-8-OC1-2.5	7,790				2	30	39	0.013
8-8-OC2-2.5	7,990				5	44	55	0.020
8-8-XC0-2.5	7,990			36	0	32	41	0.016
8-8-XC1-2.5	7,790				2	40	51	0.020
8-8-XC2-2.5	8,660				5	68	85	0.030
11-8-OC0-2	9,370	24 x 26	2	58	0	64	38	0.016
11-8-OC1-2	9,370				4	64	38	0.020
11-8-OC2-2	8,680				8	64	38	0.016
11-8-XC0-2	9,910			79	0	64	38	0.016
11-8-XC1-2	9,910				4	64	40	0.013
11-8-XC2-2	8,680				8	80	48	0.020

3.5 EVALUATION OF DEVELOPMENT EXPRESSIONS

Bond strengths (bar stresses at splice failure) for the beam-splice specimens are presented along with the failure stresses calculated using Eq. (1.1) and Eq. (1.3), the expressions that predict bond strength recommended in ACI 318-05 and ACI 408R-03, respectively. Failure stresses are calculated twice with Eq. (1.3); once using $\phi = 0.82$ and once with $\phi = 1.00$, corresponding to the design and best-fit strength reduction factors, respectively. Test-to-prediction (T/P) ratios of the bar stress at failure to that given by the predictive equation are provided to evaluate the

performance of Eq. (1.1) and Eq. (1.3). It should be noted that Eq. (1.1) and Eq. (1.3) with $\phi = 0.82$ are intended to provide an acceptable margin of safety and should significantly underpredict the bond strength, evidenced by a T/P ratio greater than 1.00, to be safely used for design purposes. As a best-fit expression, Eq. (1.3) with $\phi = 1.00$ is intended to accurately represent the actual behavior, and should yield an average T/P ratio of approximately 1.00.

For each group of specimens, the average T/P ratio is provided along with the standard deviation and coefficient of variation (COV) for the T/P ratios. A smaller COV signifies less spread and thus greater precision and a more consistent match with the experimental results. Also presented is the percentage of specimens with a T/P ratio less than 1.00, a simple measure of the number of tests for which the prediction of bond strength was unconservative. A percentage much above 10 or 15% indicates that the equation is inherently unsafe. In fact, design equations are often calibrated to limit the percentage of low tests to 5%, as is the case for anchorage design in Appendix D of ACI 318-05. Test results from NCSU (Seliem et al. 2007) and UT (Glass 2007) are considered along with those from KU.

3.5.1 Unconfined Splices

Actual and predicted bond strengths for the 10 specimens tested at KU with splices not confined by transverse reinforcement are presented in Table 3.3.

Table 3.3 shows that Eq. (1.1) unconservatively overpredicts the bond strength of the unconfined KU specimens with an average T/P ratio of 0.83, while the design version of Eq. (1.3) conservatively underpredicts the bond strength with an average T/P ratio of 1.16. Nine of the 10 tests were unconservatively predicted by Eq. (1.1), compared to only one using Eq. (1.3) for design. The best-fit version of Eq. (1.3) marginally overpredicts bond strength with an average T/P ratio of 0.95. Equation (1.1) exhibits greater scatter in the data and, thus, less overall precision at predicting the bar stress at failure, with a COV of 0.19, than Eq. (1.3) with a COV of 0.10. Table 3.4 displays the same information as Table 3.3, but also includes the test results for the unconfined beam-splice specimens tested at NCSU and UT.

Table 3.3 – Test and predicted failure stresses for unconfined KU specimens

Specimen	Stress (ksi)				Test/Prediction Ratio		
	Test	ACI 318-05 Eq. (1.1)	ACI 408R-03 Eq. (1.3) $\phi = 0.82$	ACI 408R-03 Eq. (1.3) $\phi = 1.00$	ACI 318-05 Eq. (1.1)	ACI 408R-03 Eq. (1.3) $\phi = 0.82$	ACI 408R-03 Eq. (1.3) $\phi = 1.00$
5-5-OC0-3/4	77	105	66	80	0.73	1.17	0.96
5-5-XC0-3/4	82	122	74	91	0.68	1.11	0.91
5-5-OC0-2d _b	87	78	64	77	1.12	1.37	1.12
5-5-XC0-2d _b	91	94	74	90	0.97	1.24	1.01
8-5-OC0-1.5	78	84	63	77	0.93	1.24	1.01
8-5-XC0-1.5	90	120	82	99	0.75	1.10	0.90
8-8-OC0-2.5	79	84	64	78	0.95	1.25	1.02
8-8-XC0-2.5	91	107	79	96	0.85	1.16	0.95
11-8-OC0-2	68	95	65	79	0.72	1.05	0.86
11-8-XC0-2	79	130	81	99	0.61	0.97	0.80
Average					0.83	1.16	0.95
Std. Dev.					0.16	0.11	0.09
COV					0.19	0.10	0.10
Percentage < 1.0					90%	10%	60%
Maximum					1.12	1.37	1.12
Minimum					0.61	0.97	0.80

Examination of Table 3.4 shows that the unconfined specimens from all three schools follow the trends of those tested at KU. Equation (1.1) again unconservatively overpredicts the bond strength of Grade 100 steel, with an average T/P ratio of 0.87, while the design version of Eq. (1.3) conservatively underpredicts the bond strength, with an average T/P ratio of 1.19. Further, 81% of the 31 tests were unconservatively predicted by Eq. (1.1), while 6% of the predictions using the design version of Eq. (1.3) were higher than the actual test stress. The best-fit version of Eq. (1.3) is very accurate, almost negligibly overpredicting bond strength, with an average T/P ratio of 0.98. This equation nearly bisects the data, underpredicting 45% and overpredicting 55% of the tests. Equation (1.1), with a COV of 0.20, again exhibited a less consistent prediction of bond strength than Eq. (1.3), with a COV of 0.11. Figure 3.6 displays the scatter in T/P ratios for Eq. (1.1) and the best-fit Eq. (1.3).

**Table 3.4 – Test and predicted bar stresses at failure for unconfined specimens
from all schools**

Specimen	Stress (ksi)				Test/Prediction Ratio		
	Test	ACI 318-05 Eq. (1.1)	ACI 408R-03 Eq. (1.3) $\phi = 0.82$	ACI 408R-03 Eq. (1.3) $\phi = 1.00$	ACI 318-05 Eq. (1.1)	ACI 408R-03 Eq. (1.3) $\phi = 0.82$	ACI 408R-03 Eq. (1.3) $\phi = 1.00$
University of Kansas							
5-5-OC0-3/4	77	105	66	80	0.73	1.17	0.96
5-5-XC0-3/4	82	122	74	91	0.68	1.11	0.91
5-5-OC0-2d _b	87	78	64	77	1.12	1.37	1.12
5-5-XC0-2d _b	91	94	74	90	0.97	1.24	1.01
8-5-OC0-1.5	78	84	63	77	0.93	1.24	1.01
8-5-XC0-1.5	90	120	82	99	0.75	1.10	0.90
8-8-OC0-2.5	79	84	64	78	0.95	1.25	1.02
8-8-XC0-2.5	91	107	79	96	0.85	1.16	0.95
11-8-OC0-2	68	95	65	79	0.72	1.05	0.86
11-8-XC0-2	79	130	81	99	0.61	0.97	0.80
University of Texas							
8-8-OC0-1.5	80	92	67	82	0.87	1.19	0.98
8-8-XC0-1.5	86	127	82	100	0.68	1.05	0.86
8-5-OC0-1.5	74	86	66	81	0.86	1.12	0.91
8-5-XC0-1.5	82	113	81	98	0.73	1.02	0.84
11-5-OC0-3	75	82	63	77	0.91	1.19	0.97
11-5-XC0-3	84	114	80	98	0.74	1.04	0.86
5-5-OC0-3/4	80	108	67	81	0.74	1.20	0.99
5-5-XC0-3/4	91	144	83	101	0.63	1.10	0.90
5-5-OC0-2d _b	88	87	65	79	1.01	1.36	1.11
5-5-XC0-2d _b	110	120	82	101	0.92	1.33	1.09
5-5-OC0-3d _b	97	75	70	86	1.29	1.38	1.13
5-5-XC0-3d _b	120	101	88	107	1.19	1.37	1.12
8-5-SC0-1.5	72	75	59	72	0.96	1.21	1.00
North Carolina State University							
8-5-OC0-2.5	96	80	69	84	1.20	1.40	1.14
8-5-XC0-2.5	110	104	84	103	1.06	1.30	1.07
8-8-OC0-1.5	91	98	67	81	0.93	1.36	1.12
8-8-XC0-1.5	109	145	88	107	0.75	1.24	1.02
11-5-OC0-2	74	92	67	82	0.80	1.10	0.90
11-5-XC0-2	72	105	78	95	0.69	0.93	0.76
11-8-OC0-3	78	79	62	75	0.99	1.27	1.04
11-8-XC0-3	96	123	82	101	0.78	1.16	0.95
Average					0.87	1.19	0.98
Std. Dev.					0.18	0.13	0.11
COV					0.20	0.11	0.11
Percentage < 1.0					81%	6%	55%
Maximum					1.29	1.40	1.14
Minimum					0.61	0.93	0.76

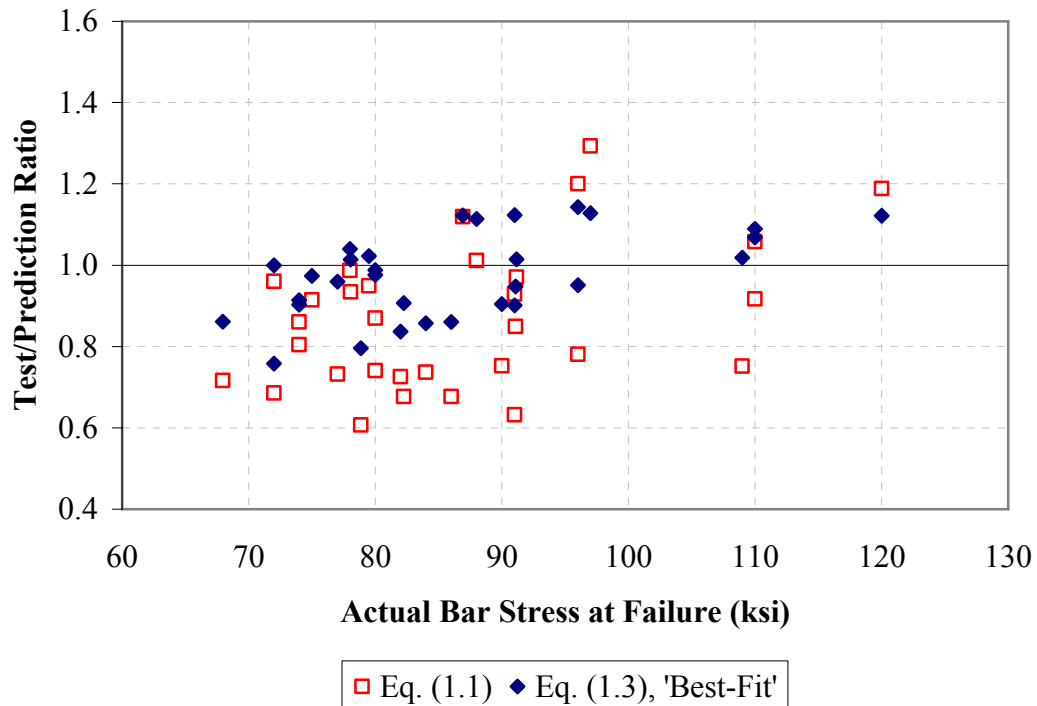


Figure 3.6 – Test-to-prediction ratios for unconfined specimens from all schools

3.5.2 Confined Splices

Table 3.5 lists the actual and predicted bond strengths of the 12 KU specimens with splices confined by transverse reinforcement. The table shows that Eq. (1.1) is an accurate predictor for the bond strength of the confined KU specimens, with an average T/P ratio of 1.01, while the design version of Eq. (1.3) conservatively underpredicts the bond strength, with an average T/P ratio of 1.25. Exactly 50% of the 12 tests had T/P ratios less than 1.00 using Eq. (1.1), while none of the tests were unconservatively predicted using the design version of Eq. (1.3). The best-fit version of Eq. (1.3) accurately predicts bond strength with an average T/P ratio of 1.02. The COVs calculated for the confined KU specimens with Eq. (1.1) and Eq. (1.3) were 0.19 and 0.10, respectively. This again shows that Eq. (1.1) is a less consistent predictor of bond strength than Eq. (1.3).

Table 3.6 displays the same information as Table 3.5, but also includes the confined beam-splice specimens tested at NCSU and UT.

Table 3.5 – Test and predicted failure stresses for confined KU specimens

Specimen	Stress (ksi)				Test/Prediction Ratio		
	Test	ACI 318-05 Eq. (1.1)	ACI 408R-03 Eq. (1.3) $\phi = 0.82$	ACI 408R-03 Eq. (1.3) $\phi = 1.00$	ACI 318-05 Eq. (1.1)	ACI 408R-03 Eq. (1.3) $\phi = 0.82$	ACI 408R-03 Eq. (1.3) $\phi = 1.00$
8-5-OC1-1.5	124	108	82	99	1.15	1.51	1.24
8-5-XC1-1.5	129	142	97	118	0.90	1.33	1.09
8-5-OC2-1.5	127	122	104	127	1.04	1.22	1.00
8-5-XC2-1.5	143	149	111	136	0.96	1.29	1.06
8-8-OC1-2.5	89	79	73	89	1.12	1.21	0.99
8-8-XC1-2.5	111	106	91	111	1.05	1.22	1.00
8-8-OC2-2.5	115	80	83	101	1.43	1.39	1.14
8-8-XC2-2.5	117	112	106	129	1.05	1.11	0.91
11-8-OC1-2	95	106	78	95	0.90	1.23	1.01
11-8-XC1-2	107	161	103	126	0.66	1.03	0.85
11-8-OC2-2	124	128	100	122	0.97	1.23	1.01
11-8-XC2-2	137	164	115	141	0.84	1.19	0.98
Average					1.01	1.25	1.02
Std. Dev.					0.19	0.13	0.10
COV					0.19	0.10	0.10
Percentage < 1.0					50%	0%	33%
Maximum					1.43	1.51	1.24
Minimum					0.66	1.03	0.85

Table 3.6 shows that, on average, Eq. (1.1) and both the design and best-fit versions of Eq. (1.3) underpredict the bond strength of confined Grade 100 splice specimens, with average T/P ratios of 1.10, 1.29, and 1.06, respectively. Equation (1.1) proved unconservative for 30% of the 33 confined specimen tests, while the design version of Eq. (1.3) was conservative for every test specimen. Twenty-seven percent of the predictions made using the best-fit version of Eq. (1.3) were above the test stress. Equation (1.1) yielded a COV of 0.21, signifying a less precise match to the experimental data than the COV of 0.10 obtained using Eq. (1.3). Figure 3.7 shows the scatter of the T/P ratios for Eq. (1.1) and the best-fit version of Eq. (1.3) by plotting the T/P ratios against the actual bar stress at failure.

**Table 3.6 – Test and predicted bar stresses at failure for confined specimens
from all schools**

Specimen	Stress (ksi)				Test/Prediction Ratio		
	Test	ACI 318-05 Eq. (1.1)	ACI 408R-03 Eq. (1.3) $\phi = 0.82$	ACI 408R-03 Eq. (1.3) $\phi = 1.00$	ACI 318-05 Eq. (1.1)	ACI 408R-03 Eq. (1.3) $\phi = 0.82$	ACI 408R-03 Eq. (1.3) $\phi = 1.00$
University of Kansas							
8-5-OC1-1.5	124	108	82	99	1.15	1.51	1.24
8-5-XC1-1.5	129	142	97	118	0.90	1.33	1.09
8-5-OC2-1.5	127	122	104	127	1.04	1.22	1.00
8-5-XC2-1.5	143	149	111	136	0.96	1.29	1.06
8-8-OC1-2.5	89	79	73	89	1.12	1.21	0.99
8-8-XC1-2.5	111	106	91	111	1.05	1.22	1.00
8-8-OC2-2.5	115	80	83	101	1.43	1.39	1.14
8-8-XC2-2.5	117	112	106	129	1.05	1.11	0.91
11-8-OC1-2	95	106	78	95	0.90	1.23	1.01
11-8-XC1-2	107	161	103	126	0.66	1.03	0.85
11-8-OC2-2	124	128	100	122	0.97	1.23	1.01
11-8-XC2-2	137	164	115	141	0.84	1.19	0.98
University of Texas							
8-8-OC1-1.5	123	120	86	104	1.03	1.44	1.18
8-8-XC1-1.5	122	155	100	121	0.79	1.23	1.01
8-8-OC2-1.5	147	121	104	126	1.21	1.41	1.17
8-8-XC2-1.5	144	159	117	142	0.91	1.23	1.01
8-5-OC2-1.5	141	111	104	126	1.27	1.35	1.12
8-5-XC2-1.5	148	142	117	142	1.04	1.26	1.04
11-5-OC1-3	104	84	80	97	1.24	1.31	1.07
11-5-XC1-3	117	116	97	118	1.01	1.20	0.99
11-5-OC2-3	128	84	91	112	1.52	1.40	1.14
11-5-XC2-3	141	116	115	139	1.22	1.23	1.01
8-5-SC1-1.5	99	95	73	88	1.04	1.36	1.13
8-5-SC2-1.5	129	96	86	104	1.34	1.51	1.24
North Carolina State University							
8-5-OC1-2.5	140	80	86	104	1.75	1.63	1.35
8-8-OC1-1.5	151	122	102	124	1.24	1.48	1.22
8-8-XC1-1.5	152	182	127	155	0.84	1.20	0.98
11-5-OC1-2	132	119	100	122	1.11	1.32	1.08
11-5-OC2-2	151	119	122	148	1.27	1.24	1.02
11-5-XC1-2	127	137	106	130	0.93	1.19	0.98
11-5-XC2-2	155	137	135	165	1.13	1.15	0.94
11-8-OC1-3	116	79	85	103	1.47	1.37	1.13
11-8-XC1-3	128	123	116	141	1.04	1.11	0.91
Average					1.10	1.29	1.06
Std. Dev.					0.23	0.13	0.11
COV					0.21	0.10	0.10
Percentage < 1.0					30%	0%	27%
Maximum					1.75	1.63	1.35
Minimum					0.66	1.03	0.85

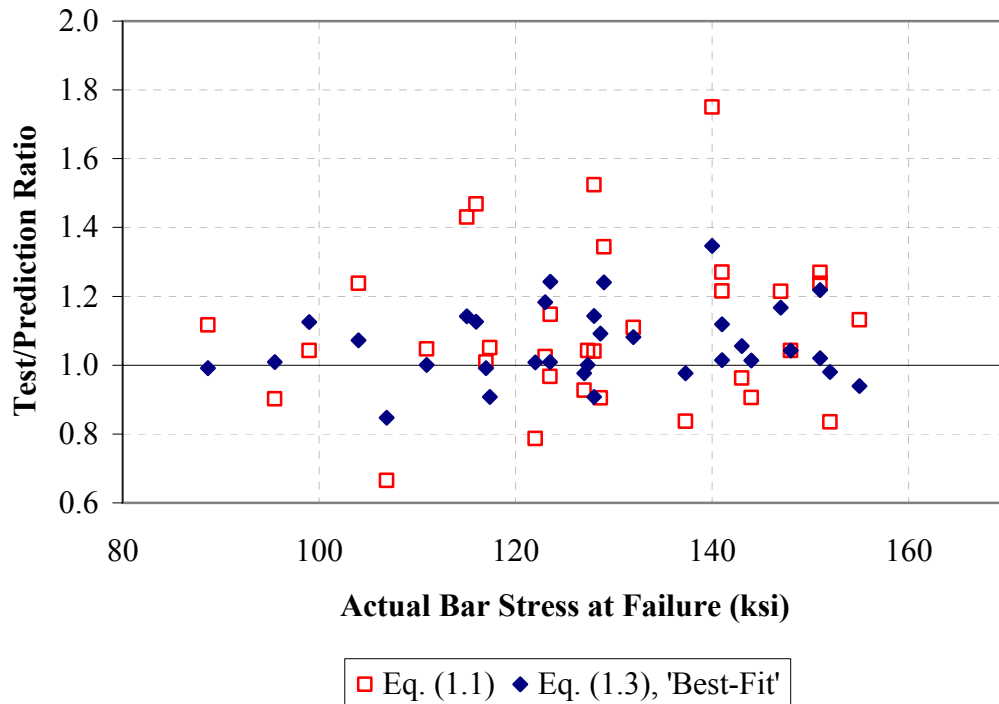


Figure 3.7 – Test-to-prediction ratios for confined specimens from all schools

3.5.3 Discussion

Given the similarity in T/P ratio comparisons between the tests performed at KU and those performed at NCSU and UT, the ensuing discussion in this section makes reference to the total dataset using the combined test results from all schools.

ACI 318-05

Equation (1.1) underestimates the addition to bond strength provided by confining transverse reinforcement. Comparing the average T/P ratio from Table 3.4 to Table 3.6 shows that confined specimens had T/P ratios averaging 0.23 higher than the unconfined specimens. This signifies that the actual increase in bar stress due to the confinement was larger than the predicted increase in bar stress.

Equation (1.2) expresses the limit placed upon the effective contribution to bond strength in Eq. (1.1) of the confinement term, represented as a combination of the concrete cover c_b and c_{so} , clear spacing c_{si} , and the transverse reinforcement index

K_{tr} . Thirty-four of these tests fall above the limit of 2.5 because large amounts of confinement are required to achieve the bar stresses targeted in this research program and the specimens were designed using Eq. (1.3), which calculates confinement in an alternative manner. ACI 318R-05 Section 12.2 states that above the limit specified in Eq. (1.2), a pullout failure is likely to occur. In this testing program, however, all specimens exhibited splitting bond failures, rather than pullout failures, including the specimens with confinement terms well above the given limit. Figure 3.8 displays the T/P ratios calculated with Eq. (1.1) as a function of the confinement term. Figure 3.9 again displays the Eq. (1.1) T/P ratios as a function of the confinement term. In this figure, however, the limit of 2.5 prescribed in Eq. (1.2) is not applied, thus including the unmodified confinement term in the calculation of Eq. (1.1).

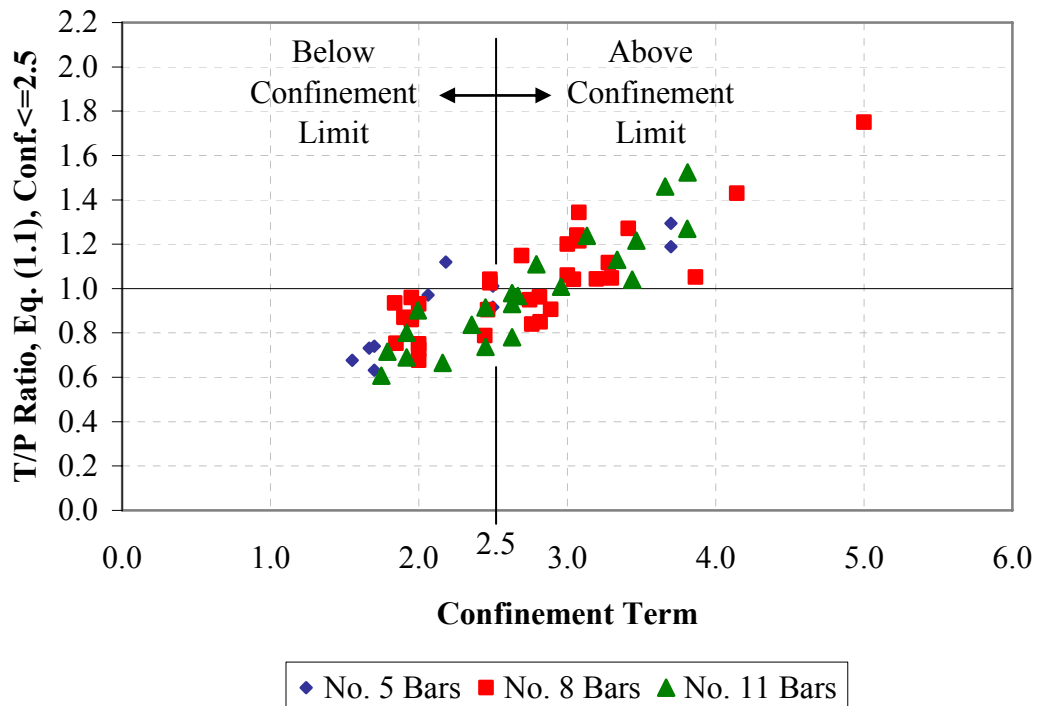


Figure 3.8 – Eq. (1.1) T/P scatterplot with the limit of Eq. (1.2) applied

The marked increase in T/P ratios above the confinement limit in Figure 3.8 shows that despite the limit on the predicted bar stress at failure due to the capped

confinement term, additional confinement does increase the bar stress at failure. Elimination of the confinement limit in Eq. (1.2), shown in Figure 3.9, produces a far more unbiased, albeit uniformly unconservative, prediction of bond strength. Without the application of the upper limit on the confinement term, the accuracy of the prediction made by Eq. (1.1) displays almost no dependency on the overall amount of confinement.

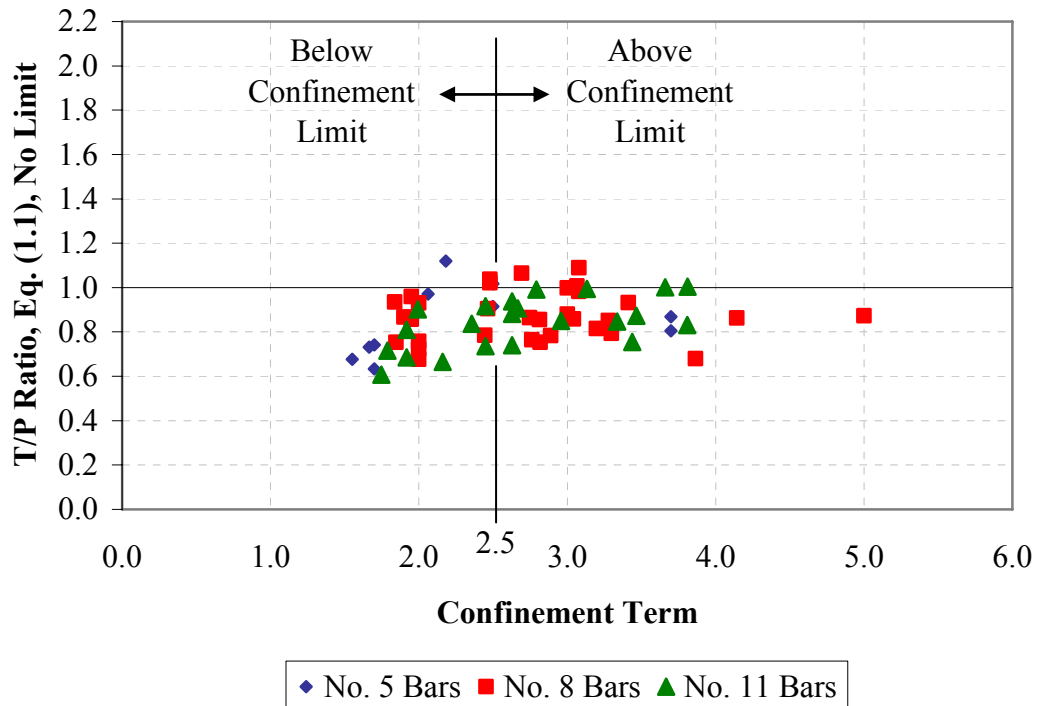


Figure 3.9 – Eq. (1.1) T/P scatterplot without the limit of Eq. (1.2) applied

Application of Eq. (1.2) caps the increase in bar stress at failure predicted by Eq. (1.1) for specimens above the confinement limit. The actual failure stress of the specimens did, however, increase with additional confinement as shown in Figure 3.8. This indicates that for splitting bond failures of Grade 100 reinforcement, the confinement limit of 2.5 does not accurately represent actual bond behavior and merits further study.

Load and Resistance Factor Design (LRFD) methodology typically achieves the desired probability of failure by balancing both the load and strength reduction factors. Although load factors are used as normal, ACI 318R-05 Section 12.1 states that the strength reduction effects are built into Eq. (1.1) for determining development length and splice strength without the use of a strength reduction factor ϕ .

Table 3.4 and Table 3.6, respectively, show that 81% of the unconfined specimens and 30% of the confined specimens would fail prior to reaching the design bar stress calculated using Eq. (1.1). This is an unacceptable margin of safety, and Eq. (1.1) should not be used for the design of development length or splices using Grade 100 reinforcing steel. The provisions in ACI 318-05, however, do not allow the designer to take advantage of yield stresses above 80 ksi. The bar stresses predicted using Eq. (1.1) varied between 75 and 182 ksi for the specimens in this research program, thus indicating that most of the specimens would not have been designed as they were had Eq. (1.1) been used as the design equation with a bar stress limit of 80 ksi. In order to use the 100 ksi yield strength of Grade 100 reinforcing steel, Eq. (1.1) must be modified to limit the probability of failure, as measured by a T/P ratio less than 1.00, to an acceptable level. The inclusion of a factor accounting for behavior at high bar stresses such that 5% or less of the T/P ratios fall below 1.00 can provide a reasonable failure threshold. Combined with the load factors in ACI 318-05, an appropriately small probability of failure may be established.

Equation (3.1) is obtained by modifying Eq. (1.1) to the format that appears in ACI 318-05 with the inclusion of an additional modification factor ψ_h to be used for design with high strength reinforcement, specifically ASTM A 1035 Grade 100 steel. ACI 318-05 Eq. (12-1) calculates a required development length using bar stress $f_s = f_y$, the minimum specified yield stress. Specimens with known development (splice) lengths were used to calculate bar stress f_s in this research program, thus, in Eq. (3.1), f_s is retained to represent bar stress rather than f_y . Other differences from Eq. (12-1) in ACI 318-05, such as the use of c for c_b and ℓ_s for ℓ_d , are the result of a desire to maintain consistent notation within this report. Equations (1.1a) through Eq. (1.1d)

are used calculate terms in Eq. (3.1), and definitions for all previously listed terms may be found in Section 1.3.2.

$$\ell_s = \left(\frac{3}{40} \frac{f_s}{\sqrt{f'_c}} \frac{\psi_t \psi_e \psi_s \psi_h \lambda}{\left(\frac{c + K_{tr}}{d_b} \right)} \right) d_b \quad (3.1)$$

where

- ψ_t = reinforcement location factor, 1.00 for bottom-cast bars
- ψ_e = coating factor, 1.00 for non-epoxy-coated reinforcement
- ψ_h = high strength reinforcement factor
- λ = lightweight concrete factor, 1.00 for normalweight concrete

Evaluation of the 64 specimens using Eq. (3.1) established $\psi_h = 1.48$ as the minimum high strength reinforcement factor for which 5% or less of the T/P ratios were below 1.00. The dataset was also examined excluding all specimens for which the predicted $f'_s > f_y$ since no member would be designed with ACI 318-05 provisions for a bar stress greater than its specified minimum yield strength. Again, $\psi_h = 1.48$ was the smallest factor at which 5% or less of the T/P ratios were below 1.00 out of the reduced dataset of 58 specimens. Across all specimens, the average T/P ratio was 1.47 and the percentage of tests with $T/P \leq 1.00$ was 4.7% when calculated using Eq. (3.1) with $\psi_h = 1.48$. Similarly, the average T/P ratio was 1.49 and the percentage of tests with $T/P \leq 1.00$ was 3.4% for the set of specimens with predicted $f'_s \leq 100$ ksi. Figure 3.10 displays the T/P ratios using Eq. (3.1) with $\psi_h = 1.48$ plotted against the predicted bar stress at failure. Tests excluded from the reduced dataset are displayed using hollow data markers.

The T/P ratios of Eq. (1.1) exhibit a large amount of scatter, as shown in Figures 3.6 and 3.7 and by the corresponding COV values of 0.20 and 0.21 for confined and unconfined specimens, respectively. Equation (1.1) is, thus, an

inconsistent predictor for bond strength of Grade 100 reinforcing steel. This lack of precision likewise carries over to predictions made using Eq. (3.1), as it is simply Eq. (1.1) modified by a scalar coefficient. The large scatter in T/P ratios and low average T/P ratio for Eq. (1.1) requires a large ψ_h to shift the T/P ratios up such that 5% or less of the values fall below 1.00, resulting in the high average T/P ratio of 1.47 for the entire dataset. The inconsistency of the prediction in matching the actual failure stress demonstrates an inherent misrepresentation in Eq. (1.1) of one or more of the factors that influence bond strength.

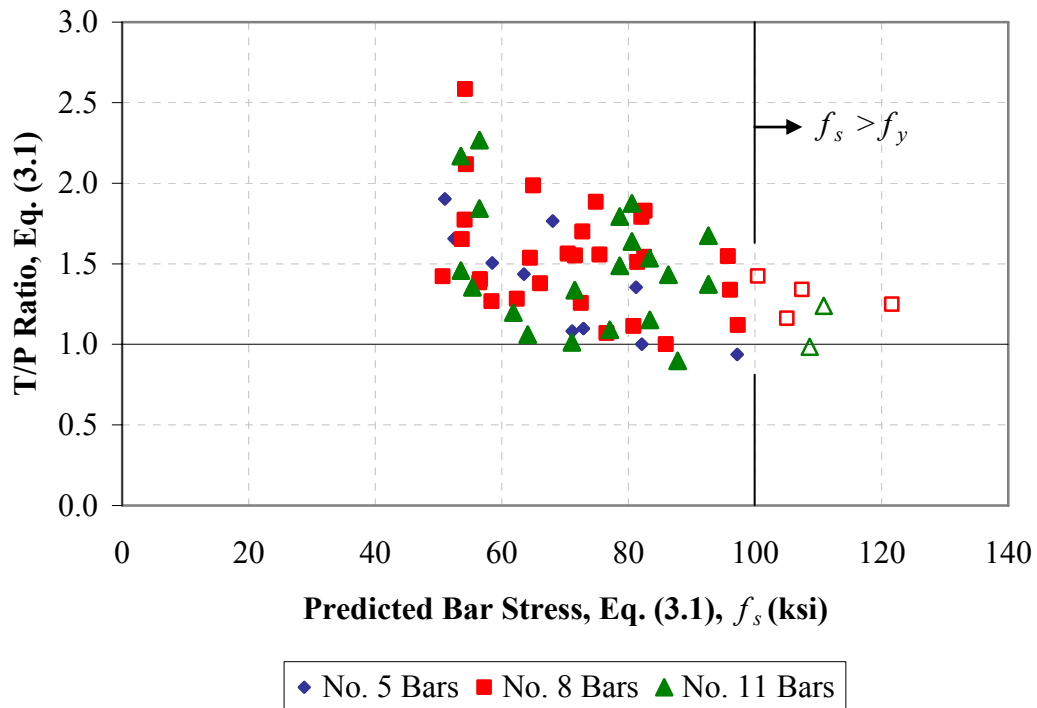


Figure 3.10 – Performance of Eq. (3.1) with $\psi_h = 1.48$

ACI 408R-03

Equation (1.3) underestimates the effect of confinement similarly to Eq. (1.1), although the effect is less pronounced. The average T/P ratio for confined specimens is 0.08 higher than that of unconfined specimens using the best-fit version of Eq. (1.3). This shows that the measured increase in bar stress at failure due to

confinement was greater than predicted by Eq. (1.3). Only seven specimens have confinement terms greater than the limit of 4.0 proscribed by Eq. (1.4). Thus, not enough data are available to draw conclusions regarding the bias of the prediction above the confinement limit. Every one of the seven specimens has a higher T/P ratio due to the limiting effect of Eq. (1.4) on the bar stress predicted by Eq. (1.3) than it would otherwise have had with no limit, ranging from 0.02 to 0.28 higher. The existence of an unbiased prediction, however, is impossible to determine with so few specimens above the limit. Further study of specimens confined beyond the limit described in Eq. (1.4) using Grade 100 reinforcing steel is warranted to help characterize the bond behavior and accuracy of Eq. (1.3) on highly confined bars or splices.

Using the design version of Eq. (1.3) with $\phi = 0.82$ results in a conservative average T/P ratio of 1.24 with 3.1% of the tests failing at a bar stress lower than the predicted stress. Exclusion of the tests with a predicted bar stress greater than the specified minimum yield stress of 100 ksi results in a dataset of 46 specimens. The average T/P ratio for these specimens with the design version of Eq. (1.3) is 1.25, and 4.3% had a T/P ratio less than or equal to 1.00. These values constitute a reasonable safety level and are suitable for design with Grade 100 reinforcement without modification to Eq. (1.3). Figure 3.11 displays the T/P ratios obtained using Eq. (1.3) with $\phi = 0.82$ against the predicted bar stress at failure. The specimens with predicted bar stresses above f_y are represented with hollow data markers.

Scatter of the T/P values calculated using Eq. (1.3), as shown in Figures 3.6 and 3.7, is minimal compared to that obtained using Eq. (1.1). The COVs of 0.11 and 0.10 obtained using Eq. (1.3) to predict the bond strength of unconfined and confined, respectively, beam-splice specimens indicate that Eq. (3.1) provides a reasonable representation of splice strength.

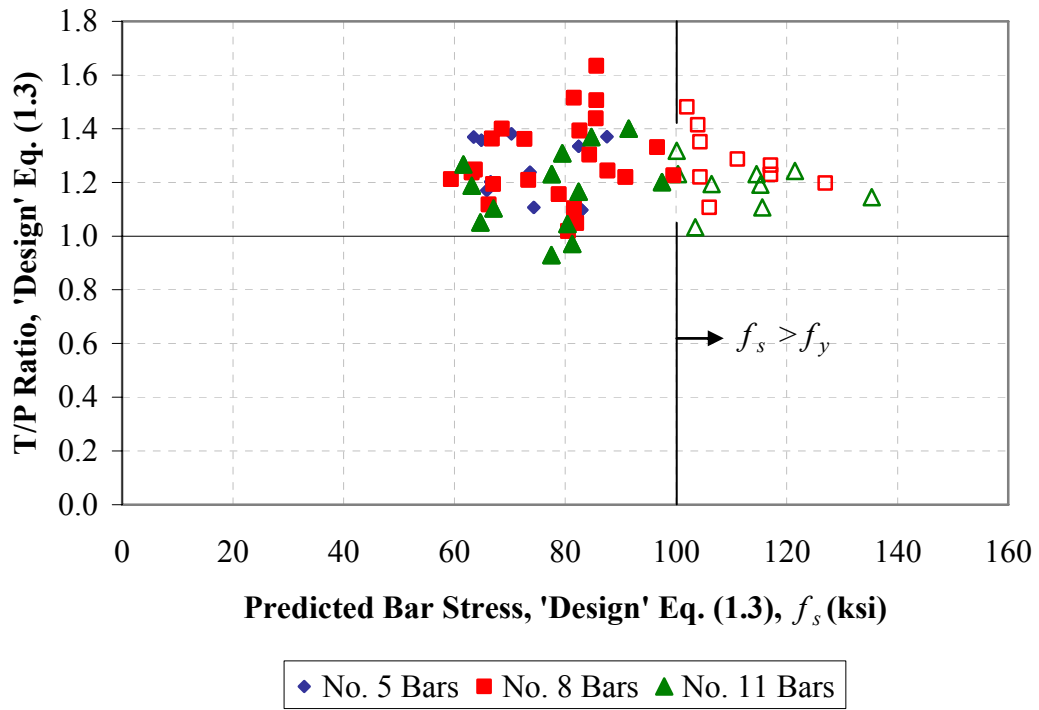


Figure 3.11 – Performance of Eq. (1.3) with $\phi = 0.82$

CHAPTER 4: CONCLUSIONS AND RECOMMENDATIONS

4.1 SUMMARY

This report describes research designed to evaluate the bond strength of ASTM A 1035 Grade 100 reinforcing steel. The joint study included 69 large-scale beam-splice tests performed at the University of Kansas (KU), North Carolina State University (NCSU), and the University of Texas at Austin (UT). Twenty-two of the specimens were tested at KU. All specimens contained bottom-cast lap-splices of No. 5, No. 8, and No. 11 Grade 100 reinforcing bars. Concrete compressive strengths ranged from 4,060 to 10,200 psi.

Specimens were designed to achieve target bar stresses at failure using the development expression recommended in ACI 408R-03. Test specimens containing splices not confined by transverse reinforcement were designed to fail at bar stresses of 80 and 100 ksi, while confined splice specimens were designed to fail at stresses 20 and 40 ksi higher than the matching unconfined specimens. Grade 60 transverse reinforcement was used to confine the spliced bars in the 38 confined specimens, using between two and 23 stirrups along the splice length.

The load-deflection and cracking behavior of the 22 KU specimens are described and evaluated. The development length equations in ACI 318-05 and ACI 408R-03 are compared with the test results from all three schools, and recommendations are made regarding the safety of their usage for design.

4.2 CONCLUSIONS AND RECOMMENDATIONS

The following conclusions are based on the observations and analyses of the 22 KU beam-splice tests.

1. Lap splices using ASTM A 1035 Grade 100 reinforcing steel developed bar stresses ranging between 68 and 143 ksi prior to splitting bond failure.
2. The use of confining transverse reinforcement significantly increases splice strength and beam deformation capacity.

3. The 0.017-in. 90% upper-bound splice-end flexural crack width at a bar stress of 40 ksi is roughly equivalent to the 0.016 in. limit referenced in Section 10.6.4 of ACI 318R-05.
4. The 0.044-in. 90% upper-bound splice-end flexural crack width at a bar stress of 67 ksi significantly exceeds the 0.016 in. limit referenced in Section 10.6.4 of ACI 318R-05 and indicates a nonlinear relationship between bar stress and crack width.

The following conclusions are based on the analyses of the beam-splice specimen test results from KU, NCSU, and UT.

5. Lap splices using ASTM A 1035 Grade 100 reinforcing steel developed bar stresses ranging between 68 and 155 ksi prior to splitting bond failure.
6. The development length expression in ACI 318-05 yielded a significantly less consistent prediction of bond strength than that of ACI 408R-03.
7. The development expressions in both ACI 318-05 and ACI 408R-03 underestimated the effect of confining transverse reinforcement on splice strength.
8. None of the 34 beam-splice specimens with confinement terms in excess of the limit of 2.5 specified in Section 12.2.3 of ACI 318-05 exhibited pullout failures.
9. Calculating the bar stress using the ACI 318-05 expression without the confinement limit resulted in an unbiased prediction, independent of the confinement term.
10. The ACI 318-05 expression is unconservative and unsafe for use with Grade 100 steel designed at its specified minimum yield stress of 100 ksi.
11. A high strength reinforcement modification factor $\psi_h = 1.48$ is recommended for the ACI 318-05 expression for use with Grade 100 reinforcement with bar stresses in excess of 80 ksi.

12. The ACI 408R-03 expression using $\phi = 0.82$ is conservative and safe for use with Grade 100 steel.

4.3 SUGGESTIONS FOR FUTURE STUDY

While the test results and analyses of the specimens from KU, NCSU, and UT have addressed numerous aspects of the bond behavior of Grade 100 reinforcing steel, further study is warranted in the following areas.

1. The behavior of highly confined lap splices.
2. The accuracy of the ACI 318-05 and ACI 408R-03 predictive equations above their respective confinement term limits.

REFERENCES

ACI Committee 318. (2005). *Building Code Requirements for Structural Concrete (ACI 318-05) and Commentary (ACI 318R-05)*, American Concrete Institute, Farmington Hills, MI, 430 pp.

ACI Committee 408. (2001). *Splice and Development Length of High Relative Rib Area Reinforcing Bars in Tension (408.3-01) and Commentary (408.3R-01)*, American Concrete Institute, Farmington Hills, MI, 6 pp.

ACI Committee 408. (2003). *Bond and Development of Straight Reinforcing Bars In Tension (ACI 408R-03)*, American Concrete Institute, Farmington Hills, MI, 49 pp.

Ansley, Marcus. (2002). "Investigation into the Structural Performance of MMFX Reinforcing," *Report*, Florida Department of Transportation, Tallahassee, FL, June, 12 pp.

ASTM A 615/A 615M – 06a. (2006). "Standard Specification for Deformed and Plain Carbon-Steel Bars for Concrete Reinforcement," ASTM International, West Conshohocken, PA, 6 pp.

ASTM A 1035/A 1035M – 06. (2006). "Standard Specification for Deformed and Plain, Low-carbon, Chromium, Steel Bars for Concrete Reinforcement," ASTM International, West Conshohocken, PA, 5 pp.

ASTM C 39/C 39M – 05e1. (2005). "Standard Test Method for Compressive Strength of Cylindrical Concrete Specimens," ASTM International, West Conshohocken, PA, 7 pp.

ASTM C 172 – 04. (2004). "Standard Practice for Sampling Freshly Mixed Concrete," ASTM International, West Conshohocken, PA, 3 pp.

ASTM C 192/C 192M – 05. (2005). "Standard Practice for Making and Curing Concrete Specimens in the Laboratory," ASTM International, West Conshohocken, PA, 8 pp.

ASTM C 617 – 98. (2003). "Standard Practice for Capping Cylindrical Concrete Specimens," ASTM International, West Conshohocken, PA, 5 pp.

Briggs, Michael; Miller, Shelby; Darwin, David; and Browning, JoAnn. (2007). "Bond Behavior of Grade 100 ASTM A 1035 Reinforcing Steel in Beam-Splice Specimens," *SL Report* No. 07-1, University of Kansas Center for Research, Lawrence, KS, 83 pp.

Darwin, David; McCabe, Steven L.; Idun, Emmanuel K.; and Schoenekase, Steven P. (1992). "Development Length Criteria: Bars Not Confined by Transverse Reinforcement," *ACI Structural Journal*, Vol. 89, No. 6, Nov.-Dec., pp. 709-720.

Darwin, David; Tholen, Michael L.; Idun, Emmanuel K.; and Zuo, Jun. (1996a). "Splice Strength of High Relative Rib Area Reinforcing Bars," *ACI Structural Journal*, Vol. 93, No. 1, Jan.-Feb., pp. 95-107.

Darwin, David; Zuo, Jun; Tholen, Michael L.; and Idun, Emmanuel K. (1996b). "Development Length Criteria for Conventional and High Relative Rib Area Reinforcing Bars," *ACI Structural Journal*, Vol. 93, No. 3, May-June, pp. 347-359.

Dawood, Mina; Seliem, Hatem; Hassan, T.; and Rizkalla, Sami H. (2004). "Design Guidelines for Concrete Beams Reinforced with MMFX Composite Reinforcing Bars," *Proceedings of the International Conference on Future Vision and Challenges for Urban Development*, Cairo, Egypt, December 20-22.

El-Hacha, Raafat; El-Agroudy, Hossam; and Rizkalla, Sami H. (2006). "Bond Characteristics of High Strength Steel Reinforcement," *ACI Structural Journal*, Vol. 103, No. 6, Nov.-Dec., pp. 771-782.

Glass, Gregory. (2007). "Performance of Tension Lap Splices with MMFX High Strength Reinforcing Bars," *Master's Thesis*, The University of Texas at Austin, TX, May, 141 pp.

Hognestad, E. (1951). "A Study of Combined Bending and Axial Load in Reinforced Concrete Members," *Bulletin 399*, University of Illinois Engineering Experiment Station, Urbana, IL, 128 pp.

Miller, Shelby. (2007). "Evaluation of Bond Strength of Grade 100 Reinforcing Bars," *Master's Thesis*, The University of Kansas, Lawrence, KS, 105 pp.

Nawy, Edward G. (2003). *Reinforced Concrete: A Fundamental Approach*, Fifth Edition, Pearson Education Inc., Upper Saddle River, NJ, 821 pp.

Orangun, C. O.; Jirsa, James O.; and Breen, John E. (1975). "The Strength of Anchored Bars: A Reevaluation of Test Data on Development Length and Splices," *Research Report No. 154-3F*, Center for Highway Research, The University of Texas at Austin, TX, Jan., 78 pp.

Orangun, C. O. Jirsa, James O.; and Breen, John E. (1977). "Reevaluation of Test Data on Development Length and Splices," *ACI Journal, Proceedings* Vol. 74, No. 3, Mar., pp. 114-122.

Peterfreund, Sean W. (2003). "Development Length of Micro-composite (MMFX) Steel Reinforcing Bars Used in Bridge Deck Applications," *Report*, University of Massachusetts Amherst, Amherst, MA, June, 52 pp.

Seliem, Hatem; Hosny, Amr; and Rizkalla, Sami H. (2007). "Evaluation of Bond Characteristics of MMFX Steel," *Technical Report* No. RD-07-02, North Carolina State University, June, Raleigh, NC, 71 pp.

VISHAY. (2007). "Strain Gage Installations for Concrete Structures," *Application Note TT-611*, Vishay Micro-measurements, August, 4 pp.

Zuo, Jun and Darwin, David. (1998). "Bond Strength of High Relative Rib Area Reinforcing Bars," *SM Report* No. 46, University of Kansas Center for Research, Lawrence, KS, 350 pp.

Zuo, Jun and Darwin, David. (2000). "Splice Strength of Conventional and High Relative Rib Area Bars in Normal and High Strength Concrete," *ACI Structural Journal*, Vol. 97, No. 4, July-Aug., pp. 630-641.

APPENDIX A: MATERIAL PROPERTIES

Table A.1 – Nominal concrete mix designs

Material	Designation	Mix		Unit
		5 ksi	8 ksi	
Cement	Ashgrove Type I/II; ASTM C 150	564	756	lb
Fine Aggregate, SSD	Kansas River Sand; ASTM C 33/KDOT S-1	1377	1415	lb
Coarse Aggregate, SSD	3/4 in. Crushed Limestone; KDOT LS-3	1823	1635	lb
Water	KDOT Potable	247	242	lb
Water Reducer	W.R. Grace Adva100; ASTM C 494 Type F	0-18	0	oz.
	W.R. Grace AdvaFlex; ASTM C 494 Type F	0	75	oz.
W/C Ratio		0.46	0.32	--
Target Slump		3	5	in.
Compressive Strength		4,670 - 6,050	7,790 - 9,910	psi
Target Age		10	7	days
Actual Age		6-42	4-7	days

*Batch weights reported per CY

Table A.2 – Aggregate properties

Material	Bulk Specific Gravity		Fineness Modulus	Unit Weight	Absorption OD
	OD	SSD			
3/4 in. Crushed Limestone KDOT LS-3	2.48	2.57	--	99 pcf	3.3%
Kansas River Sand; KDOT S-1	2.60	2.62	2.65	--	0.6%

Table A.3 – High range water-reducing admixture properties

Material	Specific Gravity	Percent Solids
W.R. Grace Adva 100 ASTM C 494 Type F	1.1	30-34%
W.R. Grace AdvaFlex ASTM C 494 Type F	1.0	28-32%

Table A.4 – MFMX Grade 100 reinforcement deformation properties

Bar Size (No.)	Average Rib Height (in.)	Average Rib Spacing (in.)	Relative Rib Area, R_r --
5	0.0386	0.415	0.0767
8	0.0644	0.680	0.0838
11	0.0738	0.834	0.0797

APPENDIX B: DETAILS OF TEST RESULTS

Table B.1 – Applied loads and moments and bar stresses at splice failure for KU specimens

Group	Specimen	Endspan to Support Distance (ft.)	Load/Load Rod				Loading System Weight at Endspan		Moment from Self Weight			Moment from Applied Loads			Calculated Bar Stress	
			NE (kips)	SE (kips)	NW (kips)	SW (kips)	East (kips)	West (kips)	East (k-ft)	West (k-ft)	East (k-ft)	West (k-ft)	East (k-ft)	West (k-ft)	M- ϕ (ksi)	Strength (ksi)
1A	5-5-OC0-3/4	4	17.3	17.2	16.8	17.0	0.370	0.384	1.4	1.4	137.8	138.8	147.5	147.5	77.0	73.9
			18.0	18.5	18.5	18.0	0.370	0.384	1.7	1.7	147.5	147.5	147.5	147.5	82.2	79.5
2A	5-5-OC0-2db	4	8.8	8.9	8.4	8.5	0.370	0.384	1.6	1.6	70.4	71.1	71.1	71.1	86.9	83.1
			8.7	9.8	9.2	9.5	0.370	0.384	1.7	1.7	75.8	75.7	75.7	75.7	91.2	87.8
3A	8-5-OC1-1.5	5.5	23.5	24.5	24.0	24.0	0.370	0.384	3.3	3.3	266.8	267.0	267.0	267.0	78.1	75.1
			37.8	38.6	38.5	37.9	0.370	0.384	3.3	3.3	422.3	422.3	422.3	422.3	123.5	122.1
			39.5	40.2	40.4	39.6	0.370	0.384	3.3	3.3	440.9	441.6	441.6	441.6	127.3	125.4
3B	8-5-XC0-1.5	5.5	27.6	28.6	27.5	27.6	0.370	0.384	4.0	4.0	306.5	309.8	309.8	309.8	90.0	87.0
			39.6	40.3	39.9	39.2	0.370	0.384	3.9	3.9	438.1	440.5	440.5	440.5	128.7	127.5
			45.5	46.1	46.1	45.7	0.370	0.384	4.9	4.9	506.7	506.2	506.2	506.2	143.0	141.4
4A	8-8-OC0-2.5	5.5	16.0	16.0	16.1	15.6	0.370	0.384	1.9	1.9	176.7	177.2	177.2	177.2	79.5	75.9
			17.0	18.0	18.2	17.8	0.370	0.384	2.0	2.0	197.9	196.7	196.7	196.7	88.7	85.3
			22.7	23.4	24.2	22.8	0.370	0.384	1.9	1.9	258.6	257.5	257.5	257.5	115.0	112.3
4B	8-8-XC0-2.5	5.5	18.1	18.3	18.7	17.7	0.370	0.384	2.1	2.1	202.3	202.3	202.3	202.3	91.1	87.7
			22.9	22.0	22.3	21.5	0.370	0.384	2.1	2.1	245.4	247.1	247.1	247.1	111.0	108.1
			24.1	23.5	23.6	23.2	0.370	0.384	2.1	2.1	262.1	260.7	260.7	260.7	117.4	114.5
5A	11-8-OC0-2	6.5	24.1	23.5	23.6	23.2	0.370	0.384	8.2	8.2	382.2	380.6	380.6	380.6	67.9	64.5
			42.0	42.3	42.3	41.7	0.370	0.384	8.2	8.2	549.0	549.9	549.9	549.9	95.5	91.7
			55.0	50.4	54.3	54.2	0.370	0.384	8.2	8.2	702.5	693.4	693.4	693.4	123.5	120.3
5B	11-8-XC0-2	6.5	33.6	34.3	33.7	34.2	0.370	0.384	9.8	9.8	443.6	443.3	443.3	443.3	78.9	75.2
			45.7	46.5	46.6	45.9	0.370	0.384	9.8	9.8	603.1	601.6	601.6	601.6	106.9	103.2
			60.8	56.2	61.8	61.1	0.370	0.384	11.2	11.2	793.6	770.7	770.7	770.7	137.3	134.4

Table B.2 – KU beam-splice specimen details in the ACI 408 Database format

Group	Specimen	ℓ_s (in.)	d_b (in.)	R_r	b (in.)	h (in.)	d (in.)	c_{s0} (in.)	c_{si} (in.)	c_b (in.)	N_b (ea.)	d_{tr} (in.)	N_s (ea.)	N_l (ea.)	A_b (in. ²)	A_t (in. ²)	f'_c (psi)	f_y (ksi)	f_{yt} (ksi)	f_{sc} Capacity (ksi)	f_{sc} Actual (ksi)	f_{su} Capacity (ksi)	f_{su} Actual (ksi)
1A	8-5-OC0-3/4	32	0.625	0.0767	14.13	20.08	19.04	1.075	1.024	0.728	4	--	--	--	0.31	--	5,490	100	--	154.5	77.0	154.5	73.9
1B	8-5-XC0-3/4	43	0.625	0.0767	14.19	20.31	19.34	0.922	1.091	0.657	4	--	--	--	0.31	--	4,670	100	--	153.8	82.2	154.0	79.5
2A	8-5-OC0-2d _b	18	0.625	0.0767	34.98	10.08	8.71	3.722	3.669	1.052	4	--	--	--	0.31	--	5,490	100	--	153.2	86.9	153.2	83.1
2B	8-5-XC0-2d _b	25	0.625	0.0767	34.98	10.18	8.89	3.796	3.641	0.976	4	--	--	--	0.31	--	4,670	100	--	152.0	91.2	152.4	87.8
	8-5-OC0-1.5	47	1.000	0.0838	14.14	30.10	28.26	1.410	3.628	1.338	2	--	--	--	0.79	--	5,260	100	--	154.2	78.1	154.3	75.1
3A	8-5-OC1-1.5	47	1.000	0.0838	14.07	30.17	28.13	1.513	3.317	1.538	2	0.50	4	2	0.79	0.20	4,720	100	60	153.1	123.5	153.4	122.1
	8-5-OC2-1.5	47	1.000	0.0838	14.15	30.12	28.29	1.435	3.369	1.335	2	0.50	8	2	0.79	0.20	6,080	100	60	155.1	127.3	154.9	125.4
	8-5-XC0-1.5	63	1.000	0.0838	14.21	30.19	28.34	1.413	3.623	1.347	2	--	--	--	0.79	--	5,940	100	--	155.0	90.0	154.9	87.0
3B	8-5-XC1-1.5	63	1.000	0.0838	14.00	30.16	28.21	1.520	3.357	1.456	2	0.50	4	2	0.79	0.20	4,720	100	60	153.0	128.7	153.4	127.5
	8-5-XC2-1.5	63	1.000	0.0838	28.16	30.22	28.42	1.530	3.227	1.297	2	0.50	8	2	0.79	0.20	5,010	100	60	156.0	143.0	156.0	141.4
	8-B-OC0-2.5	27	1.000	0.0838	14.21	21.23	18.48	2.248	2.636	2.246	2	--	--	--	0.79	--	8,660	100	--	155.1	79.5	154.5	75.9
4A	8-B-OC1-2.5	27	1.000	0.0838	14.46	21.38	18.50	2.187	2.541	2.373	2	0.50	2	2	0.79	0.20	7,790	100	60	154.8	88.7	154.1	85.3
	8-B-OC2-2.5	27	1.000	0.0838	14.25	21.21	18.55	2.281	2.634	2.162	2	0.50	5	2	0.79	0.20	7,990	100	60	154.8	115.0	154.1	112.3
	8-B-XC0-2.5	36	1.000	0.0838	14.21	21.24	18.42	2.379	2.613	2.319	2	--	--	--	0.79	--	7,990	100	--	154.8	91.1	154.1	87.7
4B	8-B-XC1-2.5	36	1.000	0.0838	14.20	21.38	18.42	2.354	2.476	2.456	2	0.50	2	2	0.79	0.20	7,790	100	60	154.7	111.0	154.0	108.1
	8-B-XC2-2.5	36	1.000	0.0838	14.11	21.15	18.40	2.437	2.566	2.253	2	0.50	5	2	0.79	0.20	8,660	100	60	155.0	117.4	154.4	114.5
	11-8-OC0-2	58	1.410	0.0797	24.23	26.32	23.80	1.833	6.891	1.815	2	--	--	--	1.56	--	9,370	100	--	161.3	67.9	160.6	64.5
5A	11-8-OC1-2	58	1.410	0.0797	24.19	26.39	24.13	1.677	7.248	1.554	2	0.50	4	2	1.56	0.20	9,370	100	60	161.3	95.5	160.7	91.7
	11-8-OC2-2	58	1.410	0.0797	24.27	26.27	23.75	1.938	6.949	1.815	2	0.50	9	2	1.56	0.20	8,680	100	60	160.9	123.5	159.9	120.3
	11-8-XC0-2	79	1.410	0.0797	24.18	26.23	23.76	1.874	7.300	1.758	2	--	--	--	1.56	--	9,910	100	--	161.5	78.9	160.9	75.2
5B	11-8-XC1-2	79	1.410	0.0797	24.22	26.28	23.64	2.016	6.975	1.938	2	0.50	4	2	1.56	0.20	9,910	100	60	161.5	106.9	160.9	103.2
	11-8-XC2-2	79	1.410	0.0797	38.27	26.19	23.78	2.118	6.881	1.708	2	0.50	9	2	1.56	0.20	8,680	100	60	162.0	137.3	161.9	134.4

Table B.3 – Splice-end flexural crack widths at bar stresses bounding 40 and 67

ksi

Specimen	<40 ksi			>40 ksi			<67 ksi			>67 ksi		
	Total Load	Bar Stress, f_s	Crack Width, w_{cr}	Total Load	Bar Stress, f_s	Crack Width, w_{cr}	Total Load	Bar Stress, f_s	Crack Width, w_{cr}	Total Load	Bar Stress, f_s	Crack Width, w_{cr}
	(kips)	(ksi)	(in.)	(kips)	(ksi)	(in.)	(kips)	(ksi)	(in.)	(kips)	(ksi)	(in.)
5-5-OC0-3/4	32	36.9	0.010	40	45.7	0.013	48	54.5	0.013			
5-5-XC0-3/4	28	32.2	0.010	36	41.5	0.010	52	59.1	0.016	60	67.9	0.016
5-5-OC0-2db	14	37.3	0.010	18	46.9	0.013	22	56.5	0.016			
5-5-XC0-2db	14	36.8	0.010	18	46.3	0.013	26	65.1	0.020	30	74.5	0.020
8-5-OC0-1.5	48	39.8	0.013	56	46.1	0.016	64	52.5	0.020			
8-5-XC0-1.5	48	39.7	0.013	64	52.4	0.016	80	65.0	0.020	88	71.3	0.040
8-5-OC1-1.5	40	33.6	0.013	48	40.0	0.013	80	65.6	0.020			
8-5-XC1-1.5	40	33.7	0.010	56	46.5	0.013	72	59.3	0.040	88	72.0	0.060
8-5-OC2-1.5	48	39.6	0.013	64	52.3	0.016	80	64.9	0.020	88	71.2	0.030
8-5-XC2-1.5	32	27.7	0.010	56	46.2	0.016	80	64.8	0.020	104	83.3	0.020
8-8-OC0-2.5	24	31.1	0.010	32	40.9	0.013						
8-8-XC0-2.5	24	31.4	0.013	32	41.2	0.016	48	60.8	0.020	56	70.6	0.030
8-8-OC1-2.5	30	38.5	0.013	40	50.7	0.020	48	60.5	0.030			
8-8-XC1-2.5	30	38.8	0.013	40	51.1	0.020	48	60.9	0.020	56	70.7	0.030
8-8-OC2-2.5	20	26.2	0.010	32	40.8	0.016	44	55.4	0.020	56	70.0	0.030
8-8-XC2-2.5	<i>Removed as outlier</i>			32	41.2	0.010	44	55.9	0.016	56	70.5	0.020
11-8-OC0-2	64	38.1	0.016	<i>Removed as outlier</i>								
11-8-XC0-2	64	38.4	0.016	80	47.5	0.020	112	65.5	0.040			
11-8-OC1-2	64	37.6	0.020	<i>Removed as outlier</i>			104	59.8	0.050			
11-8-XC1-2	64	39.8	0.013	80	48.9	0.016	96	57.9	0.020	112	67.0	0.050
11-8-OC2-2	64	38.3	0.016	80	47.4	0.020	96	56.4	0.030	120	70.0	0.050
11-8-XC2-2	48	30.5	0.010	80	48.4	0.020	112	66.2	0.030	128	75.1	0.030

B.1 SERIES 1 SPECIMENS

Both specimens in Series 1 contained four No. 5 Grade 100 MMFX longitudinal tension bars. Lap splices of 32 in. (1A) or 43 in. (1B) were centered at the midspan of the beam. The total span for Series 1 specimens was 15 ft, with an internal span of 7 ft between supports. The specimens were designed with four No. 5 Grade 60 bars as compression reinforcement. Both specimens contained 14 No. 4 closed stirrups spaced at 4 in. center-to-center in the shear regions outside the central supports. Both specimens had unconfined splices.

The specimens in this series were cast with a total depth of 21 in. in the shear regions on either end of the beam and a depth of 20 in. in the central, constant-moment region. The additional depth was added to provide adequate cover around the stirrups which, as designed, had ¼ in. or less clear cover to the tension face. The design cover of ¾ in. was maintained in the test region between supports by placing a

6-ft long, 1-in. thick insert centered at the middle of the beam. The bottom cover in the end regions was 1 ¾ in. to the longitudinal steel and 1 ¼ in. to the stirrups.

The ends of the insert were tapered at a 45° angle to minimize the effect of the stress concentration, although during testing flexural cracks did form at the notch before forming at other sites. The 6-ft length allowed the reduced section to be placed completely between the pin and roller support. In effect, the beams were cast as “dog-bone” sections, with the reduced section covering nearly the entire constant-moment region.

The major impacts of the increased section height in the end spans were a higher pre-cracked section stiffness, the notch’s localizing effect on the initial flexural crack location away from a point directly over the support, and better anchorage for the longitudinal and shear reinforcement in the end spans due to increased cover. Figure B.1, below, shows a contour line along specimen 5-5-XC0-3/4.



Figure B.1 – Specimen 5-5-XC0-3/4 showing the “dog-bone” reduced section

Cover was maintained within the splice region by suspending the spliced bars from a No. 4 cross bar, placed above the splices, which was then tied to standard 2-in.

reinforcing bar chairs protruding up through the splices. Deformations were ground down on the cross bar to reduce its bond to the surrounding concrete and limit any influence it may have had on splitting crack development. The cross bar was cut to prevent any overhang beyond the outermost bar in the exterior splices. Three chairs were used per cross bar, one between each splice.

The load-deflection behavior of the two test specimens in Series 1, shown in Figure B.2, is similar despite the differences in splice length. Specimen 5-5-XC0-3/4, with the longer of the two splice lengths, appears slightly stiffer.

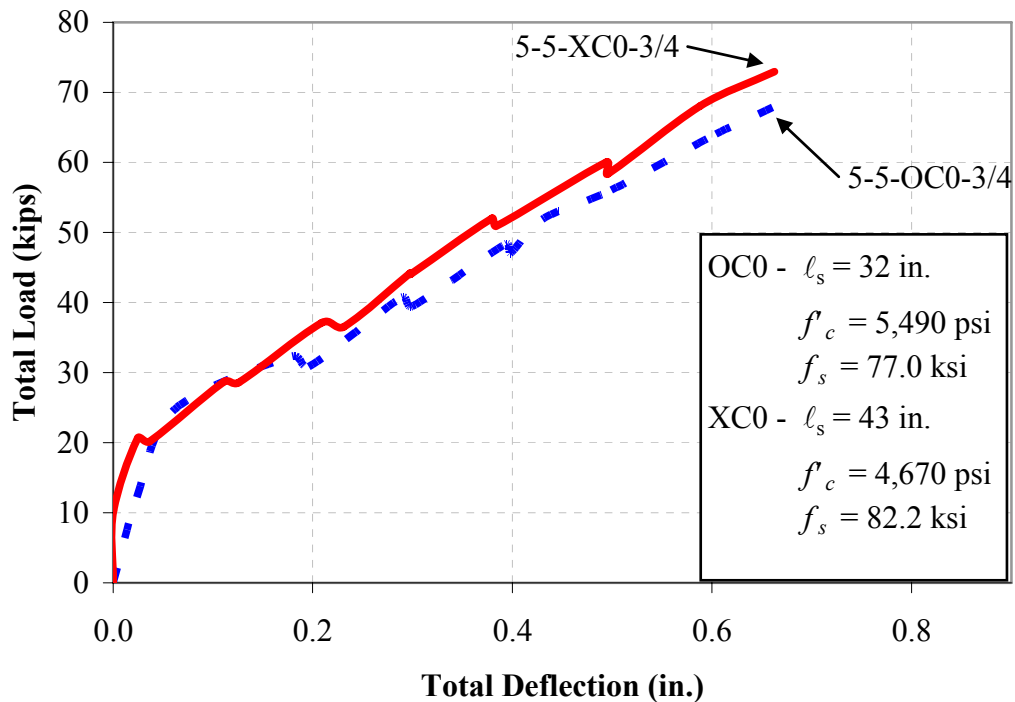


Figure B.2 – Load-deflection behavior of Series 1 beam-splice specimens

B.1.1 Group 1A

Specimen 5-5-OC0-3/4

Specimen 5-5-OC0-3/4 failed due to the formation of splitting cracks in the splice region at a bar stress of 77.0 ksi, or 97% of the value predicted by Eq. (1.3). A

photograph of the specimen following the completion of the test is shown in Figure B.3.



Figure B.3 – Specimen 5-5-OC0-3/4 at the conclusion of the test

B.1.2 Group 1B

Specimen 5-5-XC0-3/4

Specimen 5-5-XC0-3/4 failed due to the formation of splitting cracks in the splice region at a bar stress of 82.2 ksi, or 91% of the value predicted by Eq. (1.3). A photograph of the specimen following the completion of the test is shown in Figure B.4.

B.2 SERIES 2 SPECIMENS

Both specimens in Series 2 contained four No. 5 Grade 100 MMFX longitudinal tension bars. Each bar was spliced with a lap length of 18 in. (2A) or 25 in. (2B) centered at the midspan of the beam. The total span for Series 2 specimens was 15 ft, with an internal span of 7 ft between supports. Series 2 specimens were

designed without compression reinforcement, but contained four No. 4 Grade 60 bars to support the upper corners of the shear reinforcement. Both specimens contained 14 rows of two No. 4 closed stirrups spaced at 4 in. center-to-center in each shear region beyond the support, or 28 per end region. Both specimens had unconfined splices.

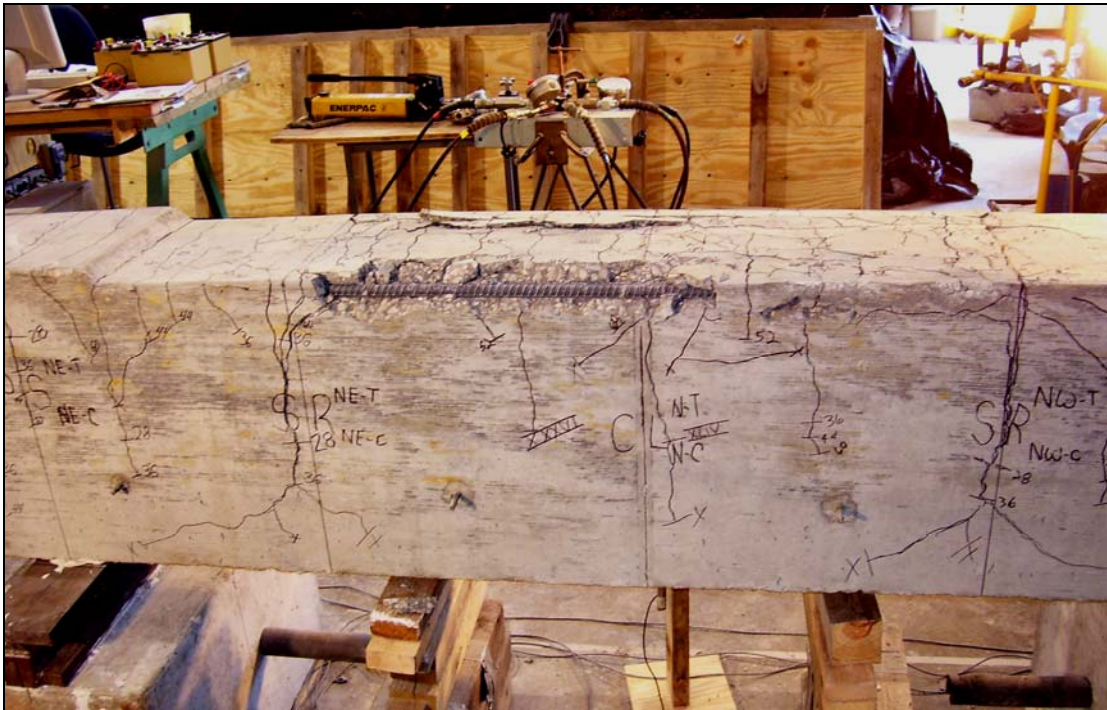


Figure B.4 – Specimen 5-5-XC0-3/4 at the conclusion of the test

Series 2 specimens were constructed using two separate reinforcement cages in each beam, with each consisting of two tension bars, and two compression bars with their own closed stirrups. This was done to provide shear reinforcement across the entire width of the beam, rather than just at the exterior edges. The two cages were tied together using eight No. 4 bars per specimen.

Because of the 35-in. width of the specimens in Series 2, blockouts were used to reduce the width at the ends of the beam to accommodate the load rods, which were spaced apart transversely 36 in. 9-in. long by 10-in. tall by 1½-in. deep blockouts were used, reducing the section width to 32 in. at both beam ends over the full height of the specimen. Specimen 5-5-XC0-2d_b used a further 45° transition for

each breakout to make the end angled, giving it a total length of 10 ½ in., with 1 ½ in. of transition to the full depth of 1 ½ in.

No chairs or other supports were placed within the splice region for either specimen in Series 2, given the very short splice length. Standard chairs were placed about 4 inches immediately outside of the splice region on both ends of each splice.

The load-deflection curves for the two Series 2 specimens are plotted in Figure B.5. The stiffness of the two specimens appears to diverge near 15 kips total load, after which specimen 5-5-OC0-2db displays a higher stiffness but lower ultimate load and deflection.

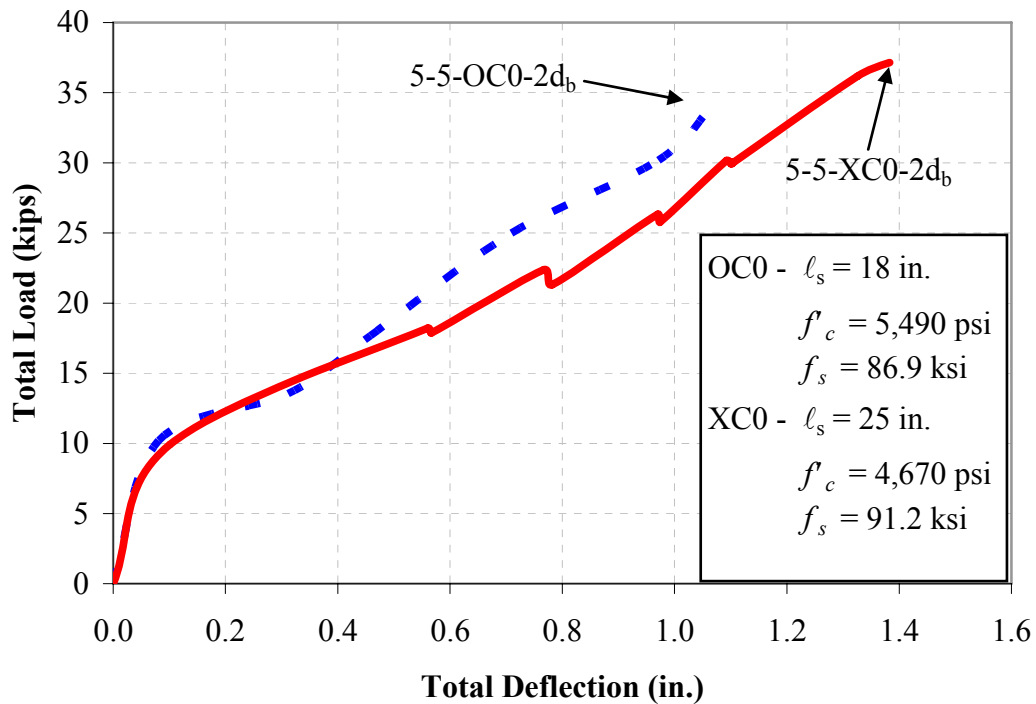


Figure B.5 – Load-deflection behavior of Series 2 beam-splice specimens

B.2.1 Group 2A

Specimen 5-5-OC0-2db

Specimen 5-5-OC0-2db failed due to the formation of bond splitting cracks along the splice at a bar stress of 86.9 ksi, or 113% of the value predicted by Eq.

(1.3). A photograph of the specimen following the completion of the test is shown in Figure B.6.



Figure B.6 – Specimen 5-5-XC0-2d_b after testing, as viewed from above

B.2.2 Group 2B

Specimen 5-5-XC0-2d_b

Specimen 5-5-XC0-2d_b failed due to the formation of bond splitting cracks in the splice region at a bar stress of 91.2 ksi, or 102% of the value predicted by Eq. (1.3). A photograph of the specimen following the completion of the test is shown in Figure B.7.

B.3 SERIES 3 SPECIMENS

The Series 3 specimens contained two No. 8 Grade 100 MMFX longitudinal tension bars. These bars were lap-spliced with lengths of 47 in. (4A) or 63 in. (4B) centered at the midspan of the beam. The total span for Series 3 specimens was 21 ft, with an internal span of 10 ft between supports. Series 3 specimens were designed

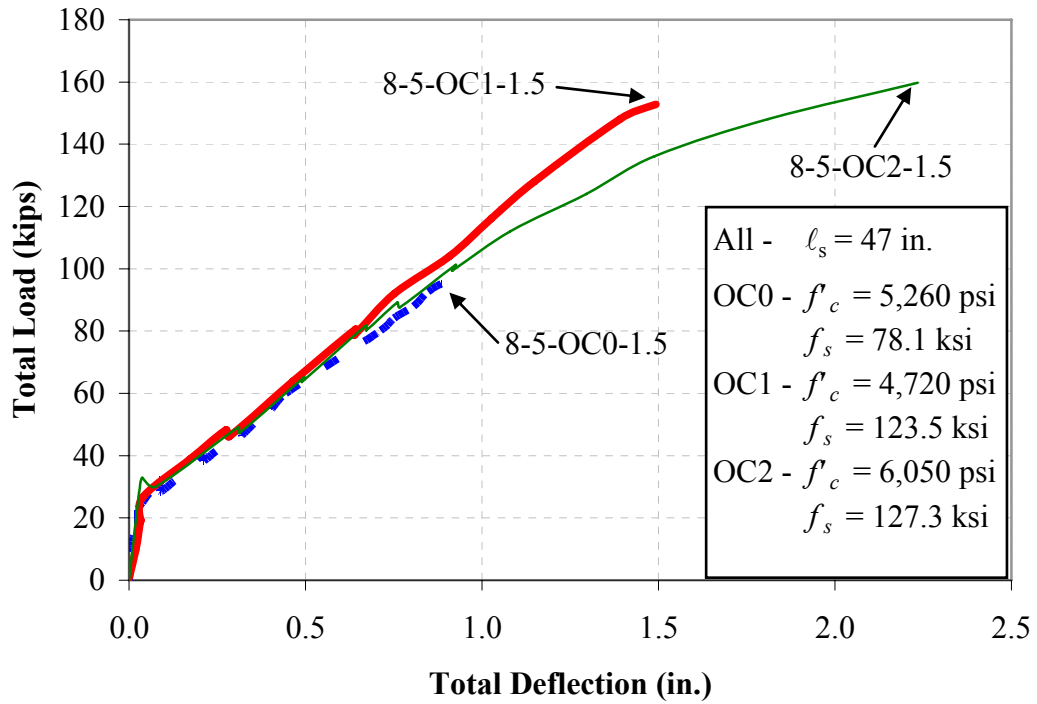


Figure B.8 – Load-deflection behavior of Group 3A beam-splice specimens



Figure B.9 – Specimen 8-5-OC0-1.5 at the conclusion of the test

Specimen 8-5-OC1-1.5

Specimen 8-5-OC1-1.5 failed due to the formation of bond splitting cracks in the splice region at a bar stress of 123.5 ksi, or 122 % of the value predicted by Eq. (1.3). A photograph of the specimen following the completion of the test is shown in Figure B.10.



Figure B.10 – Specimen 8-5-OC1-1.5 at the conclusion of the test

Specimen 8-5-OC2-1.5

Specimen 8-5-OC2-1.5 failed due to the formation of bond splitting cracks in the splice region at a bar stress of 127.3 ksi, or 99% of the value predicted by Eq. (1.3). A photograph of the specimen following the completion of the test is shown in Figure B.11.

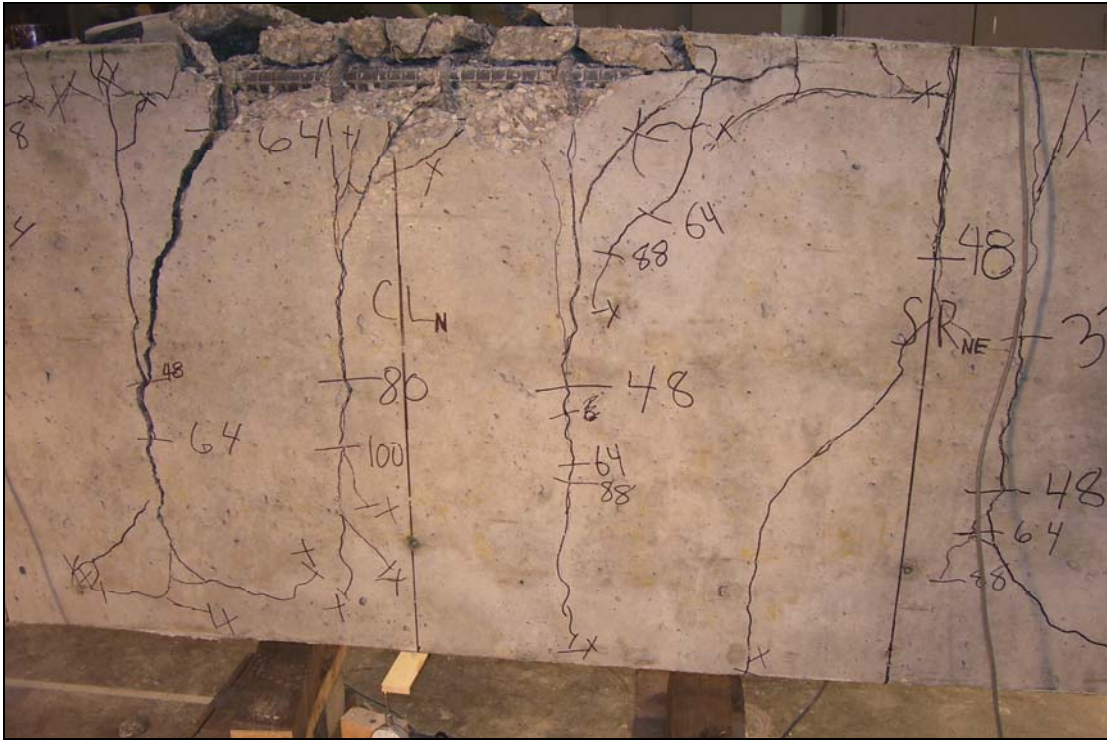


Figure B.11 – Specimen 8-5-OC2-1.5 at the conclusion of the test

B.3.2 Group 3B

All beams in Group 3B had a splice length of 63 in. Specimen 8-5-XC2-1.5 was cast as a T-beam with a 28-in. wide, 7-in. deep flange. Specimen 8-5-XC2-1.5 also contained significantly more compression steel than the other beams in the group, 3.16 in.² compared to the 0.40 in.². As expected, the load-deflection behavior for that specimen indicates less overall deflection than the other two specimens in the group at an equivalent load, but the stiffness was ultimately similar, as shown below in Figure B.12.

Specimen 8-5-XC0-1.5

Specimen 8-5-XC0-1.5 failed due to the formation of bond splitting cracks in the splice region at a bar stress of 90.0 ksi, or 91% of the value predicted by Eq. (1.3). A photograph of the specimen following the completion of the test is shown in Figure B.13.

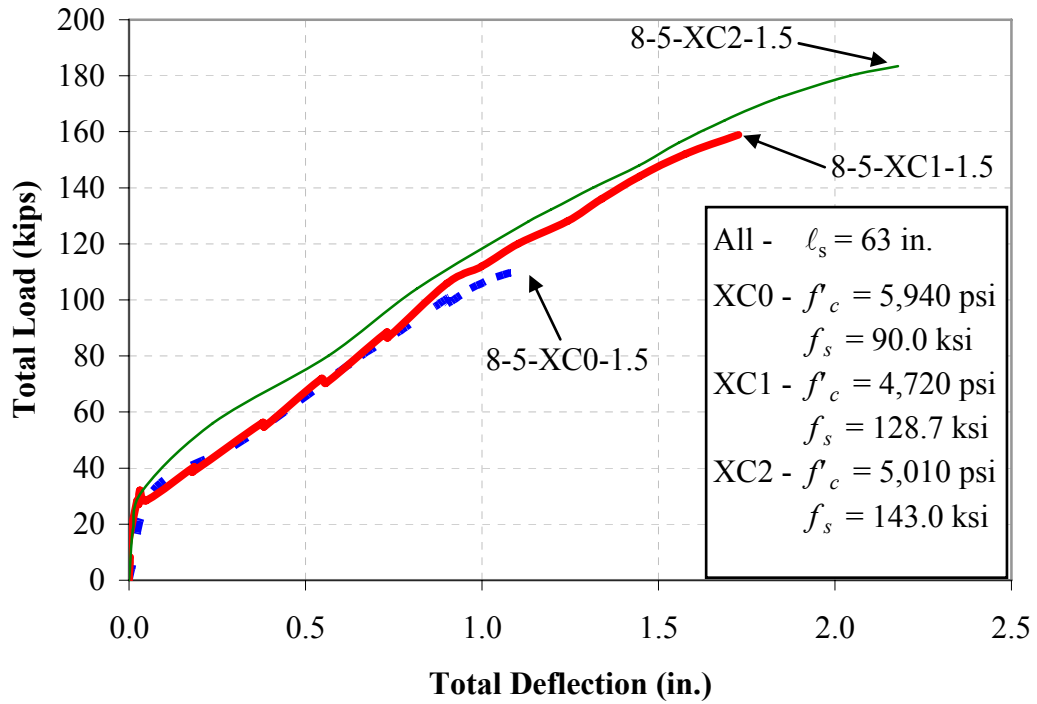


Figure B.12 – Load-deflection behavior of Group 3B beam-splice specimens



Figure B.13 – Specimen 8-5-XC0-1.5 at the conclusion of the test

the four strain gages at each end of the splices. Although all four gages failed prior to splice failure, a stiffness of 0.800 ksi/kip was established from the approximately linear region after the specimen cracked. This yielded an estimated failure stress of 148.9 ksi.



Figure B.15 – Specimen 8-5-XC2-1.5 at the conclusion of the test

In addition to being cast as a T-beam, specimen 8-5-XC2-1.5 differed from other beams in this program in that it contained U-stirrups with seismic hooks in the shear regions outside of the supports rather than the closed stirrups used in all other beams. U-stirrups were chosen to conserve material given that specimen 8-5-XC2-1.5 was a duplicate of a previously cast beam that failed in flexure. Closed stirrups were used, as normal, in the splice region for confinement.

The U-stirrups were closed with opposing inverted U-stirrups that extended into the flanges to support two of the four No. 8 Grade 60 bars used as compression reinforcement. The other two No. 8 bars were placed within the hooks on the primary

U-stirrups that confined the longitudinal steel in the ends. Two No. 3 bars were cast into specimen 8-5-XC2-1.5 at a depth of 5 ¼ in. from the top of the flange to anchor the hooks of the upper U-stirrups, but were not considered in the analysis of the beam for either tension or compression.

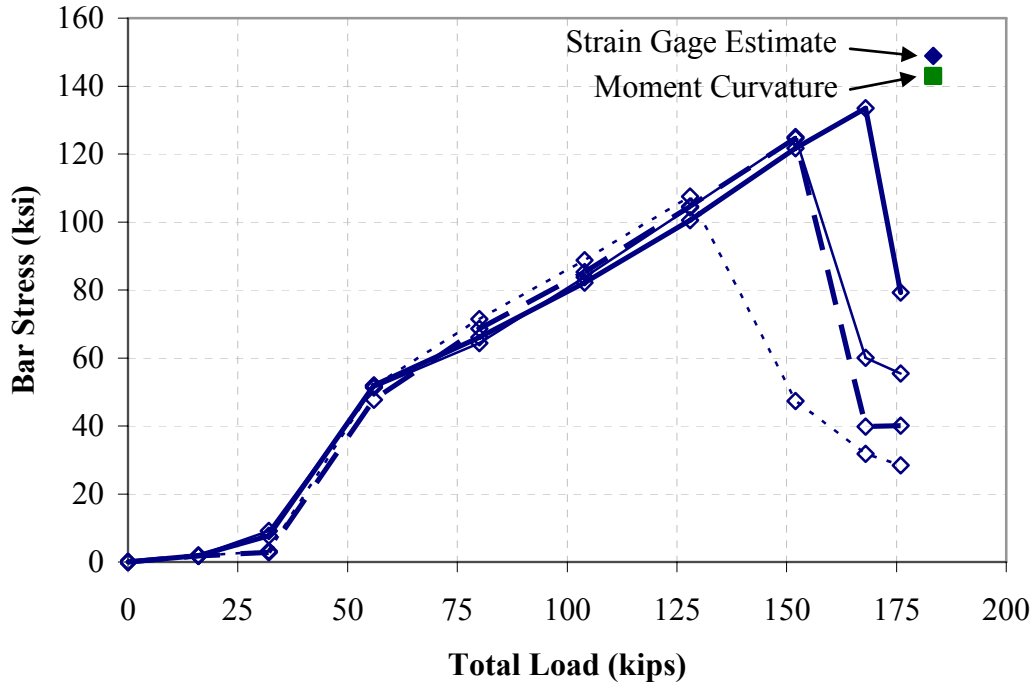


Figure B.16 – Measured bar stress for specimen 8-5-XC2-1.5

B.4 SERIES 4 SPECIMENS

All beams in Series 4 contained two No. 8 Grade 100 MMFX longitudinal tension bars. The beams had a lap splice length of 27 in. (4A) or 36 in. (4B) centered at the midspan of the beam. The total span for Series 4 beams was 21 ft with an internal span of 10 ft between supports. Series 4 beams contained two No. 8 Grade 60 bars as compression reinforcement. All specimens contained 15 closed stirrups spaced at 5 in. center-to-center in each shear region beyond the support. C0 specimens had unconfined splices, while C1 and C2 specimens contained 2 and 5 No. 4 closed stirrups, respectively.

B.4.1 Group 4A

All beams in Group 4A had a splice length of 27 in. The load-deflection behavior is shown in Figure B.17.

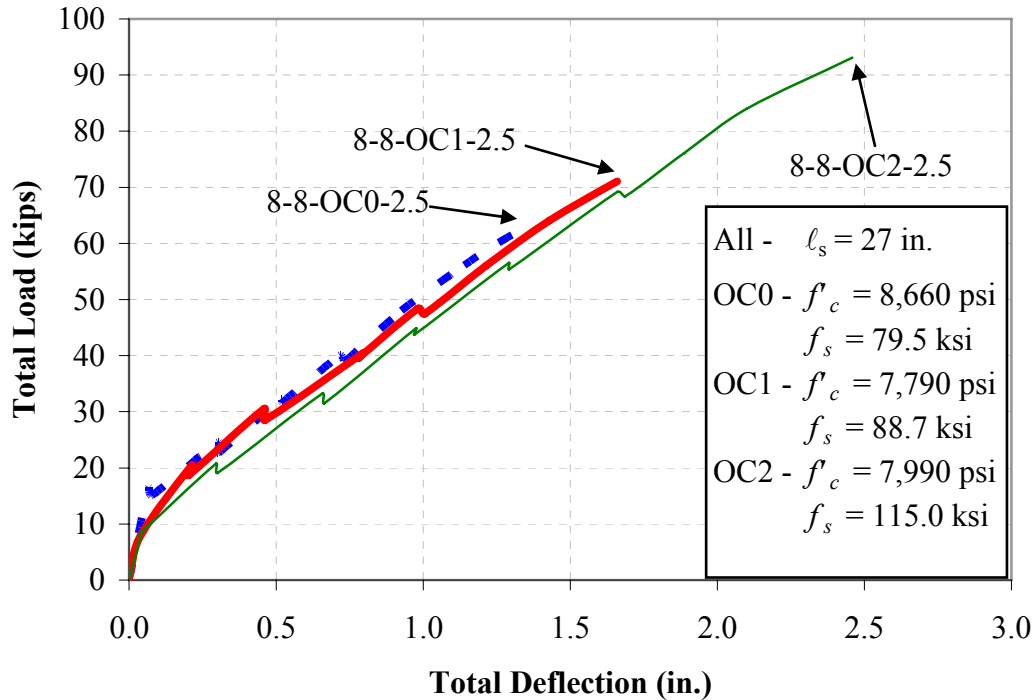


Figure B.17 – Load-deflection behavior of Group 4A beam-splice specimens

Specimen 8-8-OC0-2.5

Specimen 8-8-OC0-2.5 failed due to the formation of bond splitting cracks in the splice region at a bar stress of 79.5 ksi, or 103% of the value predicted by Eq. (1.3). A photograph of the specimen following the completion of the test is shown in Figure B.18.

Specimen 8-8-OC1-2.5

Specimen 8-8-OC1-2.5 failed due to the formation of bond splitting cracks in the splice region at a bar stress of 88.7 ksi, or 96% of the value predicted by Eq. (1.3). A photograph of the specimen following the completion of the test is shown in Figure B.19.



Figure B.18 – Specimen 8-8-OC0-2.5 at the conclusion of the test



Figure B.19 – Specimen 8-8-OC1-2.5 at the conclusion of the test

Figure B.20 displays the bar stress measured from the strain gages placed at each end of the lap-splices in specimen 8-8-OC1-2.5. Although all strain gages failed prior to splice failure, a stiffness of 1.091 ksi/kip was calculated from the approximately linear behavior following initial flexural cracking, yielding an estimated 81.1 ksi bar stress at failure.

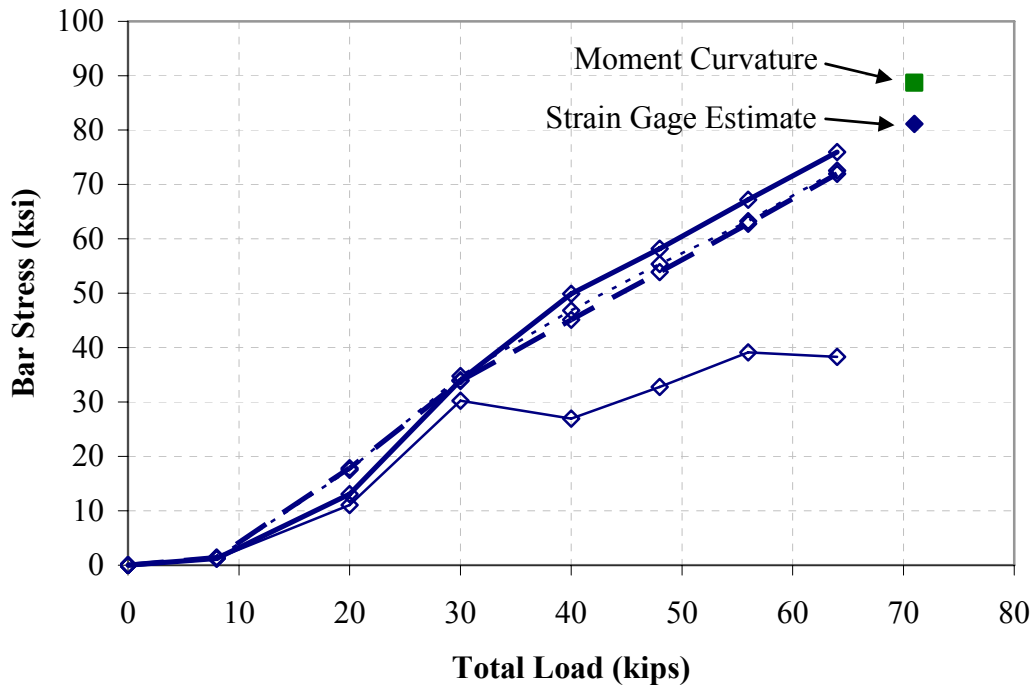


Figure B.20 – Measured bar stress for specimen 8-8-OC1-2.5

Specimen 8-8-OC2-2.5

Specimen 8-8-OC2-2.5 failed due to the formation of bond splitting cracks in the splice region at a bar stress of 115.0 ksi, or 101% of the value predicted by Eq. (1.3). Figure B.21 shows the specimen after completion of the test.

B.4.2 Group 4B

All beams in Group 4B had a splice length of 36 in. The load-deflection behavior is shown in Figure B.22.



Figure B.21 – Specimen 8-8-OC2-2.5 at the conclusion of the test

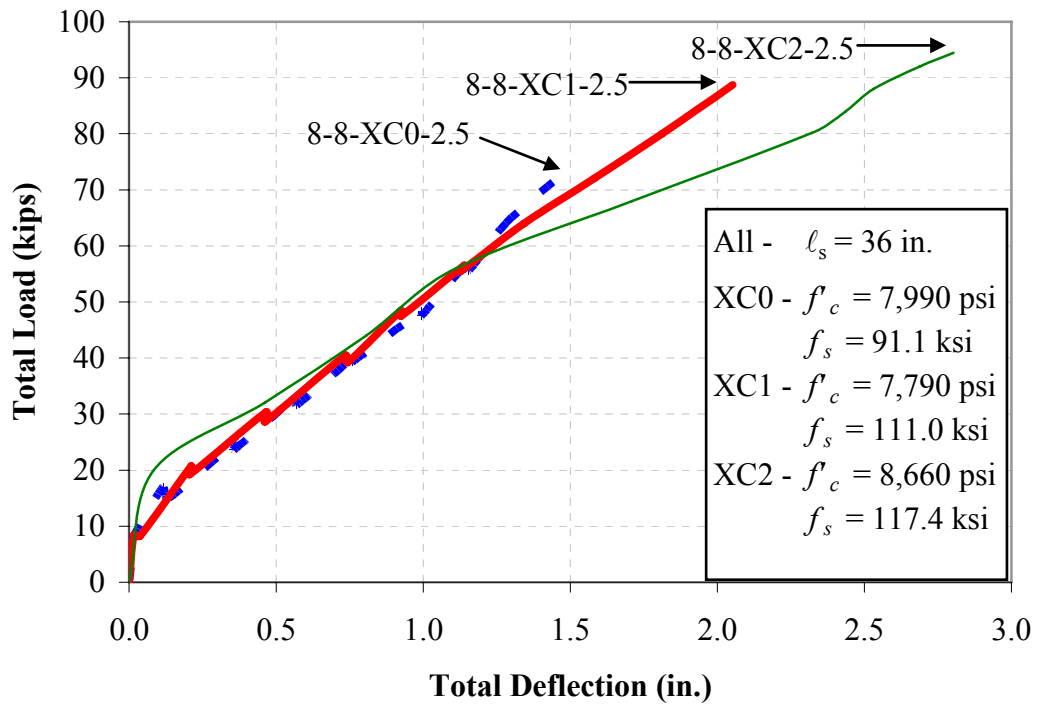


Figure B.22 – Load-deflection behavior of Group 4B beam-splice specimens

Specimen 8-8-XC0-2.5

Specimen 8-8-XC0-2.5 failed due to the formation of bond splitting cracks in the splice region at a bar stress of 91.1 ksi, or 95% of the value predicted by Eq. (1.3). A photograph of the specimen following the completion of the test is shown in Figure B.23.



Figure B.23 – Specimen 8-8-XC0-2.5 at the conclusion of the test

Specimen 8-8-XC1-2.5

Specimen 8-8-XC1-2.5 failed due to the formation of bond splitting cracks in the splice region at a bar stress of 111.0 ksi, or 98% of the value predicted by Eq. (1.3). A photograph of the specimen following the completion of the test is shown in Figure B.24.

Specimen 8-8-XC2-2.5

Specimen 8-8-XC2-2.5 failed due to the formation of bond splitting cracks in the splice region at a bar stress of 117.4 ksi, or 85% of the value predicted by Eq. (1.3). A photograph of the specimen following the completion of the test is shown in Figure B.25.

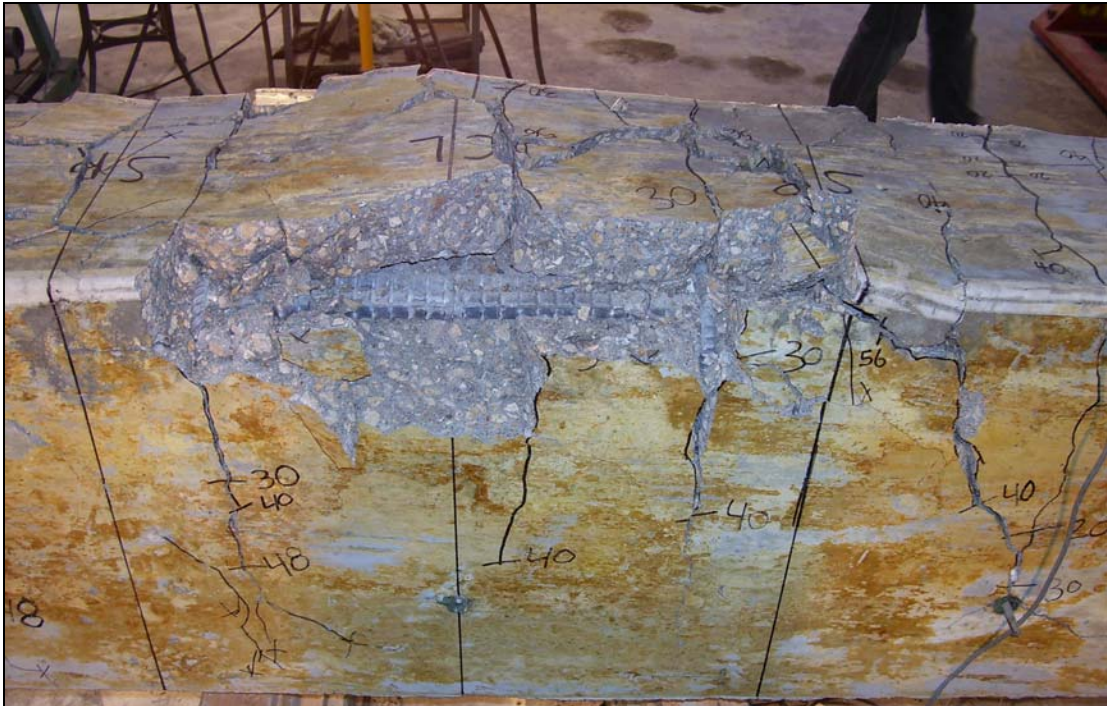


Figure B.24 – Specimen 8-8-XC1-2.5 at the conclusion of the test



Figure B.25 – Specimen 8-8-XC2-2.5 at the conclusion of the test

Specimen 8-8-XC2-2.5 was the sole specimen with a nominal target bar stress of 140 ksi that was not cast as a T-beam. Due to the first duplicate of specimen 8-5-XC2-1.5 experiencing a flexural failure at a bar stress near 140 ksi after the casting of this specimen, external stirrups were used in an attempt to confine the concrete at the highest moment regions away from the test region. Each external stirrup consisted of one C6x8.2 channel on both the top and bottom of the beam connected with ½-in. all-thread rod on each side of the beam. Four stirrups were used sequentially on each side of the splice region beginning at the edge of the bearing plate for the support and terminating roughly 10 in. from the end of the splice region. The bearing faces of the channels were attached with Hydrostone to the beam. Figure B.26 displays a photograph showing the external stirrups applied to specimen 8-8-XC2-2.5. The weight of the external stirrups was not included in the applied loads for moment calculation.



Figure B.26 – External stirrups used to confine specimen 8-8-XC2-2.5

B.5 SERIES 5 SPECIMENS

All beams in Series 5 contained two No. 11 Grade 100 MMFX longitudinal tension bars. The beams had a lap splice of length 58 in. (5A) or 79 in. (5B) centered at the midspan of the beam. The total span for Series 5 beams was 24 ft with an internal span of 11 ft between supports. Series 5 beams were designed without compression reinforcement, but contained two No. 4 Grade 60 bars to support the upper corners of the shear reinforcement. Specimen 11-8-XC2-2, a T-beam, is an exception, as described below. All specimens contained 19 No. 5 closed stirrups spaced at 4.5 in. center-to-center in each shear region beyond the support. The C0 specimens had unconfined splices, while the C1 and C2 specimens contained four and nine No. 4 closed stirrups, respectively.

B.5.1 Group 5A

All beams in Group 5A had a splice length of 58 in. The load-deflection behavior is shown below in Figure B.27.

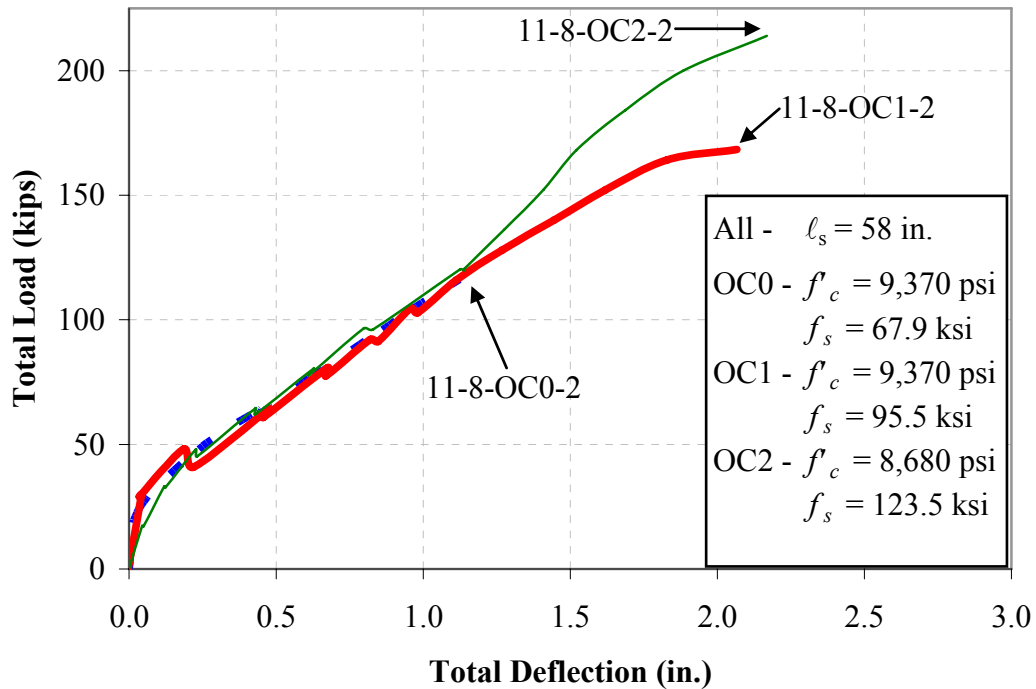


Figure B.27 – Load-deflection behavior of Group 5A beam-splice specimens

Specimen 11-8-OC0-2

Specimen 11-8-OC0-2 failed due to the formation of bond splitting cracks in the splice region at a bar stress of 67.9 ksi, or 86% of the value predicted by Eq. (1.3). A photograph of the specimen following the completion of the test is shown in Figure B.28. By averaging the strain recorded by the four gages immediately prior to failure, the measured bar stress at splice failure was determined to be 70.6 ksi. Figure B.29 displays the bar stress recorded by the strain gages versus the total load on the beam.



Figure B.28 – Specimen 11-8-OC0-2 at the conclusion of the test

Specimen 11-8-OC1-2

Specimen 11-8-OC1-2 failed due to the formation of bond splitting cracks in the splice region at a bar stress of 95.5 ksi, or 99% of the value predicted by Eq. (1.3). A photograph of the specimen following the completion of the test is shown in Figure B.30. By averaging the strain recorded by the four gages immediately prior to failure, the measured bar stress at splice failure was determined to be 98.8 ksi. Figure B.31 displays the bar stress recorded by the strain gages versus the total load on the beam.

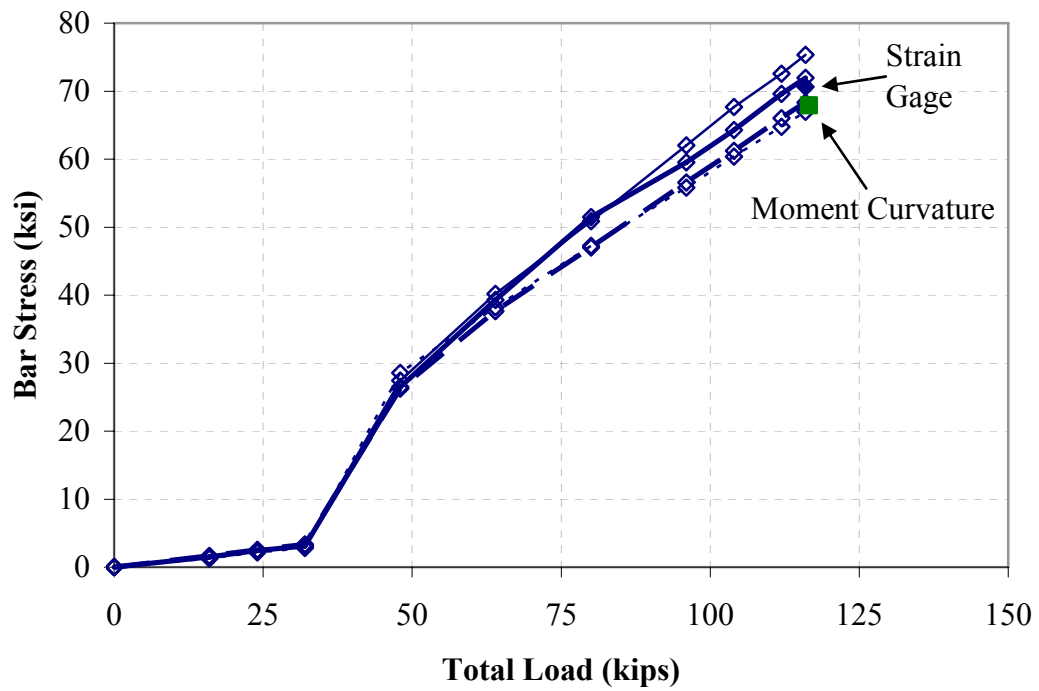


Figure B.29 – Measured bar stress for specimen 11-8-OC0-2

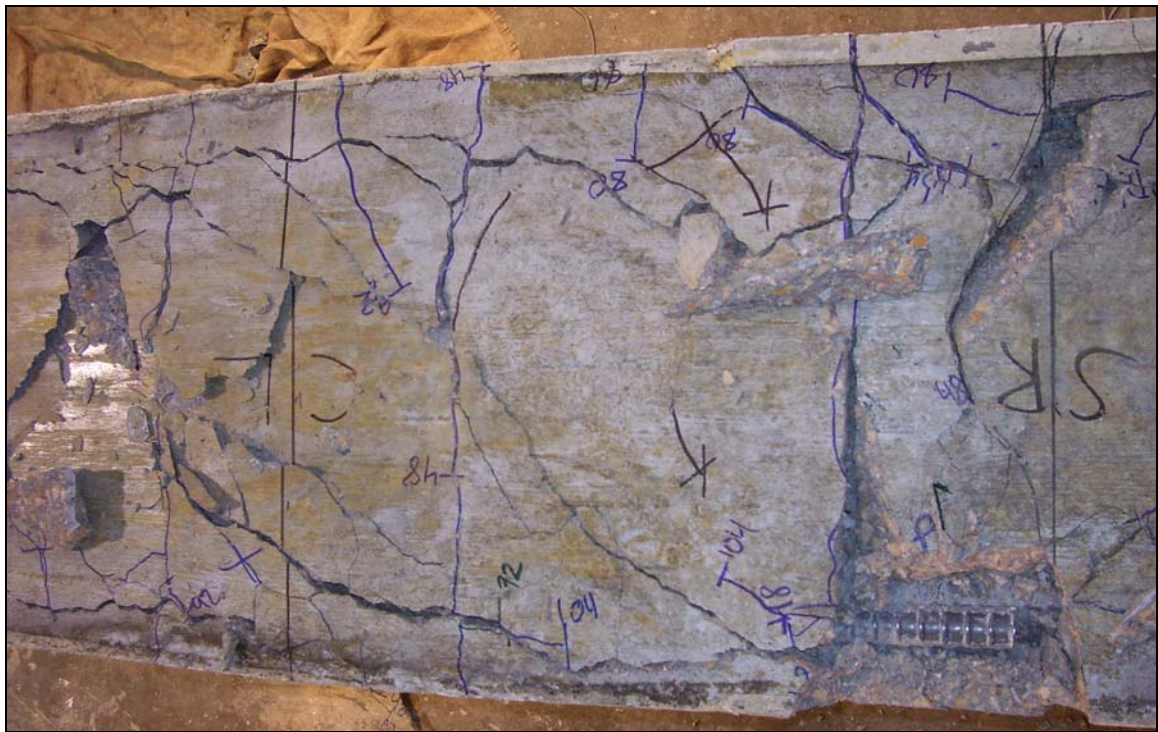


Figure B.30 – Specimen 11-8-OC1-2 after testing, as viewed from above

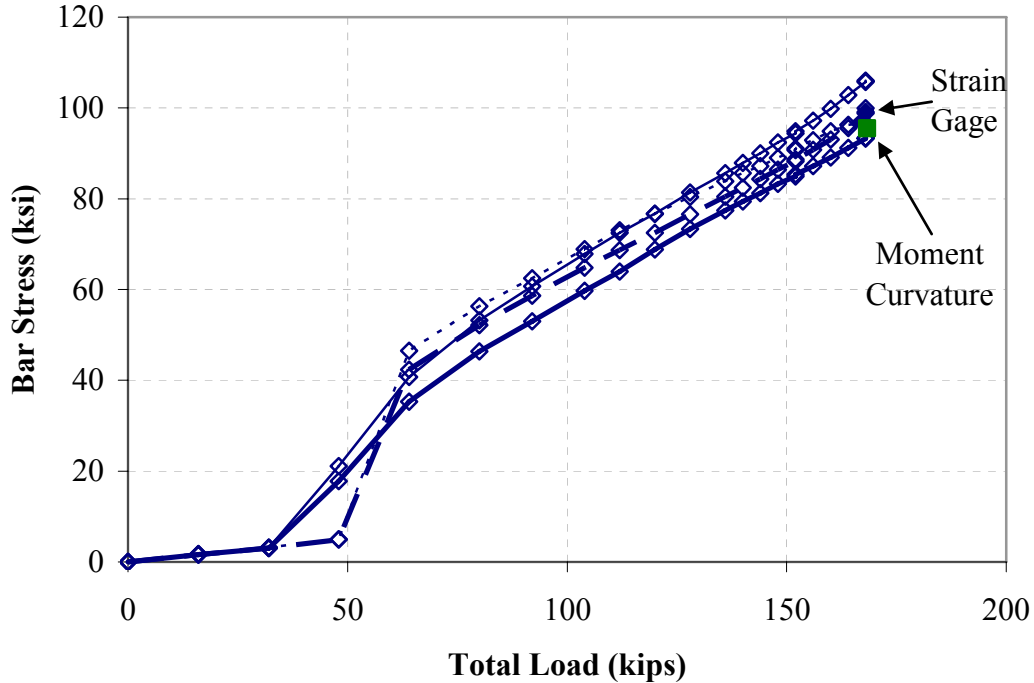


Figure B.31 – Measured bar stress for specimen 11-8-OC1-2

Specimen 11-8-OC2-2

Specimen 11-8-OC2-2 failed due to the formation of bond splitting cracks in the splice region at a bar stress of 123.5 ksi, or 100% of the value predicted by Eq. (1.3). A photograph of the specimen following the completion of the test is shown in Figure B.32. By averaging the strain recorded by the four gages immediately prior to failure, the measured bar stress at splice failure was determined to be 123.4 ksi. Figure B.33 displays the bar stress recorded by the strain gages versus the total load on the beam.

Beam 11-8-OC2-2 was loaded to approximately 48 kips total load, at which point it was noted that the load distribution across the four load rods was uneven compared to that typically observed during tests. Additionally, at that load step, a severe and continual reduction in load was noted. As such, although the beam was beyond the cracking load, all load was removed from the beam and the hydraulic system was completely reset and tightened. The beam was then reloaded from zero, and stable results were obtained for the remainder of the test.



Figure B.32 – Specimen 11-8-OC2-2 at the conclusion of the test

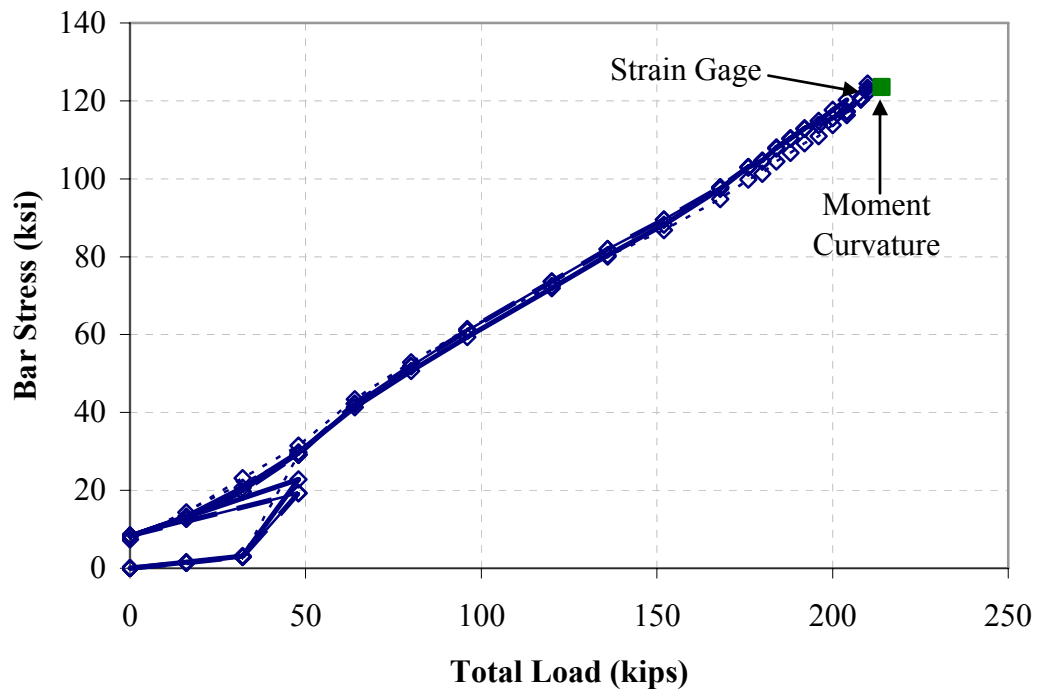


Figure B.33 – Measured bar stress for specimen 11-8-OC2-2

B.5.2 Group 5B

All beams in Group 5B had a splice length of 79 in. Specimen 11-8-XC2-2 was cast as a T-beam with a 38-in. wide, 7-in. deep flange. Specimen 11-8-XC2-2 was also cast with significantly more compression steel, 3.56 in.² compared with the 0.40 in.² found in the other beams in the group. The load-deflection behavior is slightly stiffer for the T-beam compared to the other two specimens in the group, as shown in Figure B.34.

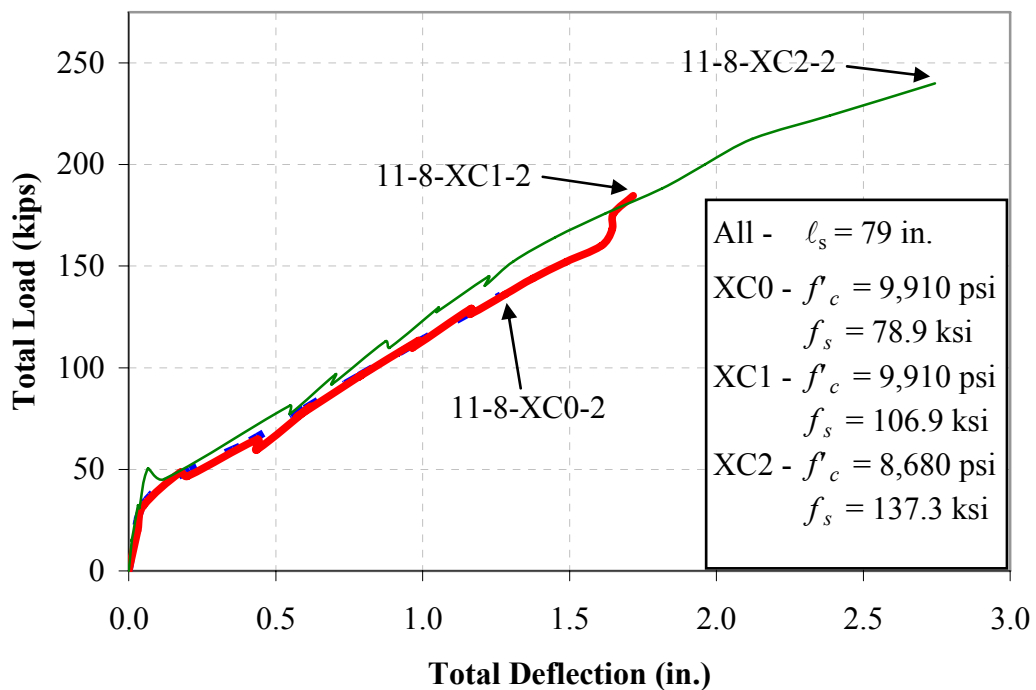


Figure B.34 – Load-deflection behavior of Group 5B beam-splice specimens

Specimen 11-8-XC0-2

Specimen 11-8-XC0-2 failed due to the formation of bond splitting cracks in the splice region at a bar stress of 78.9 ksi, or 80% of the value predicted by Eq. (1.3). A photograph of the specimen following the completion of the test is shown in Figure B.35. By averaging the strain recorded by the three accurate gages immediately prior to failure, the measured bar stress at splice failure was determined to be 83.3 ksi. Figure B.36 displays the bar stress recorded by the strain gages versus the total load.



Figure B.35 – Specimen 11-8-XC0-2 at the conclusion of the test

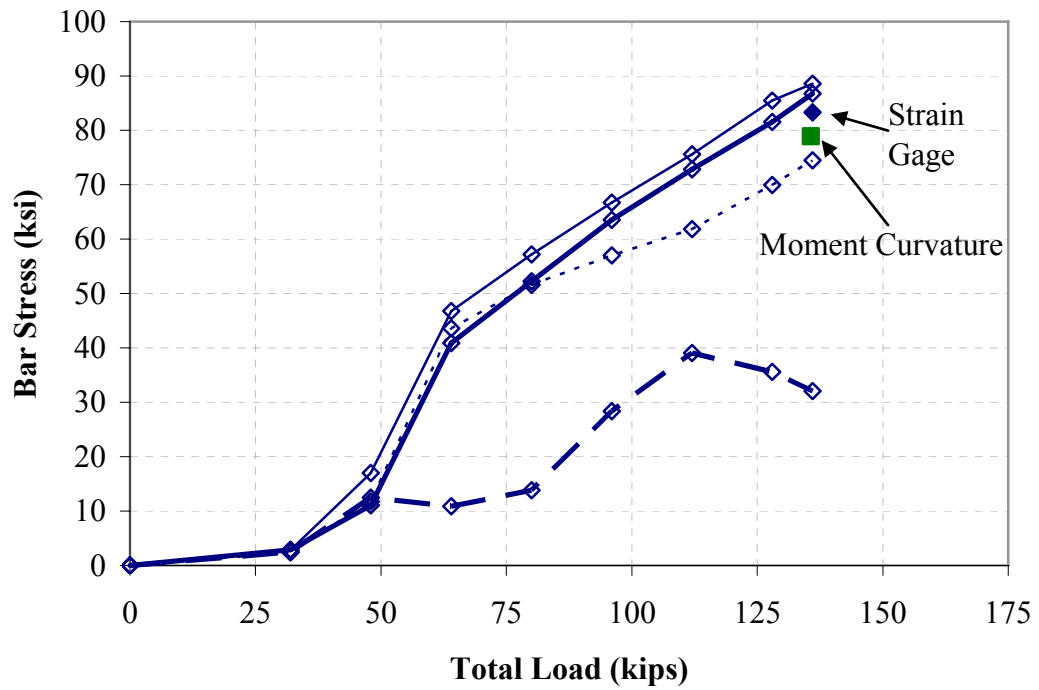


Figure B.36 – Measured bar stress for specimen 11-8-XC0-2

Specimen 11-8-XC1-2

Specimen 11-8-XC1-2 failed due to the formation of bond splitting cracks in the splice region at a bar stress of 106.9 ksi, or 84% of the value predicted by Eq. (1.3). A photograph of the specimen following the completion of the test is shown in Figure B.37. By averaging the strain recorded by the three functioning gages immediately prior to failure, the measured bar stress at splice failure was determined to be 103.9 ksi. Figure B.38 displays the bar stress recorded by the strain gages versus the total load.



Figure B.37 – Specimen 11-8-XC1-2 at the conclusion of the test

Specimen 11-8-XC2-2

Specimen 11-8-XC2-2 failed due to the formation of bond splitting cracks in the splice region at a bar stress of 137.3 ksi, or 97% of the value predicted by Eq. (1.3). A photograph of the specimen following the completion of the test is shown in Figure B.39. By averaging the strain recorded by the four gages immediately prior to failure, the measured bar stress at splice failure was determined to be 136.7 ksi. Figure B.40 displays the bar stress recorded by the strain gages versus the total load.

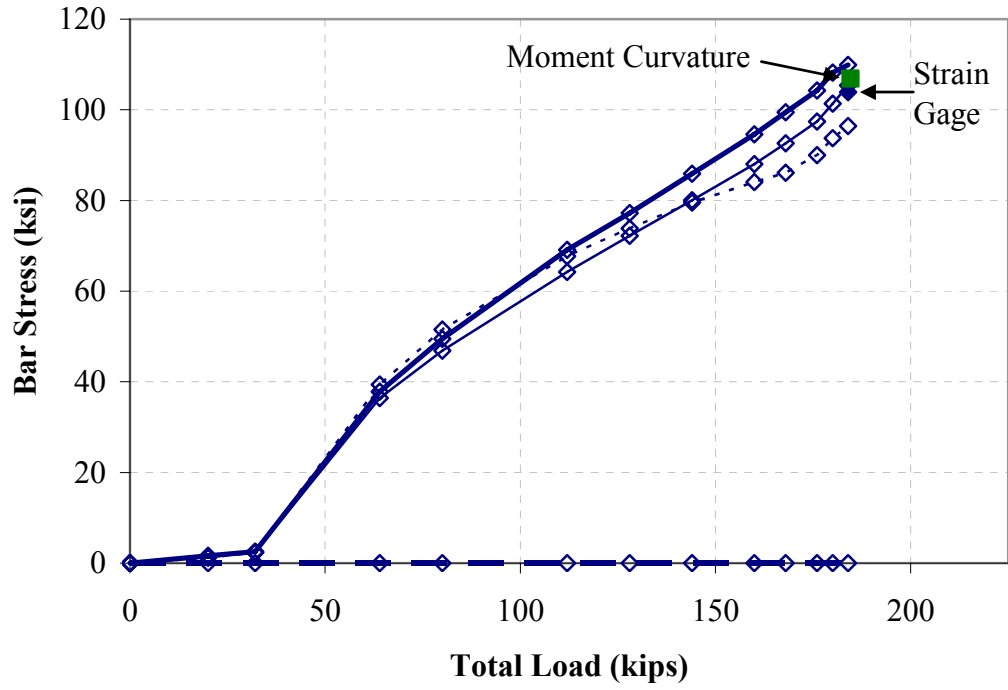


Figure B.38 – Measured bar stress for specimen 11-8-XC1-2



Figure B.39 – Specimen 11-8-XC2-2 at the conclusion of the test

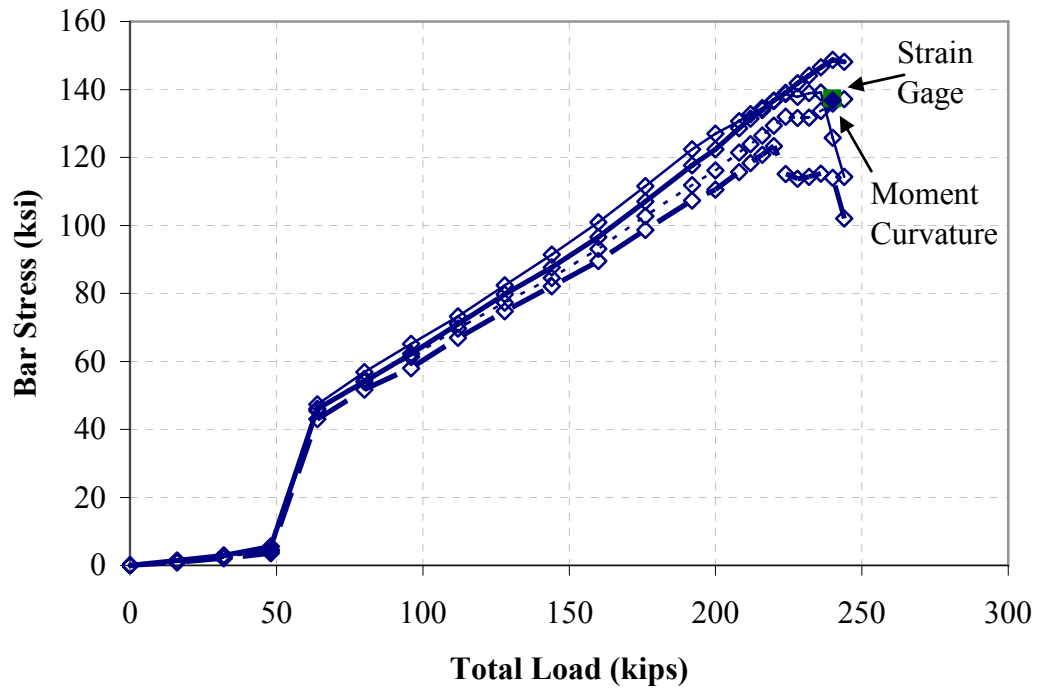


Figure B.40 – Measured bar stress for specimen 11-8-XC2-2

Given the 38-in. flange width of specimen 11-8-XC2-2, blockouts were used to reduce the flange width at the ends of the beam to accommodate the load rods, which were spaced apart transversely 36 in. 9-in. long by 7-in. tall by 4-in. deep block-outs were used to eliminate a portion of the final nine inches of the flange, resulting in a final reduced flange width at both ends of approximately 30 in.